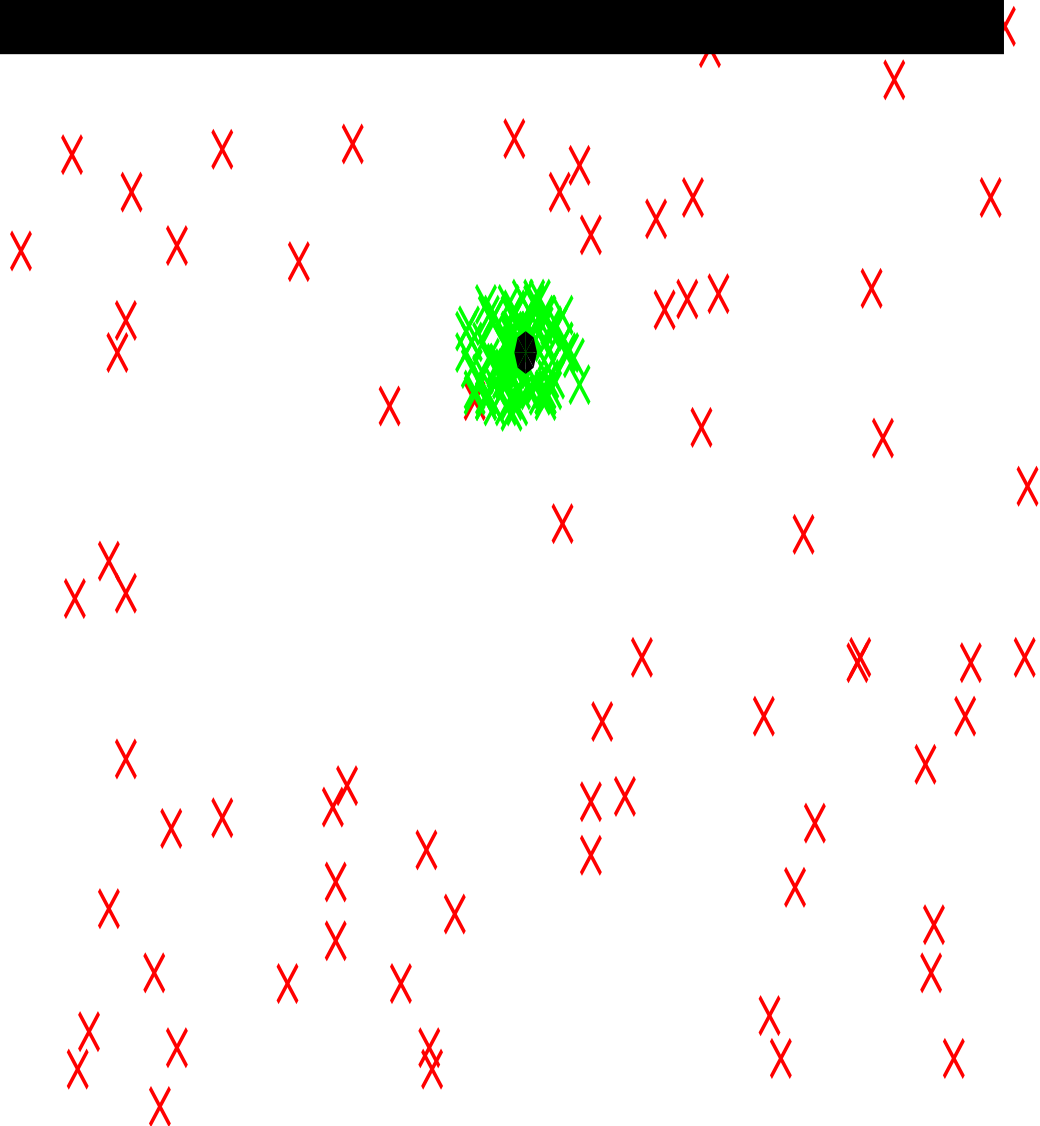


# Feedback Control for Course Correction of a Spin Stabilized Projectile

D. Mutters

Master of Science Thesis





# Feedback Control for Course Correction of a Spin Stabilized Projectile

MASTER OF SCIENCE THESIS

For the degree of Master of Science in Systems and Control at Delft  
University of Technology

D. Mutters

July 1, 2020

Faculty of Mechanical, Maritime and Materials Engineering (3mE) · Delft University of  
Technology



The work in this thesis was supported by TNO. Their cooperation is hereby gratefully acknowledged.



Copyright © Delft Center for Systems and Control (DCSC)  
All rights reserved.

DELFT UNIVERSITY OF TECHNOLOGY  
DEPARTMENT OF  
DELFT CENTER FOR SYSTEMS AND CONTROL (DCSC)

The undersigned hereby certify that they have read and recommend to the  
Faculty of Mechanical, Maritime and Materials Engineering (3mE) for  
acceptance a thesis entitled

FEEDBACK CONTROL FOR COURSE CORRECTION OF A SPIN STABILIZED  
PROJECTILE

by

D. MUTTERS

in partial fulfillment of the requirements for the degree of  
MASTER OF SCIENCE SYSTEMS AND CONTROL

Dated: July 1, 2020

Supervisor(s):

\_\_\_\_\_  
Dr. R. Ferrari

\_\_\_\_\_  
Dr.ir. H. Tol

Reader(s):

\_\_\_\_\_  
Dr.Ing. S. Grammatico

\_\_\_\_\_  
Z. Feng



---

# Abstract

This report presents the results of the graduation thesis from the TU Delft, performed at TNO unit Defence, Safety and Security, expertise group Weapon Systems. The goal of this graduation project is to develop a controller for a projectile equipped with the Precision Guidance Kit (PGK). The PGK is a Course Correction Fuze (CCF) which can be used to retrofit 'dumb' artillery projectiles. It has canards to provide course correction and contains a GPS sensor to determine its position and velocity.

The dynamics of the projectile are described by a nonlinear 6 Degrees of Freedom (DoF) non-rolling body frame model. A static model is made of the PGK where its aerodynamics are calculated using Computational Fluid Dynamics.

A Jacobian based guidance algorithm is developed for the 6 DoF model which calculates the changes in velocity needed along the perturbed trajectory to set the projectile back on the ideal path towards the target. These guidance signals function as a reference to be tracked by the controller.

A switching mode controller is designed, tuned and tested empirically in simulation. A nonlinear controller is designed to set the PGK actuator at an angle based on the guidance signals. Three switching laws are designed, the first to set the starting time of the controller, the second to switch the actuator off when the projectile is on a new ideal trajectory, and a third to avoid chattering, excessive switching, between the control modes.

The combination of the PGK actuator, the Jacobian guidance and the switching controller is shown to provide course correction successfully for four different trajectories with random offsets in initial velocity and pitch and yaw angle. The average miss distance and Circular Error Probable are decreased by 90%, to less than 50 m, without destabilizing the projectile.



---

# Table of Contents

<b>Preface</b>	<b>ix</b>
<b>1 Introduction</b>	<b>1</b>
1-1 Literature study . . . . .	2
1-1-1 Models . . . . .	2
1-1-2 Control techniques . . . . .	3
1-1-3 Conclusion . . . . .	3
1-2 Problem description . . . . .	4
1-3 Thesis outline . . . . .	5
<b>2 Model</b>	<b>7</b>
2-1 Projectile model . . . . .	7
2-1-1 Inertial reference frame . . . . .	8
2-1-2 Body frame . . . . .	8
2-1-3 Non-rolling body frame . . . . .	10
2-1-4 Nominal trajectory . . . . .	12
2-2 Actuator model . . . . .	13
2-2-1 Actuator description . . . . .	14
2-2-2 Nonlinear actuator model . . . . .	15
2-3 Linearization . . . . .	18
2-3-1 Linear projectile model . . . . .	18
2-3-2 Validation of linearized projectile model . . . . .	20
2-3-3 Linearized actuator model . . . . .	24
2-4 Conclusion . . . . .	28

<b>3</b>	<b>Guidance</b>	<b>29</b>
3-1	Jacobian guidance . . . . .	29
3-2	Guidance example . . . . .	31
3-3	Conclusion . . . . .	36
<b>4</b>	<b>Control</b>	<b>37</b>
4-1	Switching controller . . . . .	37
4-1-1	Impact point analysis . . . . .	38
4-1-2	Controlling the PGK angle . . . . .	41
4-1-3	Switching criteria . . . . .	44
4-2	Model predictive control . . . . .	56
4-2-1	Pendulum . . . . .	57
4-2-2	PGK . . . . .	66
4-3	Conclusion . . . . .	66
<b>5</b>	<b>Simulations</b>	<b>69</b>
5-1	trajectory 1: high velocity, high pitch angle . . . . .	70
5-2	trajectory 2: high velocity, low pitch angle . . . . .	73
5-3	trajectory 3: low velocity, high pitch angle . . . . .	76
5-4	trajectory 4: low velocity, low pitch angle . . . . .	78
5-5	conclusion . . . . .	80
<b>6</b>	<b>Conclusions</b>	<b>83</b>
6-1	Recommendations . . . . .	84
<b>A</b>	<b>Jacobian linearization</b>	<b>87</b>
A-1	Deviation dynamics . . . . .	87
A-2	Jacobian Linearization of projectile model . . . . .	88
	<b>Bibliography</b>	<b>91</b>
	<b>Glossary</b>	<b>95</b>
	List of Acronyms . . . . .	95
	List of Symbols . . . . .	96

---

# List of Figures

1-1	block diagram . . . . .	4
2-1	Used coordinate systems . . . . .	8
2-2	nominal trajectory . . . . .	13
2-3	ATK XM1156 Precision Guidance Kit . . . . .	14
2-4	schematic front-view of PGK . . . . .	15
2-5	actuator model at a quarter of the nominal trajectory . . . . .	17
2-6	actuator model halfway nominal trajectory . . . . .	17
2-7	actuator model at three quarters of the nominal trajectory . . . . .	18
2-8	comparison trajectories zero offset . . . . .	20
2-9	comparison trajectories pitch offset . . . . .	21
2-10	comparison trajectories yaw offset . . . . .	21
2-11	comparison trajectories velocity offset . . . . .	22
2-12	comparison sampling time for zero offset simulation . . . . .	23
2-13	comparison sampling time for pitch offset simulation . . . . .	24
2-14	Linear actuator model, update step $d\alpha = 0.001 * 2\pi$ . . . . .	25
2-15	Linear actuator model, update step $d\alpha = 0.01 * 2\pi$ . . . . .	26
2-16	Linear actuator model, update step $d\alpha = 0.02 * 2\pi$ . . . . .	26
2-17	Linear actuator model, update step $d\alpha = 0.05 * 2\pi$ . . . . .	27
2-18	Linear actuator model, update step $d\alpha = 0.1 * 2\pi$ . . . . .	27
3-1	Jacobian elements along nominal trajectory . . . . .	30
3-2	proportional forces example guidance . . . . .	33

3-3	proportional moments example guidance . . . . .	35
4-1	PGK model test: actuation between 20s and 25s, at $\alpha_{PGK} = 0\pi$ . . . . .	39
4-2	PGK model test results . . . . .	41
4-3	effect of actuator on guidance . . . . .	42
4-4	<i>BlockdiagramPGKangle</i> . . . . .	43
4-5	$\alpha_{PGK}$ . . . . .	43
4-6	$t_c$ sensitivity analysis . . . . .	45
4-7	$t_c = 10s$ . . . . .	46
4-8	$G_c$ sensitivity analysis . . . . .	47
4-9	$G_c = 2 m/s$ . . . . .	49
4-10	$t_d$ sensitivity analysis . . . . .	50
4-11	$t_d = 5s$ . . . . .	51
4-12	switching parameters analyses for depressed trajectory . . . . .	52
4-13	$t_d = 5s$ . . . . .	54
4-14	$t_d = 5s$ . . . . .	55
4-15	Model Predictive Control Scheme . . . . .	57
4-16	pendulum schematic . . . . .	58
4-17	MPC stabilizing pendulum at $\theta = 0$ degrees . . . . .	63
4-18	MPC predictions from discrete times $k$ to $k + N$ . . . . .	64
4-19	MPC stabilizing pendulum at $\theta = -10$ degrees . . . . .	65
5-1	nominal trajectory 1 . . . . .	71
5-2	miss distance trajectory 1 . . . . .	71
5-3	miss distance trajectory 1 close up . . . . .	72
5-4	nominal trajectory 2 . . . . .	73
5-5	miss distance trajectory 2 . . . . .	74
5-6	Jacobian elements nominal trajectory . . . . .	75
5-7	nominal trajectory 3 . . . . .	76
5-8	miss distance trajectory 3 . . . . .	77
5-9	nominal trajectory 4 . . . . .	78
5-10	miss distance trajectory 4 . . . . .	79
5-11	miss distance trajectory 4 with specific tuning . . . . .	80

---

# List of Tables

2-1	influence of $d\alpha_{PGK}$ on the error, with $d\alpha = 0.001$	27
2-2	influence of $d\alpha$ on the error, with $d\alpha_{PGK} = 0.01 * 2\pi$	28
3-1	proportional example guidance: delivery error for different offsets	35
4-1	PGK model test end point coordinates in m	39
4-2	PGK model test results changes in impact point	40
4-3	effect of actuator setting on guidance signals	42
5-1	simulations results trajectory 1	72
5-2	simulations results trajectory 2	75
5-3	simulations results trajectory 3	77
5-4	simulations results trajectory 4	80



---

# Preface

This report is the Master of Science graduation thesis from the Delft Center for Systems and Control (DCSC) department within the faculty of Mechanical, Maritime and Materials Engineering (3mE) at DUT. The topic of this thesis, the control design for a projectile equipped with the PGK is of interest to the Weapon Systems (WS) department of TNO.

This research was performed within the Defence Safety and Security (DSS) unit of TNO, under supervision of Dr.ir. Henry Tol and Ir. Wouter Halswijk, to whom I want to express my enormous gratitude. Thank you for your time and guidance during my time at TNO and even after that. It has not always been easy, and without your help and motivational speeches I would have never made it this far.

I would also like to thank my TU Delft supervisor, Dr. Riccardo Ferrari for all the meetings and discussions we had to try to solve the many problems we have run into along the way. Even though this subject is not closely related to your research, you have been able to coach me towards this finished thesis. And also Dr.ir. J. Sijs for the supervision at first part of this thesis work.

Of course I want to thank my parents, who have supported me in every possible way, for which I remain forever grateful. Unfortunately my sister could not wait for me and graduated before me, but thanks for the cookies and all the times we have studied together. Furthermore I would like to thank all my friends and family who have supported me along this journey and for making me forget about my thesis struggles once in a while. Last but not least, special thanks to Angela, could not have done this without you.

Delft, University of Technology  
July 1, 2020

D. Mutters

Master of Science Thesis

D. Mutters



---

# Chapter 1

---

## Introduction

Most of the innovation on modern weapon systems currently contributes to improving accuracy. Among the many motivations driving this effort are reduction of collateral damage, tactical advantages, and costs. Military operations are often conducted in urban environments, which makes artillery support rather tricky because there is great risk of collateral damage. When the projectiles can be delivered at higher accuracy at longer range, there is less collateral damage, and the operating speed increases, since the gun has to be repositioned less. Also the gun can operate at a larger distance from the enemy which increases the safety. Less rounds are needed to effectively engage the target, which provides another tactical advantage: the element of surprise, and of course a reduction in cost.

Currently the gun is aimed based on the target coordinates and meteorological data available previous to launch. The error in the gun-orientation and the muzzle velocity error have a large impact on the delivery accuracy when firing artillery projectiles. Conventional artillery uses unguided projectiles or dumb munition with low accuracy, half of the shells land more than 300m from the target when fired at maximum range [1].

Guided missiles offer a great increase in precision but also in cost, because of the propulsion, high-end sensors, actuators and Guidance Navigation and Control (GNC) systems. Retrofitting so called dumb ammunition with a Course Correction Fuze (CCF) fills the gap between precise, but expensive guided missiles and cheap, but inaccurate conventional artillery rounds. A Course Correction Fuze replaces the original fuze of the projectile and has built in sensors and actuators to provide course correction. This way the existing stockpiles of ballistic shells will be used with increases in accuracy and range, and decreases in collateral damage and round expenditure. Due to extreme accelerations

at launch and limited amount of available space the sensors and actuators are subject to challenging requirements, which complicate the design of Course Correction Fuzes.

This study focuses on the ATK XM1156 Precision Guidance Kit (PGK), a mechanically simple Course Correction Fuze for spin-stabilized 155 mm ammunition. The simplicity of the PGK ensures low cost and easy implementation, but creates additional requirements on the controller. The PGK fits in the conventional 155 mm deep fuze well and is screwed onto the projectile like the original fuze, compatibility with other calibers, 105 mm for example will be introduced in future increments [2]. The available size of the fuze is limited, and not all of the usual sensors and actuators which are used for guided missiles can be placed in the fuze head, for this the controller has to compensate.

## 1-1 Literature study

In preparation for this thesis a literature study was performed, of which a summary is presented in this section. The literature survey presents an overview of available CCFs, the most commonly used dynamical models, and focuses on different types of guidance and control currently applied to artillery projectiles equipped with a CCF.

### 1-1-1 Models

The Models of ballistic projectiles commonly use the highly nonlinear 6 Degrees of Freedom (DoF) Equations of Motion (EoM) as a starting point and are based on references [3, 4, 5]. It is shown how this model can be transformed to the non rolling body frame, used for spin-stabilized ammunition in reference [6]. This model is used for unguided spinners, but also as simplified model for guided projectiles, where forces on a general guidance-fuze are taken into account without specifying the actuators.

Both 6 DoF and 7 DoF models are highly nonlinear and are usually linearized before they are used in controller design as in references [7, 8, 9, 10]. Projectile linear theory or Linear Parameter Varying (LPV) techniques can be used to obtain a linear model [11, 12, 13, 14]. The more simplified models neglect the coupling between the yaw and pitch dynamics, so two separate controllers can be designed for the lateral and longitudinal control. However, more complex and detailed models show that the pitch and yaw channel dynamics are tightly coupled, therefore a multivariable feedback law is required. Designing separate controllers for each axis could lead to poor performance or even instability [15]. and more complex control techniques are required. The linearized models based on projectile linear theory have the benefit of less computational power requirements and the combination with an LPV technique provides a more accurate system model.

## 1-1-2 Control techniques

**Switching control** can be found everywhere in daily life. For example in the thermostats to heat your house often a simple bang-bang switching controller is used, when the temperature drops below the lower boundary the heating is switched on, when the temperature rises to above the top boundary the heating is switched off again [16]. In general switching control combines continuous dynamics with discrete switching events [17]. Switching controllers are amongst others used in combination with gain-scheduling controllers, which are one of the most popular control techniques for missile autopilot design [18, 19]. Stability and the avoidance of chattering, excessive switching between modes, are two typical challenges because of the involved switching [19, 20, 17]. Lyapunov's stability theory for general nonlinear systems can be used to find switching signals that preserve stability [17].

**MPC** is used in projectile guidance. However important differences are noted, mostly caused by the type of projectile, actuator, or application. Some of the different applications of Model Predictive Control (MPC) are: fin-stabilized projectiles [7, 8], proportional actuators, or direct-fire projectiles [7]. MPC has not yet been applied to control actuators like the PGK, but it looks promising.

**Other control methods** can also be applied to guided projectiles. Linear quadratic optimal control is used in [21, 22], both on projectiles with movable canards on the nose.  $\mathcal{H}_\infty$  control methods are used in multiple studies by the French-German research Institute of Saint Louis (ISL): in combination with PID control in [23];  $\mathcal{H}_2$  and  $\mathcal{H}_\infty$  constraints are compared in [24]; Mixed sensitivity  $\mathcal{H}_\infty$  control is used to design a gain scheduled controller in [15]; In [25, 26]  $\mathcal{H}_\infty$  loop shaping is used. Different forms of PID controllers are used in [27, 28, 29].

## 1-1-3 Conclusion

of the literature study is that a nonlinear 6 DoF non-rolling body frame model is the best suitable model to describe the dynamics of a spin stabilized projectile. This model is to be used as simulation model and can serve as the starting point for linearization. Linear models are often chosen for guided projectiles, as the computational power in the fuze is limited. A combination of (modified) projectile linear theory and jacobian linearization results in an accurate LPV model.

Switching mode control and MPC are both common control methods used in guided munitions, although they has not been applied to this kind of actuator. Stability and chattering are two main challenges to be dealt with.  $\mathcal{H}_\infty$  provides robustness but does not have the ability to deal with constraints. Linear MPC seems to be a logical choice for a controller as it has the possibility of dealing with constraints, stability, and uses linear models to decrease computational requirements.

## 1-2 Problem description

The problem statement is phrased with the following research question: How to design and evaluate a controller for a 155 mm spin-stabilized gunfired projectile equipped with the Precision Guidance Kit? The design criteria are:

- Robustness: Provide course correction without destabilizing the projectile
- Performance: Result in a Circular Error Probable (CEP) of less than 50m

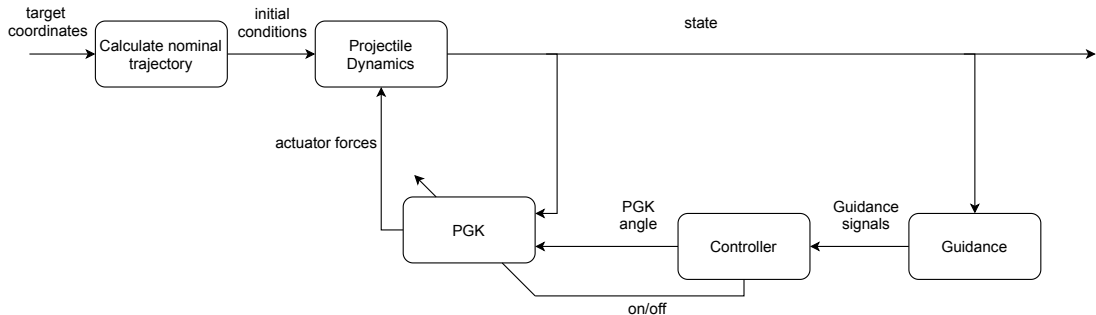


**Figure 1-1:** block diagram

The block diagram shown in figure 1-1 shows the entire system. With an exception of the first block, that calculates the nominal trajectory based on the target, all blocks need to be designed.

First of all a model of the projectile and the actuator is needed. The switching controller and MPC controller require different models. The switching controller uses nonlinear models, and the MPC controller uses linear models. So linearization of both the projectile and actuator model is needed. Secondly a Guidance algorithm has to be designed to create inputs for the controllers. Last but not least both controllers need to be designed.

Linear MPC control proved to be a significant challenge for the highly nonlinear simulation model. Application of MPC in closed-loop simulations was not achieved in this thesis. Therefore the structure of this thesis is somewhat unconventional. The design and results of the switching controller are discussed completely, but the work concerning the MPC, including theoretical derivation of the MPC structure and a working example of a controlled pendulum, is presented as a stepping stone for further research. The following research objectives are reached:

- Modeling the projectile and the PGK
- Linearization of the projectile and actuator model

- Implementing the Guidance algorithm
- Designing the switching mode controller
- Evaluation of the controller in simulation

## 1-3 Thesis outline

This thesis is structured in the following way. Chapter 2 describes the models used to describe the projectile and actuator dynamics. This includes the translations between the different reference frames, the description of the actuator, and the linearization of both projectile and actuator model. The guidance is explained in chapter 3, where the structure of the guidance algorithm is discussed and a simplified proportional example is used for demonstration. The design of the switching controller and the MPC structure is shown in chapter 4. Chapter 5 includes the simulations conducted with the switching mode controller. Finally the conclusion and recommendations of this graduation work can be found in chapter 6.

At the back of this thesis there is an appendix including the mathematical derivations of the jacobian linearization that are found to be too tedious for the main matter of this thesis.



---

# Chapter 2

---

## Model

This chapter describes the dynamical models of the projectile and actuator that are used for guidance, control, and simulation. In section 2-1 the projectile model is shown in three subsections each describing a different reference frame. The inertial frame or Earth frame, the body frame, and the non-rolling body frame, which is an intermediate frame between the inertial and body frame. The transformations between these different reference coordinate systems are included [6]. The full-nonlinear 6 Degrees of Freedom (DoF) non-rolling body frame model, based on references [3, 4, 5], is used as high-fidelity simulation model.

The actuator is described in section 2-2. A general description of the actuator is given and the nonlinear actuator model is shown.

The 6 DoF non-rolling body model is linearized according to projectile linear theory [13] and is shown in section 2-3. The resulting Linear Parameter Varying (LPV) model is verified by comparison to the nonlinear model and the same is done for the actuator model.

### 2-1 Projectile model

This section describes the Equations of Motion (EoM) of the projectile body with 6 DoF. Starting at the inertial reference frame, the equations of motion are transformed to the body frame. An intermediate frame, the non-rolling body frame, is a commonly used reference frame for highly spinning projectiles because of the lower computational demand. This model will be used as simulation model, and as a starting point for a linear control model.

### 2-1-1 Inertial reference frame

The Flat earth frame is used as inertial reference frame. This frame omits the rotation and curvature of the earth, which is sufficiently accurate for short flight trajectories [11]. The x-axis is positive towards the target, parallel to the surface of the earth. The y-axis is perpendicular to the x-axis, parallel to the earth's surface and positive to the right when looking from gun to target. The z-axis is perpendicular to both x- and y-axis and positive downwards as in figure 2-1a.

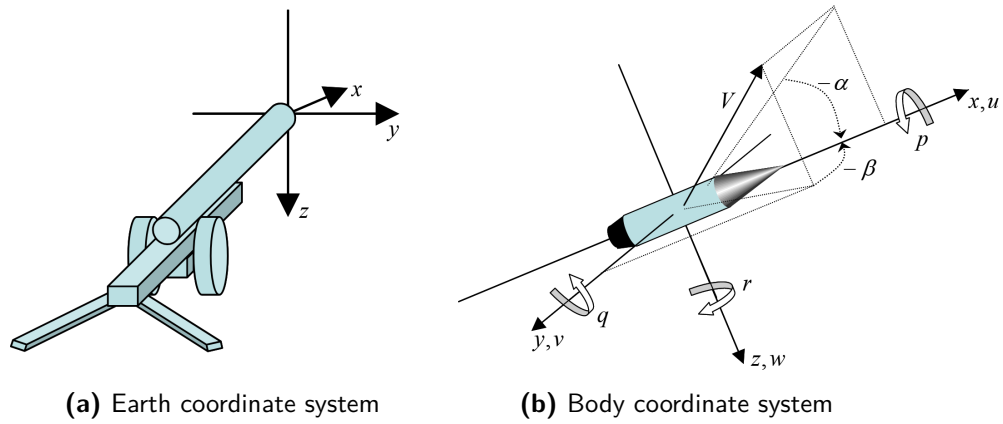


Figure 2-1: Used coordinate systems

Source: [11]

### 2-1-2 Body frame

Standard Euler angles are used to transfer the earth frame to the rolling body frame, which has its origin at the center of mass of the projectile. The x-axis of this frame points forward out of the nose of the projectile. The y-axis is positive to the right, and z-axis downwards, when looking along the x-axis in positive direction. Where  $u$ ,  $v$ , and  $w$  are the velocity vector components,  $p$ ,  $q$ , and  $r$  are the angular velocity vector components, and  $\alpha$  and  $\beta$  are the angle of attack and sideslip, respectively, see figure 2-1b.  $I$  is the inertia matrix,  $F_X$ ,  $F_Y$ , and  $F_Z$  the force components, and  $M_X$ ,  $M_Y$ , and  $M_Z$  the moment components. The 6 DoF **EOM!** (**EOM!**) are given by:

$$\begin{bmatrix} \dot{u} \\ \dot{v} \\ \dot{w} \end{bmatrix} = \frac{1}{m} \begin{bmatrix} F_X \\ F_Y \\ F_Z \end{bmatrix} - \begin{bmatrix} 0 & -r & q \\ r & 0 & -p \\ -q & p & 0 \end{bmatrix} \begin{bmatrix} u \\ v \\ w \end{bmatrix} \quad (2-1)$$

$$\begin{bmatrix} \dot{p} \\ \dot{q} \\ \dot{r} \end{bmatrix} = [I]^{-1} \left( \begin{bmatrix} M_X \\ M_Y \\ M_Z \end{bmatrix} - \begin{bmatrix} 0 & -r & q \\ r & 0 & -p \\ -q & p & 0 \end{bmatrix} [I] \begin{bmatrix} p \\ q \\ r \end{bmatrix} \right). \quad (2-2)$$

Equations (2-3) and (2-4) relate the body frame to the earth frame.

$$\begin{bmatrix} \dot{x}_E \\ \dot{y}_E \\ \dot{z}_E \end{bmatrix} = \begin{bmatrix} \cos \theta \cos \psi & \sin \phi \sin \theta \cos \psi - \cos \phi \sin \psi & \cos \phi \sin \theta \cos \psi + \sin \phi \sin \psi \\ \cos \theta \sin \psi & \sin \phi \sin \theta \sin \psi + \cos \phi \cos \psi & \cos \phi \sin \theta \sin \psi - \sin \phi \cos \psi \\ -\sin \theta & \sin \phi \cos \theta & \cos \phi \cos \theta \end{bmatrix} \begin{bmatrix} u \\ v \\ w \end{bmatrix} \quad (2-3)$$

$$\begin{bmatrix} \dot{\phi} \\ \dot{\theta} \\ \dot{\psi} \end{bmatrix} = \begin{bmatrix} 1 & \sin \phi \tan \theta & \cos \phi \tan \theta \\ 0 & \cos \phi & -\sin \phi \\ 0 & \frac{\sin \phi}{\cos \theta} & \frac{\cos \phi}{\cos \theta} \end{bmatrix} \begin{bmatrix} p \\ q \\ r \end{bmatrix} \quad (2-4)$$

The force vector  $F = [F_X \ F_Y \ F_Z]^T$  can be decomposed into four elements, namely an aerodynamic force acting on the projectile body,  $F_b$ , the Magnus force,  $F_m$ , caused by the combination of the spinning of the projectile and angle of attack, the gravity,  $F_g$ , and the actuator force  $F_a$ . The actuator model is discussed in section 2-2, but the other three forces are shown below. Here  $\bar{q}$  is the dynamic pressure,  $S$  the aerodynamic reference surface of the projectile,  $d$  the diameter of the projectile,  $V$  the total velocity.  $C_{A0}$  and  $C_{A2}$  are the terms of the aerodynamic drag coefficient,  $C_{N\alpha}$  is the normal coefficient, and  $C_{yp\alpha}$  the Magnus force coefficient. The normal coefficient is the same for  $Y$  and  $Z$  direction because of projectile symmetry. The aerodynamic coefficients are obtained by table lookup, as a function of Mach number  $\mathcal{M}$ .

$$F = \begin{bmatrix} X \\ Y \\ Z \end{bmatrix} = F_b + F_m + F_g + F_a \quad (2-5)$$

$$F_b = -\bar{q}S \begin{bmatrix} C_{A0} + C_{A2} \left( \frac{v^2 + w^2}{V^2} \right) \\ C_{N\alpha} \frac{v}{V} \\ C_{N\alpha} \frac{w}{V} \end{bmatrix} \quad (2-6)$$

$$F_m = -\bar{q}S \left( \frac{pd}{V} \right) \begin{bmatrix} 0 \\ C_{yp\alpha} \frac{w}{V} \\ -C_{yp\alpha} \frac{v}{V} \end{bmatrix} \quad (2-7)$$

$$F_g = mg \begin{bmatrix} -\sin \theta \\ \cos \theta \sin \phi \\ \cos \theta \cos \phi \end{bmatrix} \quad (2-8)$$

$$F = -\bar{q}S \left\{ \begin{bmatrix} C_{A0} + C_{A2} \left( \frac{v^2 + w^2}{V^2} \right) \\ C_{N\alpha} \frac{v}{V} \\ C_{N\alpha} \frac{w}{V} \end{bmatrix} + \left( \frac{p_a d}{V} \right) \begin{bmatrix} 0 \\ C_{yp\alpha} \frac{w}{V} \\ -C_{yp\alpha} \frac{v}{V} \end{bmatrix} \right\} + mg \begin{bmatrix} -\sin \theta \\ \cos \theta \sin \phi \\ \cos \theta \cos \phi \end{bmatrix} + F_a \quad (2-9)$$

The moments  $M = [M_X \ M_Y \ M_Z]^T$  are decomposed in the same way as the forces. The moment caused by aerodynamics on the body,  $M_b$ , and the Magnus effect,  $M_m$ , are shown. Additionally there is a term containing the damping,  $M_d$ . And the actuator moments are  $M_a$ , explained in more detail in section 2-2.  $C_{m\alpha}$  is the aerodynamic body overturning moment coefficient,  $C_{np\alpha}$  the Magnus moment coefficient, and  $C_{lp}$ ,  $C_{mq}$ , and  $C_{nr}$  the damping moment coefficients. Which are also obtained by table lookup based on the Mach number, however the Magnus moment coefficient is also a function of  $\alpha'$ , which is the angle of incidence.  $\alpha' = \arccos \frac{u}{V}$ .

$$M = \begin{bmatrix} M_X \\ M_Y \\ M_Z \end{bmatrix} = M_b + M_m + M_d + M_a \quad (2-10)$$

$$M_b = \bar{q}Sd \begin{bmatrix} 0 \\ C_{m\alpha} \frac{w}{V} \\ -C_{m\alpha} \frac{v}{V} \end{bmatrix} \quad (2-11)$$

$$M_m = -\bar{q}Sd \left( \frac{p_a d}{V} \right) \begin{bmatrix} 0 \\ C_{np\alpha} \frac{v}{V} \\ C_{np\alpha} \frac{w}{V} \end{bmatrix} \quad (2-12)$$

$$M_d = \bar{q}Sd \left( \frac{d}{V} \right) \begin{bmatrix} C_{lp} p \\ C_{mq} q \\ C_{nr} r \end{bmatrix} \quad (2-13)$$

$$M = \bar{q}Sd \left\{ \begin{bmatrix} 0 \\ C_{m\alpha} \frac{w}{V} \\ -C_{m\alpha} \frac{v}{V} \end{bmatrix} - \left( \frac{p_a d}{V} \right) \begin{bmatrix} 0 \\ C_{np\alpha} \frac{v}{V} \\ C_{np\alpha} \frac{w}{V} \end{bmatrix} + \left( \frac{d}{V} \right) \begin{bmatrix} C_{lp} p \\ C_{mq} q \\ C_{nr} r \end{bmatrix} \right\} + M_a \quad (2-14)$$

### 2-1-3 Non-rolling body frame

The last coordinate system used is the non-rolling body frame (or body fixed plane frame) [6, 30]. This frame will pitch and yaw with the projectile, but not roll, which makes it a convenient frame for spinning projectiles. In the body frame the forces acting on the projectile body rotate with the body which requires significant computational

power since the roll rate is high (order of magnitude 200 Hz). In the non-rolling body frame these forces are decoupled from the rolling of the projectile, but still follow the changes in pitch and yaw. Rewriting the equations from the body frame to the non-rolling body frame does not change the physics, it is a mathematical 'trick' to decrease computational time.

In the non-rolling body frame,  $\phi = 0$ , and  $\dot{\phi} = 0$ , which will lead to  $p = -r \tan \theta$ . The 6 DoF equations of motion, in the non-rolling body frame are

$$\begin{bmatrix} \dot{u} \\ \dot{v} \\ \dot{w} \end{bmatrix} = \frac{1}{m} \begin{bmatrix} F_X \\ F_Y \\ F_Z \end{bmatrix} - \begin{bmatrix} 0 & -r & q \\ r & 0 & r \tan \theta \\ -q & -r \tan \theta & 0 \end{bmatrix} \begin{bmatrix} u \\ v \\ w \end{bmatrix} \quad (2-15)$$

$$\begin{bmatrix} \dot{p} \\ \dot{q} \\ \dot{r} \end{bmatrix} = [I]^{-1} \left( \begin{bmatrix} M_X \\ M_Y \\ M_Z \end{bmatrix} - \begin{bmatrix} 0 & -r & q \\ r & 0 & r \tan \theta \\ -q & -r \tan \theta & 0 \end{bmatrix} [I] \begin{bmatrix} p \\ q \\ r \end{bmatrix} \right) \quad (2-16)$$

$$\begin{bmatrix} \dot{x}_E \\ \dot{y}_E \\ \dot{z}_E \end{bmatrix} = \begin{bmatrix} \cos \theta \cos \psi & -\sin \psi & \sin \theta \cos \psi \\ \cos \theta \sin \psi & \cos \psi & \sin \theta \sin \psi \\ -\sin \theta & 0 & \cos \theta \end{bmatrix} \begin{bmatrix} u \\ v \\ w \end{bmatrix} \quad (2-17)$$

$$\begin{bmatrix} \dot{\phi} \\ \dot{\theta} \\ \dot{\psi} \end{bmatrix} = \begin{bmatrix} 1 & 0 & \tan \theta \\ 0 & 1 & 0 \\ 0 & 0 & \frac{1}{\cos \theta} \end{bmatrix} \begin{bmatrix} p \\ q \\ r \end{bmatrix} \quad (2-18)$$

As  $\phi = 0$  the equation of the gravitational force will change to

$$F_g = mg \begin{bmatrix} -\sin \theta \\ 0 \\ \cos \theta \end{bmatrix} \quad (2-19)$$

The equations of aerodynamic forces and moments are identical to those in the rolling body frame. The variables change however, since they are now calculated in the non-rolling body frame. Therefore the total equation describing the forces changes to

$$F = -\bar{q}S \left\{ \begin{bmatrix} C_{A0} + C_{A2} \left( \frac{v^2 + w^2}{V^2} \right) \\ C_{N\alpha} \frac{v}{V} \\ C_{N\alpha} \frac{w}{V} \end{bmatrix} + \left( \frac{p_{ad}}{V} \right) \begin{bmatrix} 0 \\ C_{yp\alpha} \frac{w}{V} \\ -C_{yp\alpha} \frac{v}{V} \end{bmatrix} \right\} + mg \begin{bmatrix} -\sin \theta \\ 0 \\ \cos \theta \end{bmatrix} + F_a \quad (2-20)$$

while the equation describing the moments remains the same as in the rolling body frame.

$$M = \bar{q} S d \left\{ \begin{bmatrix} 0 \\ C_{m\alpha} \frac{w}{V} \\ -C_{m\alpha} \frac{v}{V} \end{bmatrix} - \left( \frac{p_a d}{V} \right) \begin{bmatrix} 0 \\ C_{np\alpha} \frac{v}{V} \\ C_{np\alpha} \frac{w}{V} \end{bmatrix} + \left( \frac{d}{V} \right) \begin{bmatrix} C_{lp} p \\ C_{mq} q \\ C_{nr} r \end{bmatrix} \right\} + M_a \quad (2-21)$$

#### 2-1-4 Nominal trajectory

The trajectory without actuator forces and moments, and without an initial offset is called the nominal trajectory. The target is known before launch and ideally the initial firing settings will launching the projectile on a trajectory that will end at the target position, this trajectory is the nominal trajectory. In practice however there are errors in the initial settings that will cause the trajectory to deviate, for which the actuator will compensate. Still the nominal trajectory is used for guidance and control as the actual trajectories are close to the nominal trajectory. The nominal trajectory is known before launch, so any calculations involving the nominal trajectory can be done off-line and do not use the limited computational power in flight. In this report the nominal trajectory is used to show the working the actuator model in section 2-2-2 and in the construction and verification of the linear projectile model in sections 2-3-1, and 2-3-2 respectively.

The initial state of this nominal trajectory is

$$\begin{aligned} x_0 &= \left[ u_0 \quad v_0 \quad w_0 \quad p_0 \quad q_0 \quad r_0 \quad x_{E_0} \quad y_{E_0} \quad z_{E_0} \quad \phi_0 \quad \theta_0 \quad \psi_0 \right]^T \\ &= \left[ 655 \text{m/s} \quad 0 \quad 0 \quad 1324/\text{s} \quad 0 \quad 0 \quad 0 \quad 0 \quad 0 \quad 0 \quad 45^\circ \quad 0 \right]^T. \end{aligned}$$

The trajectory is shown in figure 2-2 and has a final position of  $[x_E \ y_E \ z_E] = [21855 \ 665 \ 0]$  m.

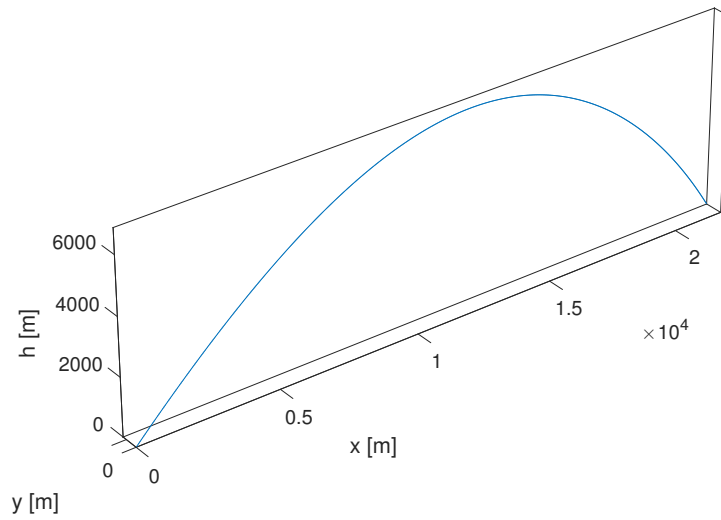


**Figure 2-2:** nominal trajectory

## 2-2 Actuator model

This section is split in two parts. The first part explains how the actuator, the Precision Guidance Kit (PGK), looks and functions. The second part will discuss the modeling of the actuator and ends with the equations that describe  $F_a$  and  $M_a$  to complete the equations of motion from the previous section.

### 2-2-1 Actuator description

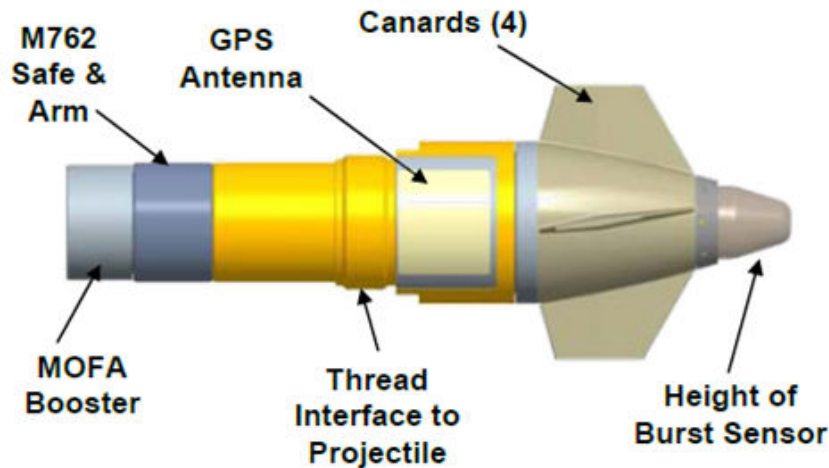
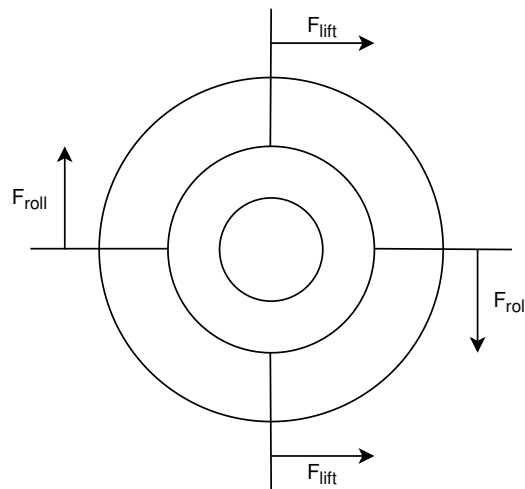


Figure 2-3: ATK XM1156 Precision Guidance Kit

Source: [31]

The ATK XM1156 PGK can be used to retrofit unguided munitions, see figure 2-3. The regular 'dumb' fuze of the projectile can be replaced by the PGK which can deal with the detonation, like the old fuze, and adds guidance possibilities at the same time. It is a roll-decoupled fuze, which means that the fuze can rotate with respect to the projectile body. It is equipped with four canards, two for anti-roll rotation of the nose and two to generate lift for the course correction. Because of the anti-roll canards the fuze will spin in the opposite direction of the projectile's spin when in flight. The ring with the canards can be despun using a roll-brake. When the braking power is fully applied, the ring will act as if fixed to the projectile. Without braking the ring will spin freely in the opposite direction of the projectile's spin. And when the braking power is somewhere in between, the ring can be fixed with respect to the earth. If the PGK ring is set fixed with respect to the earth it can deliver force and moment in a certain direction. It's important to note that the PGK is not a proportional actuator, the direction of the actuator forces and moments can be chosen, but the magnitude cannot. So the controller will have two options, apply the actuator at a certain angle, or letting it spin freely. When the last setting is chosen there will be no resulting actuator forces perpendicular to the projectile's movement, only a drag force.



**Figure 2-4:** schematic front-view of PGK

So the steering canards can be stabilized in the proper roll attitude to generate a lift force in the desired direction. The two roll canards only facilitate the rotation of the ring, so it can be set at certain angle, see figure 2-4 for a schematic front-view of the PGK. This concept is originally proposed by [32] and differs from the other Course Correction Fuzes (CCFs) by its simplicity; there is no deployment of drag brakes, spin brakes or canards and there is no motor or extra battery required since an alternator generates power from the spinning of the fuze with respect to the body. The only sensor the PGK uses is a Global Positioning System (GPS) sensor with roll angle determination by a magnetometer [2]. The PGK promises to deliver significant improvements to projectile accuracy, achieving a Circular Error Probable (CEP) of less than 50 m [33].

### 2-2-2 Nonlinear actuator model

The nonlinear actuator model is a simplification. In reality the PGK is actuated by a brake, counteracting the torque caused by aerodynamics. The brake torque can be regulated, when this is zero the PGK ring can spin freely, when it's maximized the PGK ring is rotating with the body, and somewhere in between the PGK ring can be set fixed with respect to the surroundings. This model is calculating the forces and moments in the fin frame caused by the actuator, given the state of the projectile and the angle of the PGK ring. This is a static model, all dynamics of the actuator are omitted in this simplification.

The aerodynamic coefficients are calculated with Computational Fluid Dynamics (CFD) software, and are defined in the fin frame. The forces and moments in the fin frame, respectively  $F_F$  and  $M_F$  are defined as follows. With  $\bar{q}$  the dynamic pressure,  $S_r$  the reference surface of the fins,  $l_r$  the reference length of the fins,  $C_{\cdot}$  the aerodynamic coefficients,  $\mathcal{M}$  the Mach number, and  $\alpha_{Fin}$  the angle of attack of the Fins.

$$F_F = \bar{q}S_r \begin{bmatrix} CA_{Fin}(\mathcal{M}, \alpha_{Fin}) \\ CY_{Fin}(\mathcal{M}, \alpha_{Fin}) \\ CN_{Fin}(\mathcal{M}, \alpha_{Fin}) \end{bmatrix} \quad (2-22)$$

$$M_F = \bar{q}S_r l_r \begin{bmatrix} CLL_{Fin}(\mathcal{M}, \alpha_{Fin}) \\ CM_{Fin}(\mathcal{M}, \alpha_{Fin}) \\ CLN_{Fin}(\mathcal{M}, \alpha_{Fin}) \end{bmatrix} \quad (2-23)$$

The Mach number,  $\mathcal{M}$ , depends on the velocity and altitude, which are part of the current state,  $x(t)$ , and the angle of attack of the PGK Fins depend on the current state and the angle of the PGK ring,  $\alpha_{PGK}$ . So these equations can be rewritten to:

$$F_F = \bar{q}S_r \begin{bmatrix} CA_{Fin}(x(t), \alpha_{PGK}) \\ CY_{Fin}(x(t), \alpha_{PGK}) \\ CN_{Fin}(x(t), \alpha_{PGK}) \end{bmatrix} \quad (2-24)$$

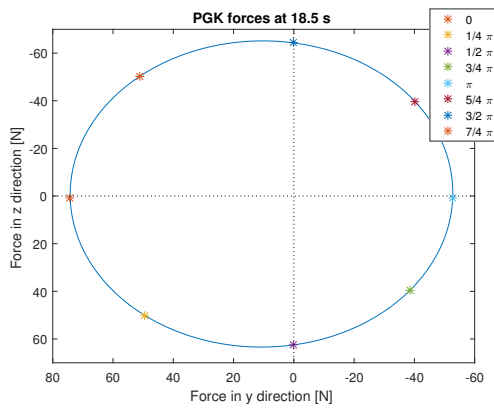
$$M_F = \bar{q}S_r l_r \begin{bmatrix} CLL_{Fin}(x(t), \alpha_{PGK}) \\ CM_{Fin}(x(t), \alpha_{PGK}) \\ CLN_{Fin}(x(t), \alpha_{PGK}) \end{bmatrix} \quad (2-25)$$

Since these Forces and Moments are located in the fin frame, at the nose of the projectile, a translation is necessary for them to be applied to the equations of motion in the non-rolling body frame. The forces remain the same, but the moment caused by these forces needs to be taken into account. The translation across the x-axis from the nose to the CoG of the projectile body is  $-0.43m$

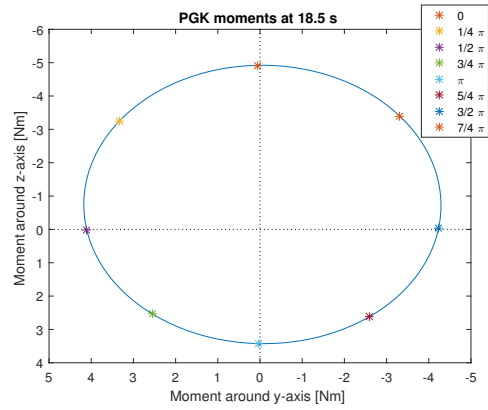
$$F_a = \begin{bmatrix} F_{a_x} \\ F_{a_y} \\ F_{a_z} \end{bmatrix} = \bar{q}S_r \begin{bmatrix} CA_{Fin}(x(t), \alpha_{PGK}) \\ CY_{Fin}(x(t), \alpha_{PGK}) \\ CN_{Fin}(x(t), \alpha_{PGK}) \end{bmatrix} \quad (2-26)$$

$$M_a = \bar{q}S_r l_r \begin{bmatrix} CLL_{Fin}(x(t), \alpha_{PGK}) \\ CM_{Fin}(x(t), \alpha_{PGK}) \\ CLN_{Fin}(x(t), \alpha_{PGK}) \end{bmatrix} + \begin{bmatrix} 0 \\ 0.43F_{a_z} \\ -0.43F_{a_y} \end{bmatrix} \quad (2-27)$$

$F_a$  and  $M_a$  are the actuator forces and moments, and can be substituted into equation (2-20) and (2-21). In figures 2-5, 2-6 and 2-7 the resulting forces and moments in y and z direction are shown. These are snapshots of the actuator model at a quarter, halfway and at three quarters of the nominal trajectory previously discussed in section 2-1-4. At this point the PGK is rotated with  $\alpha_{PGK}$  increasing from 0 to  $2\pi$ . The magnitude of the actuator forces and moments change along the trajectory, as the velocity of the projectile changes. As can be seen from the figures the shape of the force and moment plots is similar for the different times along the trajectory.

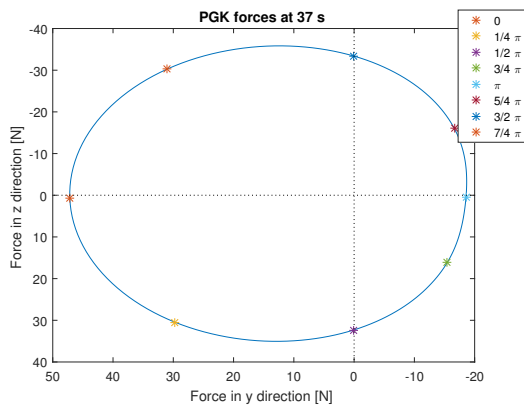


(a) actuator forces  $F_{a_y}$ , and  $F_{a_z}$

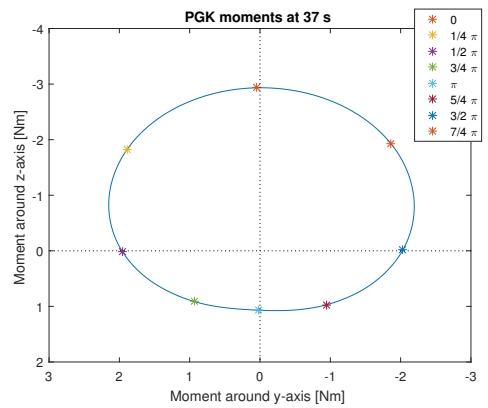


(b) actuator moments  $M_{a_y}$ , and  $M_{a_z}$

Figure 2-5: actuator model at a quarter of the nominal trajectory



(a) actuator forces  $F_{a_y}$ , and  $F_{a_z}$



(b) actuator moments  $M_{a_y}$ , and  $M_{a_z}$

Figure 2-6: actuator model halfway nominal trajectory

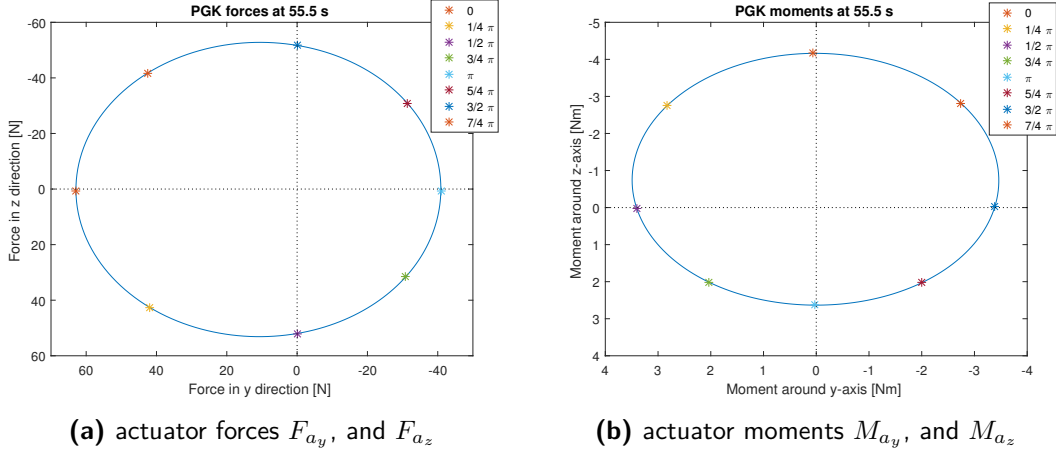


Figure 2-7: actuator model at three quarters of the nominal trajectory

## 2-3 Linearization

In section 2-1 and section 2-2 the nonlinear models of the projectile and actuator are discussed. These models are often linearized to save computational time or to be used in combination with linear controllers. This section describes how the projectile and actuator model are linearized, and also compares them to the nonlinear models for validation.

### 2-3-1 Linear projectile model

Some simplifications to the non-rolling projectile model are made according to projectile linear theory [13]:

- $V$  and  $p$  are large compared to  $\theta$ ,  $\psi$ ,  $v$ ,  $w$ ,  $q$ , and  $r$ , such that products of small quantities and their derivatives are negligible.
- $V$ ,  $p$  are slowly changing and considered to be constant for small time steps.
- $u$  is large compared to  $v$  and  $w$ :  $u \approx V$ .
- small angles of attack:  $\alpha \approx \frac{w}{V}$ , and  $\beta \approx \frac{v}{V}$ .
- since the shell has cylindrical symmetry:  $I_{yy} = I_{zz}$ .

Since  $V$  and  $p$  are considered to be constant, their derivatives are zero and can be left out of the equations of motion, changing it to a 4 DoF system. The remaining four states are dependent on the values for  $V_0$  and  $p_0$ , so these are updated along the trajectory, which makes it a parameter varying model.

$$\begin{bmatrix} \dot{v} \\ \dot{w} \\ \dot{q} \\ \dot{r} \end{bmatrix} = - \begin{bmatrix} 0 & r \tan \theta & 0 & V \\ r \tan \theta & 0 & -V & 0 \\ 0 & 0 & 0 & I_{yy}^{-1} I_{xx} * p + r \tan \theta \\ 0 & 0 & -I_{zz}^{-1} I_{xx} * p & -q \tan \theta \end{bmatrix} \begin{bmatrix} v \\ w \\ q \\ r \end{bmatrix} + \begin{bmatrix} \frac{1}{m} F_Y \\ \frac{1}{m} F_Z \\ I_{yy}^{-1} M_Y \\ I_{zz}^{-1} M_Z \end{bmatrix} \quad (2-28)$$

Now eliminating the products of small quantities, and applying assumption of constant  $V = V_0$  and  $p = p_0$ , and  $I_{yy} = I_{zz}$

$$\begin{bmatrix} \dot{v} \\ \dot{w} \\ \dot{q} \\ \dot{r} \end{bmatrix} = - \begin{bmatrix} 0 & 0 & 0 & V_0 \\ 0 & 0 & -V_0 & 0 \\ 0 & 0 & 0 & I_{yy}^{-1} I_{xx} * p_0 \\ 0 & 0 & -I_{yy}^{-1} I_{xx} * p_0 & 0 \end{bmatrix} \begin{bmatrix} v \\ w \\ q \\ r \end{bmatrix} + \begin{bmatrix} \frac{1}{m} F_Y \\ \frac{1}{m} F_Z \\ I_{yy}^{-1} M_Y \\ I_{yy}^{-1} M_Z \end{bmatrix} \quad (2-29)$$

Using linearization along the nominal trajectory these 4 DoF equations can be written into a linear equation describing the deviation of the trajectory from the nominal trajectory.

Taking the first term of the Taylor expansion, the Jacobian, from (2-29) results in equation (2-30), for details of this derivation see Appendix A:

$$A = \begin{bmatrix} -A_j & -B_j & 0 & -V_0 \\ B_j & -A_j & V_0 & 0 \\ -C_j & E_j & F_j & -G_j \\ -E_j & -C_j & G_j & F_j \end{bmatrix} \quad (2-30)$$

where

$$A_j = \frac{1}{mV_0} \bar{q} S C_{Na} \quad (2-31)$$

$$B_j = \frac{1}{mV_0} \bar{q} S \frac{p_0 d}{V_0} C_{ypa} \quad (2-32)$$

$$C_j = I_{yy}^{-1} \frac{\bar{q} S d}{V_0} \frac{p_0 d}{V_0} C_{npa} \quad (2-33)$$

$$E_j = I_{yy}^{-1} \frac{\bar{q} S d}{V_0} C_{ma} \quad (2-34)$$

$$F_j = I_{yy}^{-1} \frac{\bar{q} S d}{V_0} d C_{nr} \quad (2-35)$$

$$G_j = I_{yy}^{-1} I_{xx} p_0 \quad (2-36)$$

As can be seen, the elements in matrix  $A$  still depend on  $V_0$  and  $p_0$ , which are considered to be constant for small time intervals. Therefore matrix  $A$  will be updated along the trajectory, resulting in an LPV system describing the deviation dynamics,

$$\dot{\delta}_x(t) = A(V_0, p_0) \delta_x(t) \text{ where } \delta_x(t) = x(t) - \bar{x}(t) \quad (2-37)$$

where  $\bar{x}$  is the nominal state.

### 2-3-2 Validation of linearized projectile model

To validate the assumptions and simplifications leading to the LPV model (2-37), it is compared to the non-linear model with the same initial offset from the nominal trajectory. Four cases are shown: the first without offset, so the nonlinear trajectory in this case is the nominal trajectory, the second with a  $.5^\circ$  offset in initial pitch angle, the third with a  $.5^\circ$  offset in initial yaw angle, and the fourth with a  $10\text{ m/s}$  offset in initial velocity. Since deviation in these initial values are the main cause of delivery error of projectiles, they will be varied in the later simulations to test the controller. Therefore the linear model should be valid for these forms of deviation. As a measure of accuracy the Root-Mean-Square Error (RMSE) relative to the traveled distance is used. The relative RMSE should be small, in the order of 1%. Finally the influence of the sampling time is analyzed.

**zero offset** There is no initial offset with respect to the nominal trajectory, so the nonlinear trajectory equals the nominal trajectory.

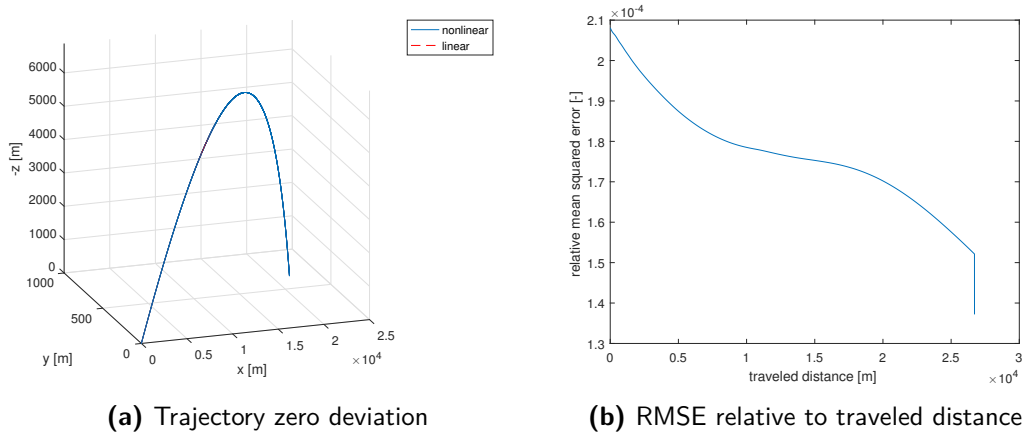


**Figure 2-8:** comparison trajectories zero offset

The two trajectories are shown in figure 2-8a, and are almost equal. The RMSE relative to the traveled distance is in the order of  $1 \times 10^{-4}$ .

**pitch offset** An offset of  $.5^\circ$  is applied to the initial pitch angle of the nominal trajectory. Both the nonlinear and the linear trajectory will therefore deviate from the nominal trajectory.

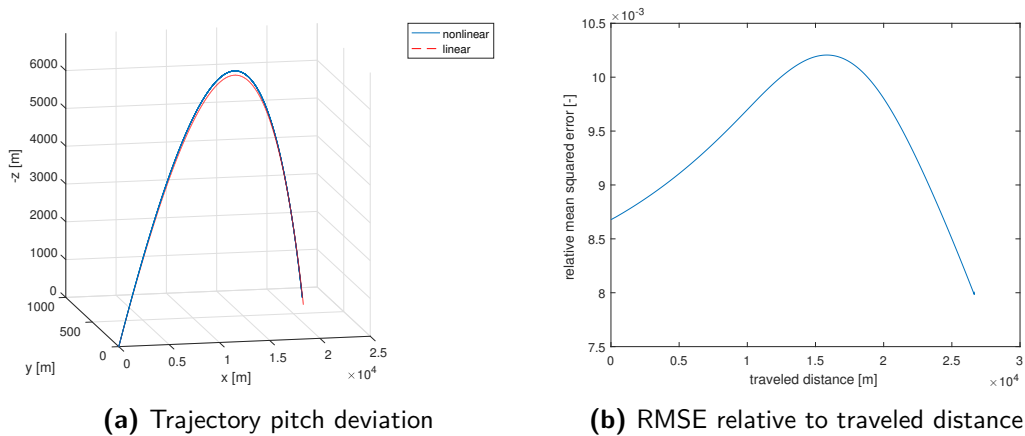


**Figure 2-9:** comparison trajectories pitch offset

The two trajectories are shown in figure 2-9a. The relative RMSE is in the order of  $5 \times 10^{-3}$ , and the maximum of the relative RMSE as can be seen from 2-9b it's maximum is around the apex of the trajectory, where the velocity is minimal.

**yaw offset** Similar to the pitch offset, in this case a yaw offset of  $.5^\circ$  is applied to the nominal trajectory's initial condition.

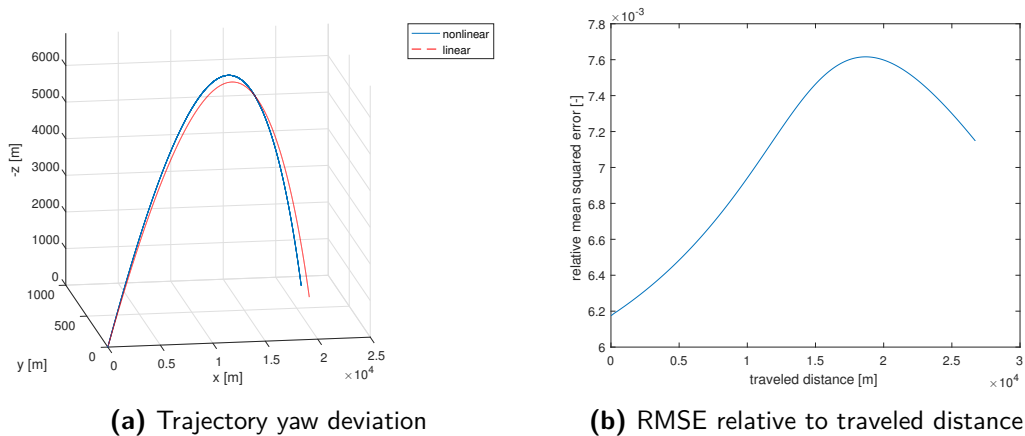


**Figure 2-10:** comparison trajectories yaw offset

The two trajectories are shown in figure 2-10a. The relative RMSE shown in figure 2-10b is in the order of  $4 \times 10^{-3}$ , with the maximum around the apex of the trajectory.

**initial velocity offset** A deviation of  $10m/s$  is applied to the nominal initial conditions.

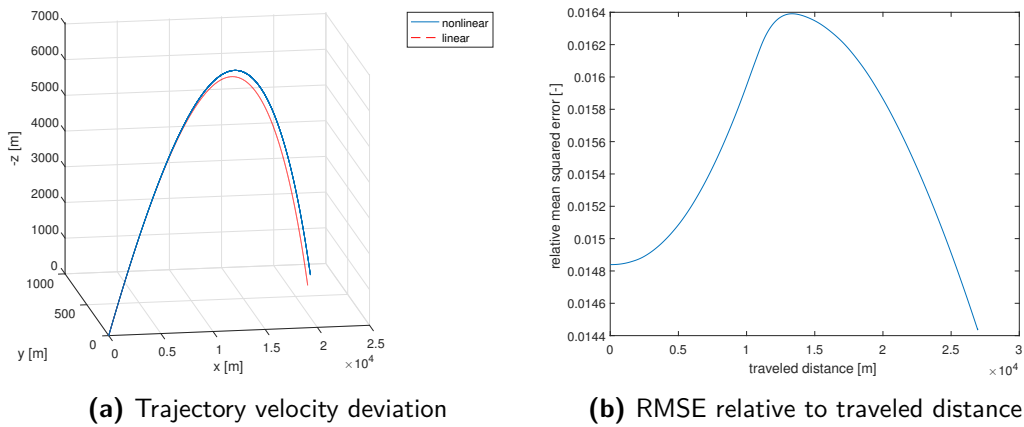
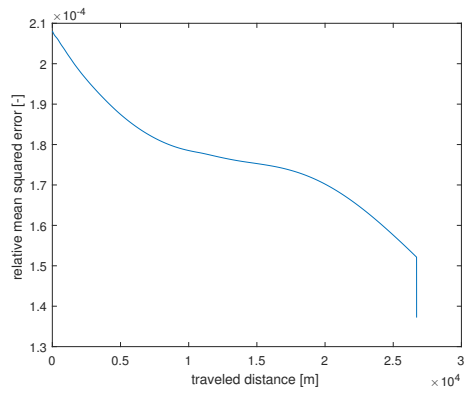


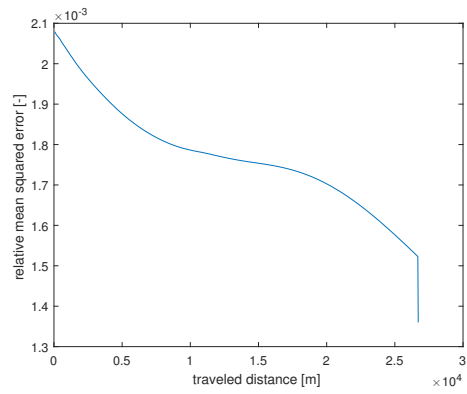
**Figure 2-11:** comparison trajectories velocity offset

The two trajectories are shown in figure 2-11a. The relative RMSE shown in figure 2-11b is in the order of  $9 \times 10^{-3}$ , with the maximum around the beginning of the apex of the trajectory.

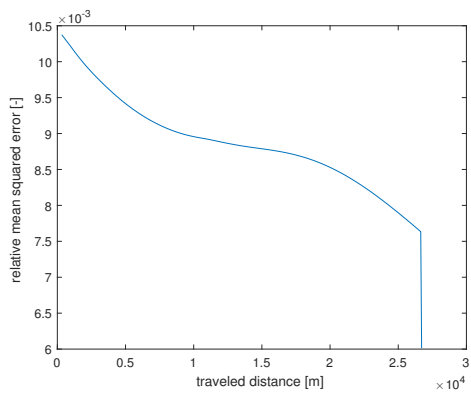
**sampling time** The sampling time is increased from 0.01s to 0.1s and 0.5s, and the zero offset and pitch offset simulation are repeated. Figure 2-12 shows that the RMSE increases with the sampling time for the zero offset simulation. The pitch offset simulation shows almost no change in RMSE between  $T_s = 0.01s$  and  $T_s = 0.1$ , but when the sampling time is increased to  $T_s = 0.5s$  the error also increases, as can be seen in figure 2-13.



(a) sampling time 0.01



(b) sampling time 0.1



(c) sampling time 0.5

Figure 2-12: comparison sampling time for zero offset simulation

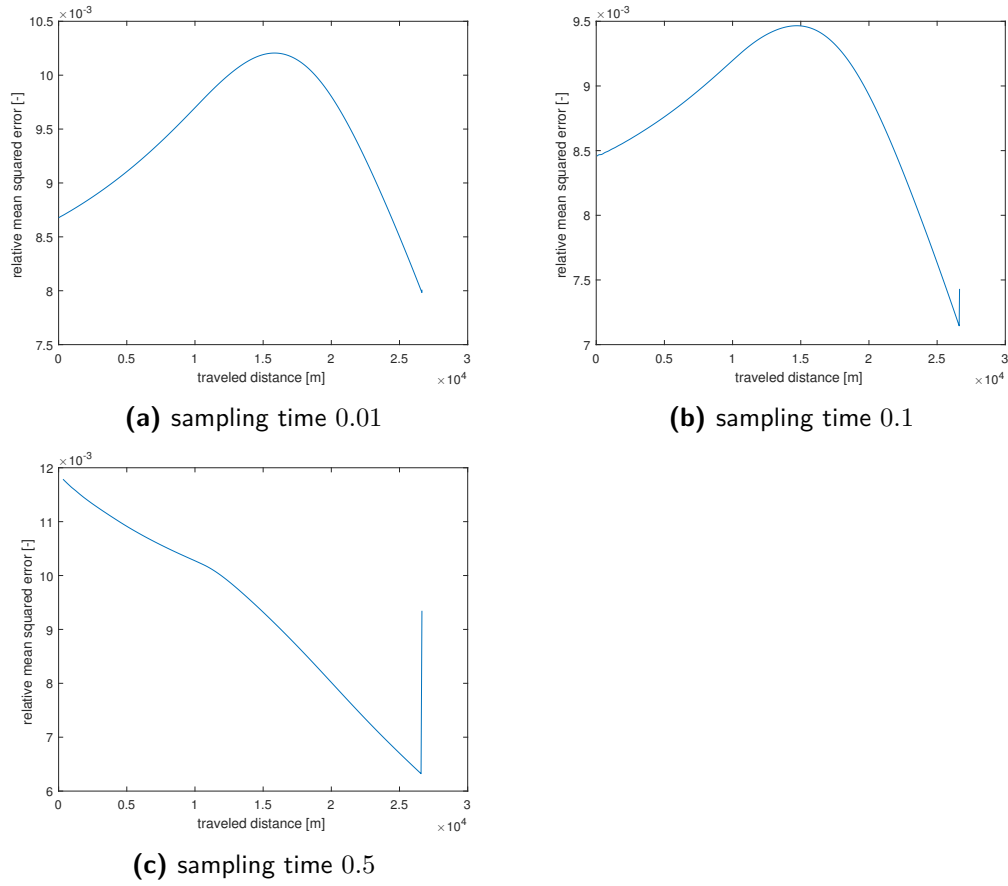


**Figure 2-13:** comparison sampling time for pitch offset simulation

### 2-3-3 Linearized actuator model

The nonlinear actuator model described in equations (2-26) and (2-27) is written in short as

$$\begin{bmatrix} F_a \\ M_a \end{bmatrix} = f_{PGK}(x(t), \alpha_{PGK}) \quad (2-38)$$

A small increase in PGK angle is applied,  $\delta_{\alpha_{PGK}}$ , resulting in a slightly different actuator force and moment,  $F_a^+$ , and  $M_a^+$ . This actuator model is linearized in the same way as the projectile model, however the linearization is done numerically instead of analytically. The actuator model contains a highly nonlinear transformation from fin frame to body frame, therefore numerical linearization is more appropriate.

$$\begin{bmatrix} F_a^+ \\ M_a^+ \end{bmatrix} = f_{PGK}(x(t), \alpha_{PGK} + \delta\alpha_{PGK}) \quad (2-39)$$

so the gradient  $m_{lin}$  is

$$m_{lin} = \frac{\begin{bmatrix} F_a^+ \\ M_a^+ \end{bmatrix} - \begin{bmatrix} F_a \\ M_a \end{bmatrix}}{\delta\alpha_{PGK}} \quad (2-40)$$

The new force and moment vector according to the linear actuator model are:

$$\begin{bmatrix} F_{lin} \\ M_{lin} \end{bmatrix} = m_{lin} * d\alpha_{PGK} + \begin{bmatrix} F_a \\ M_a \end{bmatrix} \quad (2-41)$$

which can be rewritten as

$$\begin{bmatrix} \delta F \\ \delta M \end{bmatrix} = \begin{bmatrix} F_{lin} \\ M_{lin} \end{bmatrix} - \begin{bmatrix} F_a \\ M_a \end{bmatrix} = m_{lin} * d\alpha_{PGK} = B * d\alpha_{PGK}. \quad (2-42)$$

So the linearized actuator model describing the deviation dynamics of the actuator is  $B = m_{lin}$ .

In figure 2-14 to 2-18 and table 2-1 you can see the effect of the size of the update step  $d\alpha_{PGK}$  on the accuracy of the linearization.

$d\alpha = 0.001$  is chosen for the local linearization, a sensitivity analysis on this value is performed at the end of this section in table 2-2.

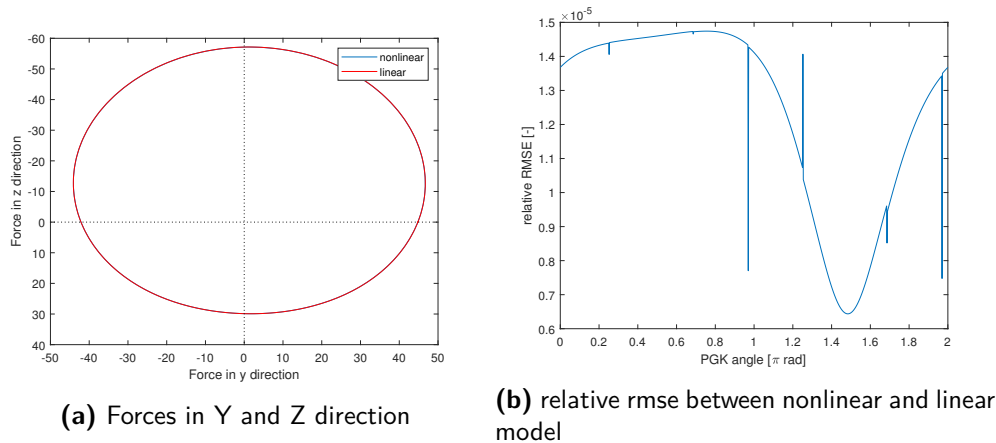


**Figure 2-14:** Linear actuator model, update step  $d\alpha = 0.001 * 2\pi$

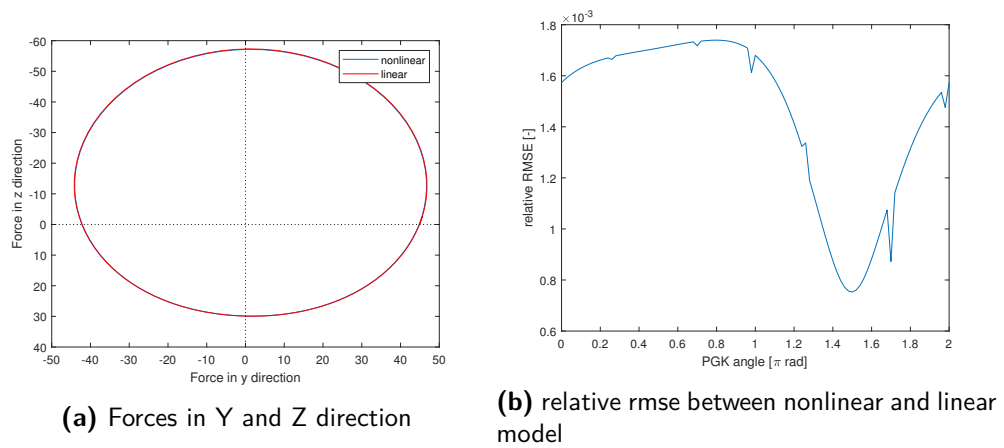


**Figure 2-15:** Linear actuator model, update step  $d\alpha = 0.01 * 2\pi$

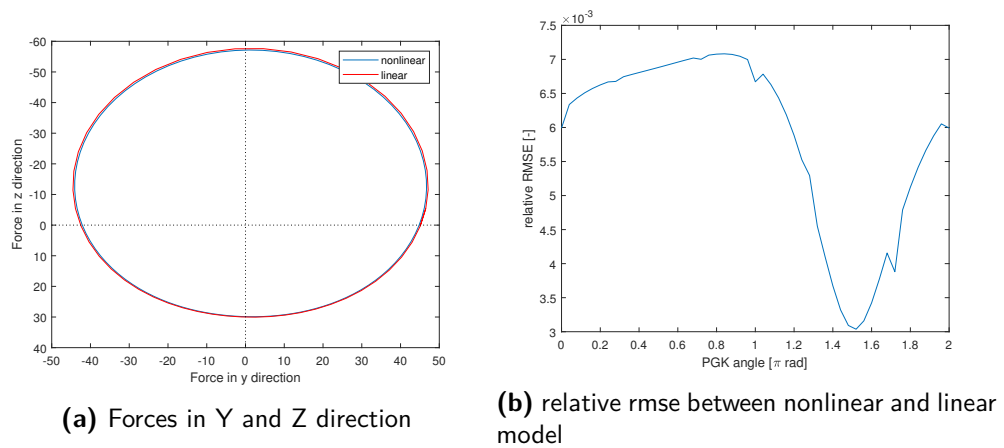


**Figure 2-16:** Linear actuator model, update step  $d\alpha = 0.02 * 2\pi$

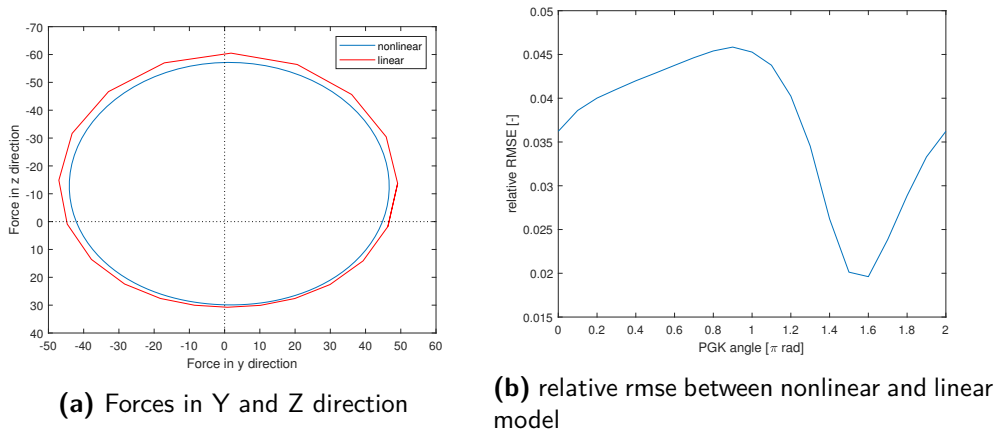


**Figure 2-17:** Linear actuator model, update step  $d\alpha = 0.05 * 2\pi$

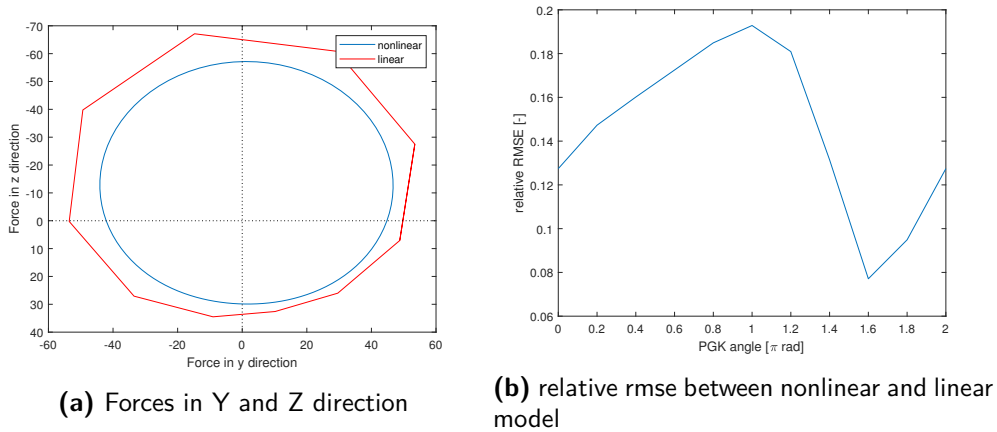


**Figure 2-18:** Linear actuator model, update step  $d\alpha = 0.1 * 2\pi$

$d\alpha_{PGK} [2\pi]$	0.001	0.01	0.02	0.05	0.1
mean error	$1.2419 \times 10^{-5}$	0.0015	0.0059	0.0368	0.1452

**Table 2-1:** influence of  $d\alpha_{PGK}$  on the error, with  $d\alpha = 0.001$

In table 2-2 it can be seen that the mean error is minimal when  $d\alpha = d\alpha_{PGK}$ , this is caused by the definition of the linear model. Then why is  $d\alpha = 0.001$  chosen as linearization value? To avoid the underestimation of the forces and moments caused by the actuator. When  $d\alpha < d\alpha_{PGK}$  the forces from the linear model are larger than those of the nonlinear model, therefore the control effort will be lower.

$d\alpha_{lin} [2\pi]$	0.002	0.004	0.006	0.008	0.01	0.012	0.014	0.016	0.018	0.2
mean error [ $\times 10^{-4}$ ]	11.8	8.85	5.91	2.96	0.00	2.96	5.91	8.86	11.8	14.8

**Table 2-2:** influence of  $d\alpha$  on the error, with  $d\alpha_{PGK} = 0.01 * 2\pi$

## 2-4 Conclusion

The dynamical models are described in this chapter, as are the transformations between the different coordinate systems. The nonlinear 6 DoF non-rolling body frame projectile model serves as a simulation model as well as the base for the linear projectile model. The derivation of the LPV projectile model and the linear actuator model is shown, based on projectile linear theory and Jacobian linearization. The linear models are both validated and are capable of accurately describing the projectile and the actuator with the expected changes in initial velocity, pitch angle, yaw angle and sampling time. Therefore they can be used in (linear) controller design.

---

# Chapter 3

---

## Guidance

In Guidance Navigation and Control (GNC) systems, the guidance provides the desired trajectory, the navigation determines the current state, and the control manipulates the actuator to follow the trajectory determined by the guidance. In this chapter the guidance is explained. The navigation is assumed to be ideal, so at any time the state of the projectile is known. To illustrate how the guidance works, a proportional controller and proportional actuator are used. This will greatly simplify the control problem and results in a simulation in which the possibilities and limitations of the guidance can be shown. The actuator and controller can be seen as ideal, so the resulting error will be caused by the guidance and not by the actuator or controller. Therefore this chapter ends with a perfect benchmark for the controller designed for the PGK in chapter 4.

### 3-1 Jacobian guidance

The guidance is developed by TNO and is modified and applied to the 6DoF non-rolling body frame in this chapter. It is a Jacobian based guidance, which calculates the change in velocity needed to deliver the projectile at the desired end-point. This is done by analyzing changes in the velocity along the nominal trajectory, and their effect on the end-point.

Intuitively this effect will change along the trajectory, velocity added at the beginning of the trajectory will cause a larger deviation of the end-point, than additional velocity a second before impact.

A Jacobian matrix is acquired of the effects of a deviation in velocity  $\Delta V_x$ ,  $\Delta V_y$  and  $\Delta V_z$  on the deviation of the impact point in range and cross-range direction  $\Delta R$  and  $\Delta CR$ . This Jacobian matrix is calculated along the nominal trajectory, is computationally expensive but can be done off line so it does not use the scarce computational power

available in the actuator itself. It is commonly assumed that the projectile trajectory is close enough to the nominal trajectory for this jacobian matrix to be used.

$$\begin{bmatrix} \Delta R \\ \Delta CR \end{bmatrix} = J_{guidance}(t) \begin{bmatrix} \Delta V_x \\ \Delta V_y \\ \Delta V_z \end{bmatrix} \quad (3-1)$$

where

$$J_{guidance}(t) = \begin{bmatrix} \frac{\partial R}{\partial V_x} & \frac{\partial R}{\partial V_y} & \frac{\partial R}{\partial V_z} \\ \frac{\partial CR}{\partial V_x} & \frac{\partial CR}{\partial V_y} & \frac{\partial CR}{\partial V_z} \end{bmatrix} \quad (3-2)$$

The elements of the jacobian matrix are calculated multiple times along the trajectory, and are interpolated between calculation points, see figure 3-1. The green and yellow line are printed in bold to highlight that  $\Delta V_y$  has the largest effect on  $\Delta CR$ , and  $\Delta V_z$  has the largest effect on  $\Delta R$ . An increase in  $\Delta V_z$  has a negative effect on the range, this is because the  $z$ -axis is positive downwards and it makes sense that the projectile will have a decreased range, with an increased velocity pointed towards the surface.

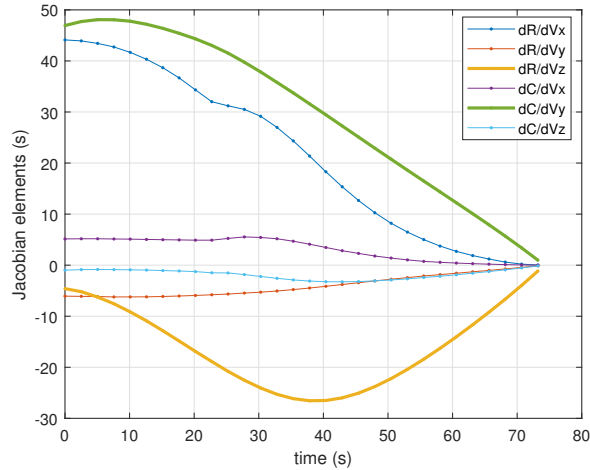


**Figure 3-1:** Jacobian elements along nominal trajectory

With this information, the effect that a change in velocity somewhere along the trajectory has on the location of the impact point is known. The goal of the guidance is to show the change in velocity needed to minimize the error between expected impact point and the desired impact point. So the inverse relationship is needed. At any time along the

trajectory, the impact point can be calculated using the current state. And the range and cross-range deviation  $\Delta R$  and  $\Delta CR$  from the impact point to the desired impact point can be obtained.

$$\begin{bmatrix} \Delta R(t) \\ \Delta CR(t) \end{bmatrix} = J_{guidance}(t)T_{vi} \begin{bmatrix} u_{E_n}(t) - u_E(t) \\ v_{E_n}(t) - v_E(t) \\ w_{E_n}(t) - w_E(t) \end{bmatrix} + I_{guidance} \begin{bmatrix} x_{E_n}(t) - x_E(t) \\ y_{E_n}(t) - y_E(t) \\ z_{E_n}(t) - z_E(t) \end{bmatrix} \quad (3-3)$$

$$T_{vi} = \begin{bmatrix} \cos \theta \cos \psi & -\sin \psi & \sin \theta \cos \psi \\ \cos \theta \sin \psi & \cos \psi & \sin \theta \sin \psi \\ -\sin \theta & 0 & \cos \theta \end{bmatrix}, \text{ and } I_{guidance} = \begin{bmatrix} 1 & 0 & \|u_{E_n}\| \\ 0 & 1 & \|v_{E_n}\| \end{bmatrix} \quad (3-4)$$

Where  $T_{vi}$  is the transformation matrix from the initial frame, or earth frame, to the non-rolling body frame. The second term in equation (3-3) is to compensate for the fact that this extrapolation method calculates the final position at the impact time of the nominal trajectory. This position is not exactly at ground level and this is corrected using the norms of the expected final velocity in x and y direction in matrix  $I_{guidance}$ .

A change in velocity needs to be applied to the projectile to end up with a desired change in impact point of, so the resulting delta between predicted impact point and desired impact point will be zero. The desired changes in velocity  $\Delta V_y^*$ , and  $\Delta V_z^*$  will be used as a reference signal for the controller. Since the PGK does not provide the possibility to change the velocity in x direction, that term is not used as a reference signal. This results in

$$\begin{bmatrix} \Delta V_x^* \\ \Delta V_y^* \end{bmatrix} = \begin{bmatrix} 0 & 1 & 0 \\ 0 & 0 & 1 \end{bmatrix} J_{guidance}^+ \begin{bmatrix} \Delta R(t) \\ \Delta CR(t) \end{bmatrix}, \quad (3-5)$$

where  $J_{guidance}^+$  is the Moore-Penrose inverse, or pseudo-inverse, of  $J_{guidance}$ .

## 3-2 Guidance example

The guidance provides reference signals  $\Delta V_y^*$ , and  $\Delta V_z^*$  as described in the previous section. The guidance is applied to a simplified problem, the nonlinear 6 DoF non-rolling body frame projectile model is used, but the actuator is assumed to be proportional.

The guidance signals are the deviations in normal velocity that would set the projectile onto a new desired trajectory leading to the target. A simple proportional control law is used to demonstrate the guidance. These signals,  $\Delta V_{y,z}^*$ , are multiplied by two proportional control gains,  $K_{1,2}$  and applied directly to the equations of motion in the non-rolling body frame as specific force  $F_{s_{y,z}}$ .

$$\begin{bmatrix} F_{s_y} \\ F_{s_z} \end{bmatrix} = \begin{bmatrix} K_1 \Delta V_y^* \\ K_2 \Delta V_z^* \end{bmatrix} \quad (3-6)$$

$$\begin{bmatrix} \dot{u} \\ \dot{v} \\ \dot{w} \end{bmatrix} = \frac{1}{m} \begin{bmatrix} X \\ Y \\ Z \end{bmatrix} - \begin{bmatrix} 0 & -r & q \\ r & 0 & r \tan \theta \\ -q & -r \tan \theta & 0 \end{bmatrix} \begin{bmatrix} u \\ v \\ w \end{bmatrix} + \begin{bmatrix} 0 \\ F_{s_y} \\ F_{s_z} \end{bmatrix} \quad (3-7)$$

$$\begin{bmatrix} \dot{p} \\ \dot{q} \\ \dot{r} \end{bmatrix} = [I]^{-1} \left( \begin{bmatrix} L \\ M \\ N \end{bmatrix} - \begin{bmatrix} 0 & -r & q \\ r & 0 & r \tan \theta \\ -q & -r \tan \theta & 0 \end{bmatrix} [I] \begin{bmatrix} p \\ q \\ r \end{bmatrix} \right) \quad (3-8)$$

The combination of the guidance and this simple controller is significantly reducing the delivery error. An initial deviation of  $\pm 1^\circ$  in pitch and yaw angle is used to show the effect of the guidance and control in this example. The gains in this example are set at  $K_1 = K_2 = 1$ , without any further tuning the guidance and control are already working satisfactory.

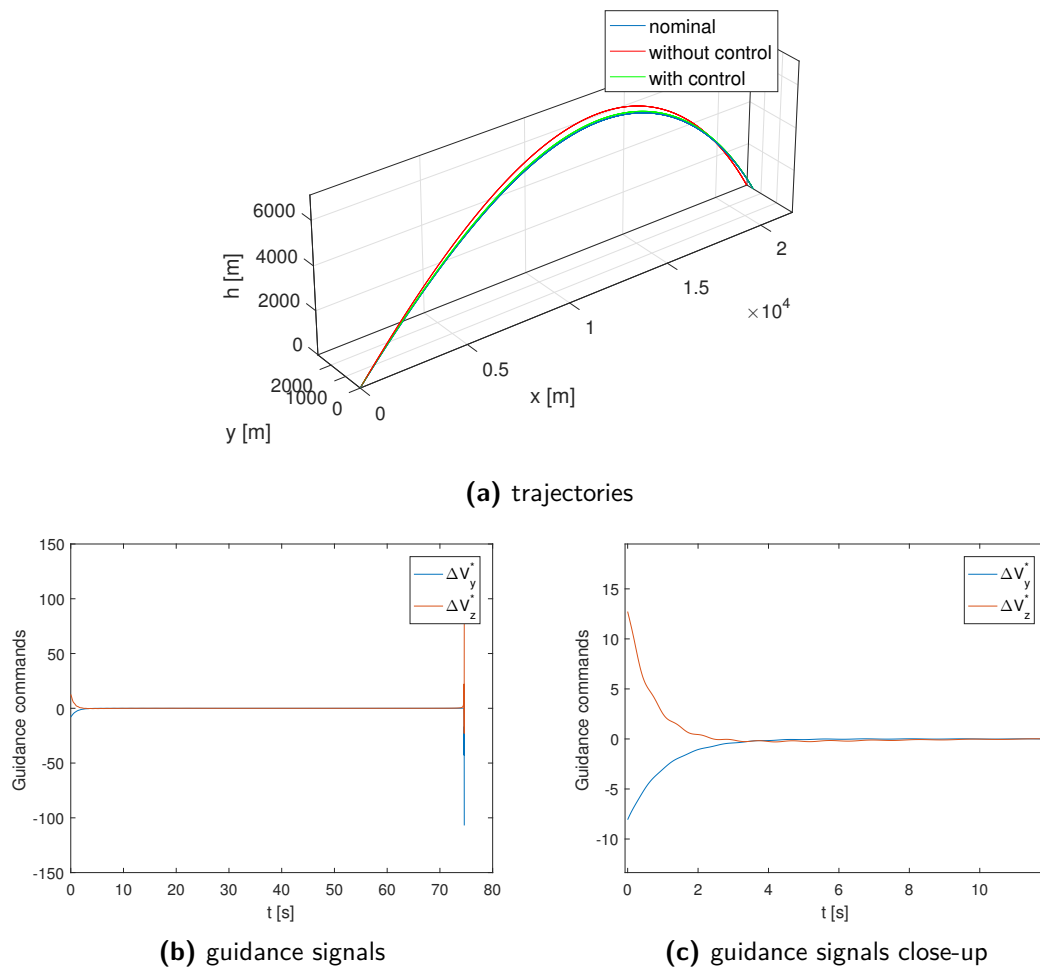


**Figure 3-2:** proportional forces example guidance

As can be seen in figure 3-2c about 4 seconds are needed for the guidance and control to change the trajectory of the projectile so it is on track to hit the target. After 4 seconds the guidance commands (and thus the specific forces since  $K_1 = K_2 = 1$ ) are close to 0. So there are no, or small, changes in velocity needed to reach the desired destination. Just before impact the forces blow up. This can be explained by the remaining error. With this guidance and control there is still a miss-distance of almost 7m. Just before impact there is little time to reach the target without an error. When the time to impact goes to 0, the required delta velocity to reach a delivery error of zero goes to infinity. This can also be seen in figure 3-2b.

The miss distance, or delivery error,  $\varepsilon$ , is defined as

$$\varepsilon = \begin{bmatrix} \varepsilon_x \\ \varepsilon_y \\ \varepsilon_z \end{bmatrix} = \begin{bmatrix} x_E(t_{impact}) \\ y_E(t_{impact}) \\ z_E(t_{impact}) \end{bmatrix} - \begin{bmatrix} T_x \\ T_y \\ T_z \end{bmatrix}, \quad (3-9)$$

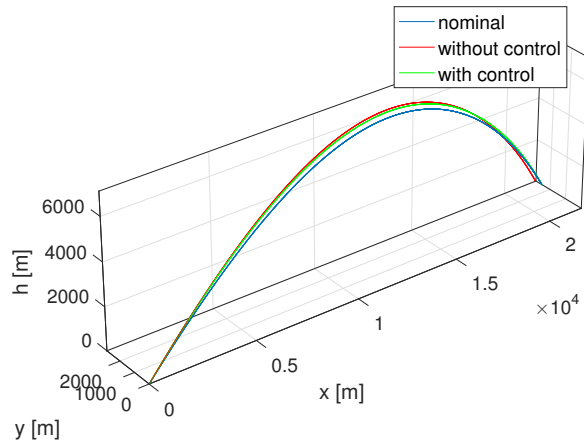
where  $T_{x,y,z}$  are the target coordinates, and  $(x, y, z)_E(t_{impact})$  the simulated coordinates in the earth frame at time of impact. The delivery errors of the uncontrolled and controlled simulations with the different offsets for initial pitch and yaw angle are listed in table 3-1. As can be seen in the table, the guidance in combination with a simple actuator and controller is capable of dealing with offsets of  $1^\circ$  in all directions. These offsets will cause delivery errors of around 400m for the uncontrolled trajectory. This guidance and controller can reduce the error to a couple of meters. Note that the simulation stops right before the projectile hits the ground, in the second row of table 3-1 this is quite large. The projectile is still 6m above ground when the simulation stops, although the delivery error is already greatly reduced, it could be reduced further when the simulation stops at exactly 0 as is the case for the other simulations shown in this table.

This test is repeated for another proportional actuator, controlling only the moments. The controller gains are  $K_1 = K_2 = 0.5$ , resulting in a trajectory and guidance signals as shown in figure 3-3. The resulting miss distances can be found in table 3-1, and are significantly smaller than the uncontrolled miss distances, but slightly larger than those of the actuator using specific forces.

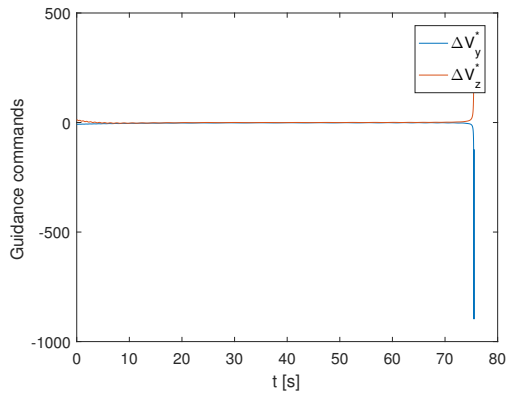
$$\begin{bmatrix} M_{s_y} \\ M_{s_z} \end{bmatrix} = \begin{bmatrix} K_1 \Delta V_y^* \\ K_2 \Delta V_z^* \end{bmatrix} \quad (3-10)$$

$$\begin{bmatrix} \dot{u} \\ \dot{v} \\ \dot{w} \end{bmatrix} = \frac{1}{m} \begin{bmatrix} X \\ Y \\ Z \end{bmatrix} - \begin{bmatrix} 0 & -r & q \\ r & 0 & r \tan \theta \\ -q & -r \tan \theta & 0 \end{bmatrix} \begin{bmatrix} u \\ v \\ w \end{bmatrix} \quad (3-11)$$

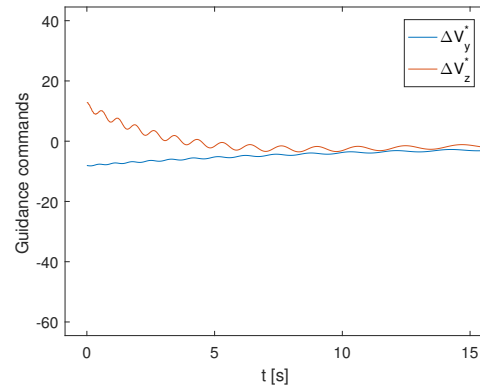
$$\begin{bmatrix} \dot{p} \\ \dot{q} \\ \dot{r} \end{bmatrix} = [I]^{-1} \left( \begin{bmatrix} L \\ M \\ N \end{bmatrix} - \begin{bmatrix} 0 & -r & q \\ r & 0 & r \tan \theta \\ -q & -r \tan \theta & 0 \end{bmatrix} [I] \begin{bmatrix} p \\ q \\ r \end{bmatrix} \right) + \begin{bmatrix} 0 \\ M_{s_z} \\ -M_{s_y} \end{bmatrix} \quad (3-12)$$



(a) trajectories



(b) guidance signals



(c) guidance signals close-up

Figure 3-3: proportional moments example guidance

Table 3-1: proportional example guidance: delivery error for different offsets

offset [°]		uncontrolled [m]			controlled by $F_s$ [m]			controlled by $M_s$ [m]		
$\theta$	$\psi$	$\varepsilon_x$	$\varepsilon_y$	$\varepsilon_z$	$\varepsilon_x$	$\varepsilon_y$	$\varepsilon_z$	$\varepsilon_x$	$\varepsilon_y$	$\varepsilon_z$
0	0	0	0	0	0	0	0	0	0	0
+1	+1	-12.6	401	0	4.2	0.5	6.1	10.1	5.8	0
+1	-1	75.6	-359	0	0.5	0	0	8.6	-2.8	0
-1	+1	-99.9	354	0	-0.7	0	0	-12.9	3.8	0
-1	-1	-13.2	-402	0	-0.6	0	0	-17.6	-5.3	0

### 3-3 Conclusion

In this chapter the principles of the jacobian guidance are explained. The mathematical derivation of the guidance signals are included. These signals will function as a reference to be tracked by a controller. To demonstrate the capabilities of the guidance, two simple proportional actuators are used, one providing only forces, and one only moments. These actuators are combined with a proportional controller. This combination results in a decrease of delivery errors by at least 95% for initial offsets in pitch and yaw angles of  $1^\circ$ .

While the actuator and controller are to be changed for more realistic ones in the next chapter, the guidance is as described in this chapter. So any increase in delivery error can be attributed to the actuator and controller.

---

# Chapter 4

---

## Control

This chapter is divided into two main parts, one for each controller. Firstly the guidance as previously described will be combined with the nonlinear actuator model and an empirical switching mode controller. The specific effect that the actuator setting has on the impact point and the guidance signals is analyzed. Based on that an empirical switching mode controller is designed. The switching points of the controller are analyzed based on their effect on miss distance and actuator signals. This analysis finishes with a tuning for the switching controller that successfully provides course correction with the Precision Guidance Kit (PGK) actuator.

Secondly the Model Predictive Control (MPC) controller is detailed. The structure of the MPC is shown, including the control model, how the prediction matrices are constructed, as well as the performance signal and the cost function. This is explained by solving the control problem of stabilizing a downward facing pendulum. This can function as a stepping stone for a model based controller to provide course correction in combination with the PGK.

### 4-1 Switching controller

A logic-based switching controller is a controller whose subsystems include not only familiar static or dynamical components such as the PGK model in this particular case. These kind of controllers contain event-driven logic and associated switches as well. In systems like this the logical component acts as the mode changer[34].

Switching control can be found everywhere in daily life. For example in the thermostats to heat your house often a simple switching controller is used, when the temperature drops below the lower boundary the heating is switched on, when the temperature rises

to above the top boundary the heating is switched off again [16]. In general switching control combines continuous dynamics with discrete switching events[17]. In the thermostat example the discrete mode changer is based on logics, if  $T > T_{upperboundary}$  control action is zero. When the temperature decreases and reaches the lower boundary  $T < T_{lowerboundary}$ , the controller is switched on again. The system used to control the temperature, when the switching controller turns it on, can be linear or nonlinear, but the switching itself is by definition discrete.

Switching controllers are amongst others used in combination with gain-scheduling controllers, which are one of the most popular control techniques for missile autopilot design [18, 19]. Stabilization and the avoidance of chattering are two typical challenges because of the involved switching [19, 20].

In this section the guidance as previously described will be combined with the nonlinear actuator model and an empirical switching mode controller. The effect that the actuator setting has on the impact point and the guidance signals is analyzed, and a switching mode controller is designed based on that. The switching laws are stepwise constructed subsequently, and tuned based on sensitivity analyses to end up with the switching controller. Stability is not theoretically proven, but is shown in simulation in chapter 5. Chattering, excessive switching between two switching laws, is dealt with by the switching laws.

#### 4-1-1 Impact point analysis

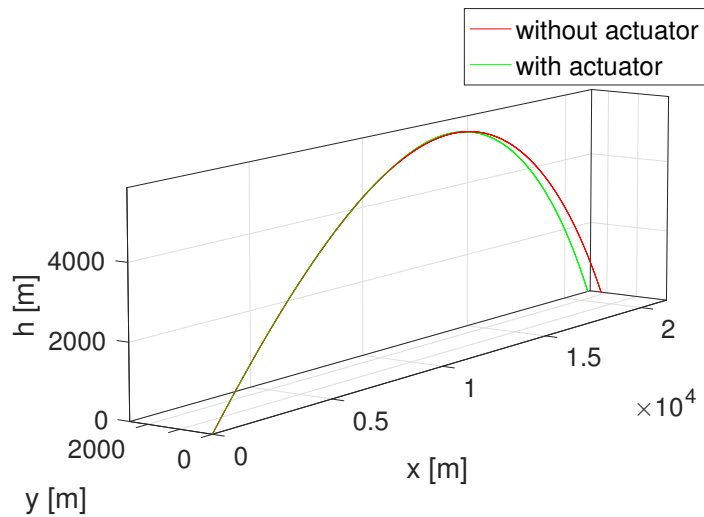
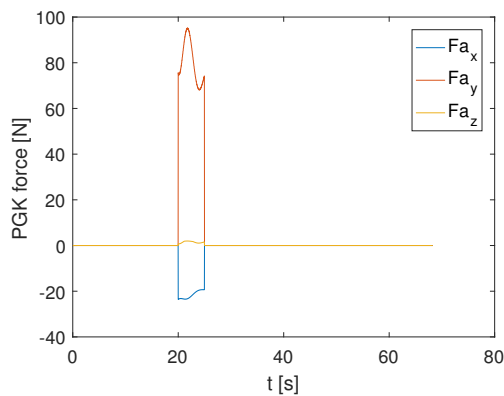
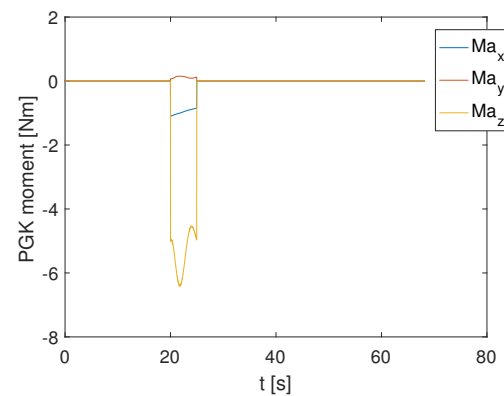
The PGK actuator model is described in section 2-2. The forces and moments caused by the actuator are known at a certain point along the trajectory, for a certain actuator angle setting. But the effect that these forces have on the projectile trajectory and the impact point are not shown yet.

A simple experiment is performed in which the PGK model is applied at a constant angle for 5 seconds. Four simulations are done, at PGK angles  $\alpha_{PGK} = 0, \frac{1}{2}\pi, \pi,$  and  $\frac{3}{2}\pi$ . The time interval for the actuation is between 20s and 25s, at this time interval the vibrations from the launch are dampened and the projectile dynamics are stable. This is repeated for another 4 simulations in which the actuation of the PGK is done between 40s and 45s. This is to find out if actuation before and after apogee affect the trajectory in a different manner.

As an example the trajectory and PGK forces and moments are shown when the PGK actuator model is applied from 20s to 25s at an angle of  $\alpha_{PGK} = 0$ . The end points are shown in table 4-1. The trajectory, forces and moments are shown in figure 4-1.

**Table 4-1:** PGK model test end point coordinates in m

	x	y	z
without actuator	21376	2198	0
with actuator	21245	2567	0
difference	-132	370	0

**(a)** trajectory**(b)** forces**(c)** moments**Figure 4-1:** PGK model test: actuation between 20s and 25s, at  $\alpha_{PGK} = 0\pi$ 

The forces, moments, and impact points of the 8 simulations with varying PGK angles and actuation times are shown in figure 4-2. The drag force caused by the actuator,  $F_{a,x}$ , is also shown. As stated before in section 2-2, this force is almost not influenced by the

PGK settings at all. For example, at  $t = 20s$ , for these four different values of  $\alpha_{PGK}$  the actuator drag force varies between  $F_{a_x} = -23.6N$  to  $F_{a_x} = -21.8N$ , and therefore the analysis focuses on the actuator forces  $F_{a_y}$ , and  $F_{a_z}$ , since they do change a lot with the PGK angle.

When the actuator is applied from 20s to 25s the change in impact point is larger than from 40s to 45s, this has two main causes. The total velocity of the projectile is higher from 20s to 25s, therefore the PGK forces and moments will also be larger. And the remaining flight time is larger at 20s, so a change in velocity has a larger effect on the impact point. Note the exception for  $\alpha_{PGK} = 3/4 \pi$ , which is caused by the difference in pitch angle. For this application of the PGK, where the initial pitch angle is always  $45^\circ$  or less, it is only important that an increase in force in -z direction will increase the range. An increase of force in this direction pre-apogee may cause a decrease in range for larger initial pitch angles, but post-apogee it will cause an increase in range for both scenarios.

It can be seen table 4-2, and in figure 4-2a that changes in x and y direction can be achieved in both negative and positive direction. So a suitable controller should be able to provide the desired course correction.

**Table 4-2:** PGK model test results changes in impact point

actuation time interval	$\alpha_{PGK}$ [rad]	change in impact point [m]		
		dx	dy	dz
20s-25s	0	-132	370	0
40s-45s	0	-52	186	0
20s-25s	$1/2 \pi$	-256	-41	0
40s-45s	$1/2 \pi$	-165	-25	6
20s-25s	$\pi$	-32	-260	0
40s-45s	$\pi$	-3	-104	0
20s-25s	$3/2 \pi$	122	12	0
40s-45s	$3/2 \pi$	140	17	0

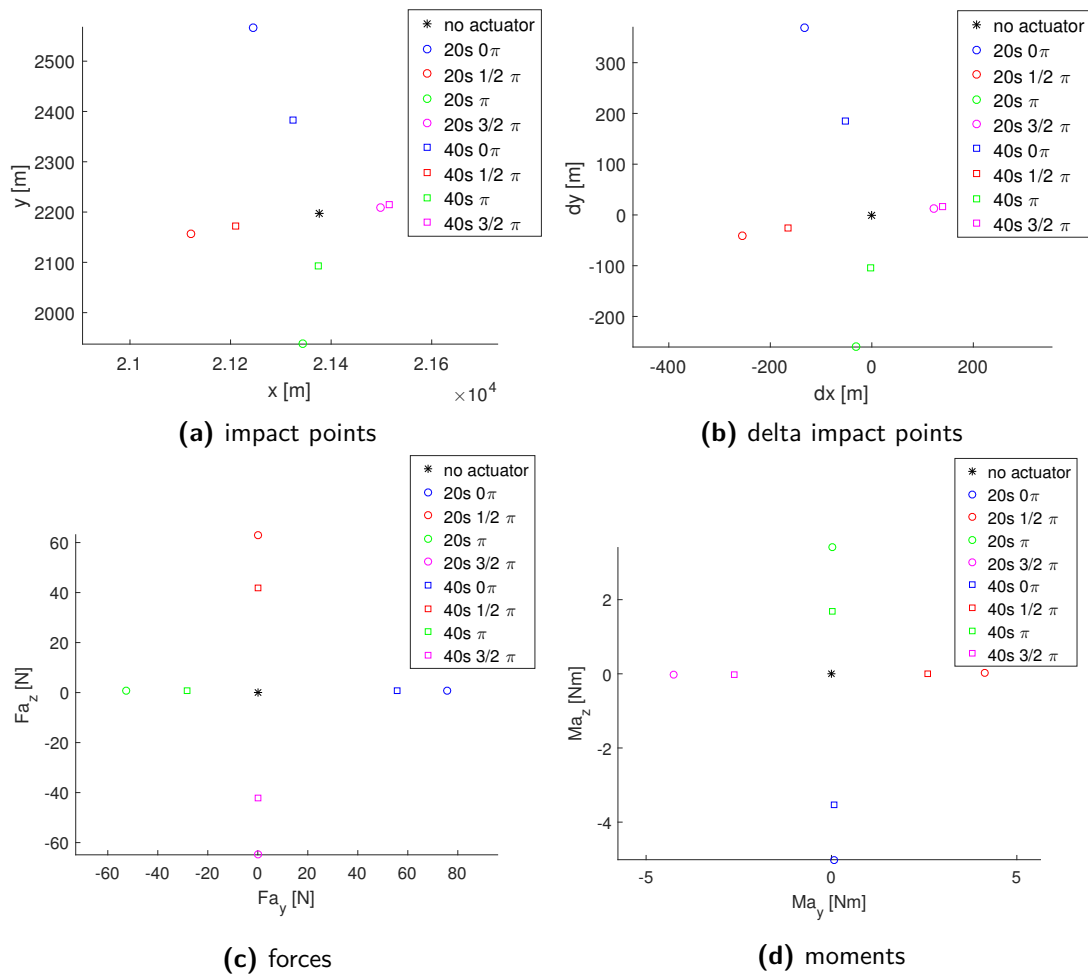
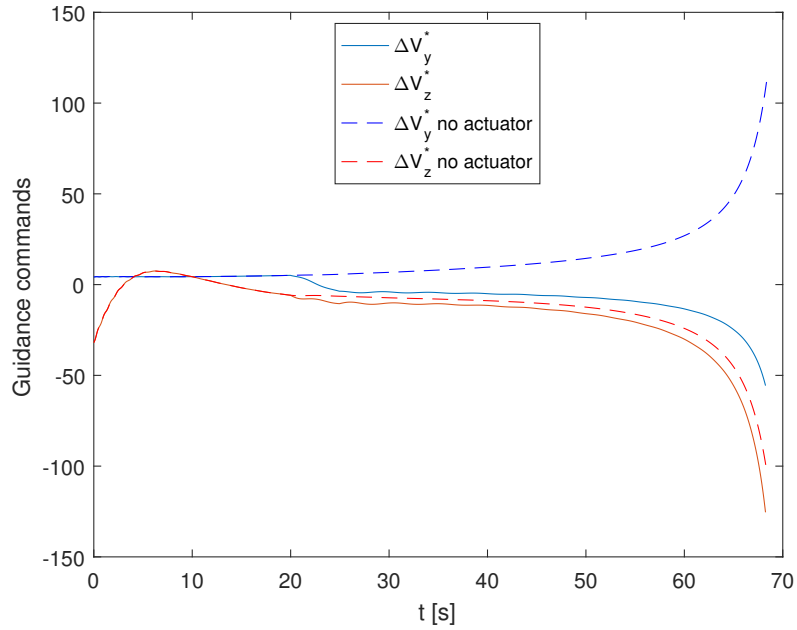


Figure 4-2: PGK model test results

### 4-1-2 Controlling the PGK angle

In the previous section the effect of the actuator on the impact point is shown. To control the PGK angle a second analysis is necessary. The required forces and moments to track the reference signal provided by the guidance need to be found. The same example is used as before, the PGK actuator model is applied from 20s to 25s at an angle of  $0\pi$ .



**Figure 4-3:** effect of actuator on guidance

In figure 4-3 the effect of the actuator on the guidance signals can be seen. The red line,  $\Delta V_z^*$  remains mostly unaffected, but the blue line shows a clear negative change of  $\Delta V_y^*$ . This is repeated for the three other angles, and the results are shown in table 4-3.

**Table 4-3:** effect of actuator setting on guidance signals

$\alpha_{PGK}$ [rad]	$F_{a_y}$ [N]	$F_{a_z}$ [N]	$M_{a_y}$ [Nm]	$M_{a_z}$ [Nm]	$\Delta V_y^*$	$\Delta V_z^*$
0	75.6	0.7	0.1	-5.0	↓	-
$1/2 \pi$	0.1	63.1	4.1	0.0	-	↓
1	-52.5	0.7	0.0	3.4	↑	-
$3/2 \pi$	0.1	-64.9	-4.3	0.0	-	↑

Given the guidance signals  $\Delta V_y^*$  and  $\Delta V_z^*$ , the angle of the PGK,  $\alpha_{PGK}$ , can be determined to apply the required forces and moments to the projectile to provide course correction. This is the part of the control block diagram shown in blue in figure 4-4. The calculation for PGK angle is as shown in figure 4-5.

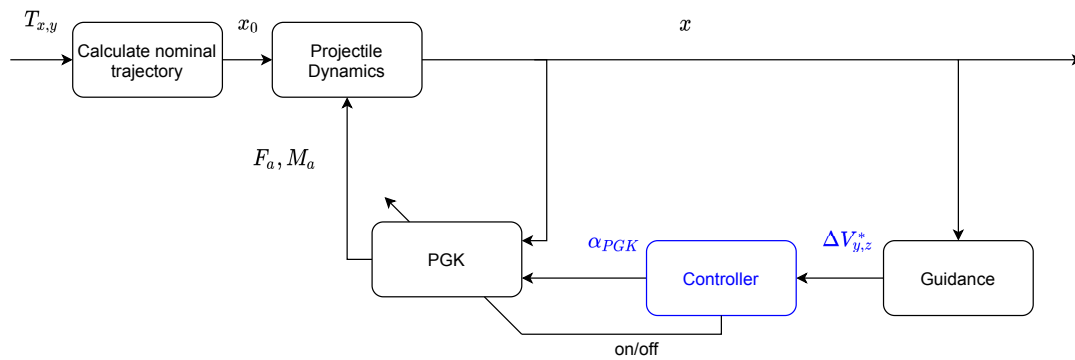


Figure 4-4: Block diagram PGK angle

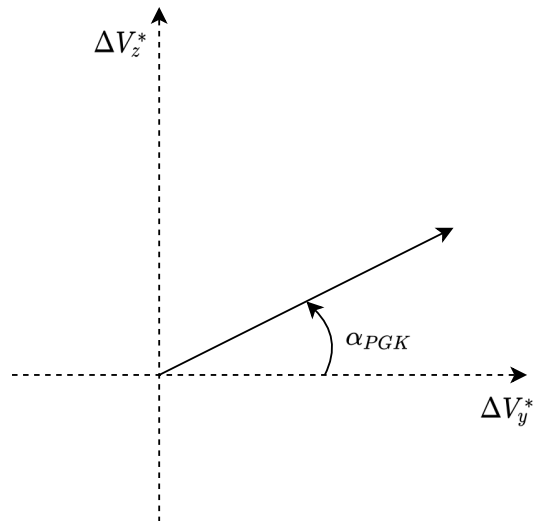


Figure 4-5:  $\alpha_{PGK}$

The function  $\arctan$ , or  $\tan^{-1}$  is limited to values on the interval  $(-1/2\pi, 1/2\pi)$ . To calculate  $\alpha_{PGK}$  the function  $atan2$  is used, which results in the value for the angle in all four quadrants on the interval  $(-\pi, \pi]$ .

$$\alpha_{PGK} = atan2(\Delta V_z^*, \Delta V_y^*) \quad (4-1)$$

where  $atan2$  is defined as

$$atan2(y, x) = \begin{cases} \arctan\left(\frac{y}{x}\right) & \text{if } x > 0, \\ \arctan\left(\frac{y}{x}\right) + \pi & \text{if } x < 0 \text{ and } y \geq 0, \\ \arctan\left(\frac{y}{x}\right) - \pi & \text{if } x < 0 \text{ and } y < 0, \\ 1/2\pi & \text{if } x = 0 \text{ and } y > 0, \\ -1/2\pi & \text{if } x = 0 \text{ and } y < 0, \\ \text{undefined} & \text{if } x = 0 \text{ and } y = 0. \end{cases} \quad (4-2)$$

### 4-1-3 Switching criteria

In this section the controller described in (4-1) is implemented in a switching control law. The switching criteria are explained and tuned based on a sensitivity analysis on the resulting delivery error and actuator signals. The analysis is performed using the nominal trajectory described in section 2-1-4, with an offset of  $+1^\circ$  in initial pitch and yaw angle.

Three switching laws are used and are stepwise added to the controller in this section. The first one determines when to switch on the controller after launch. At the beginning of the trajectory there are multiple vibrations present, which are dampened by the stable design or spin of the projectile. Therefore it is common practice not to start the control from the beginning of the trajectory, but after a certain time  $t_c$ .

To avoid excessive control action the second switching law is added. This law will shut the controller off when the guidance signals are below a certain threshold. When the projectile is on a trajectory ending at the target, the guidance signals are zero. For any other trajectory the guidance will calculate a certain  $\Delta V$  that needs to be applied to the projectile for it to end up at the desired location. However if this trajectory is close enough to the ideal trajectory, or the guidance signals smaller than threshold  $G_c$  the controller will be switched off by this control law. The third law is added to prevent excessive switching, or chattering, when the actuator is turned off at time  $t = t_{off}$  by the second control law, it can only be switched on again after a certain downtime at time  $t = t_{off} + t_d$ . The three parameters  $t_c$ ,  $G_c$ , and  $t_d$  are analyzed, resulting in the final switching mode controller. This will cause a larger hysteresis loop but chattering is avoided.

#### Controller starting time $t_c$

$$\begin{bmatrix} F_a \\ M_a \end{bmatrix} = \begin{cases} 0 & \text{if } t < t_c, \\ f_{PGK}(x(t), \alpha_{PGK}) & \text{for all other situations.} \end{cases} \quad (4-3)$$

Common in controlling ballistic projectiles is to start actuation at apogee, so any vibrations caused by the launch are dampened, and an increase in pitch angle extends the

range, which is not always the case before apogee. Choosing to activate the acPGK before apogee may increase the course correction it can provide. An analysis is performed with different controller starting times  $t_c$ .

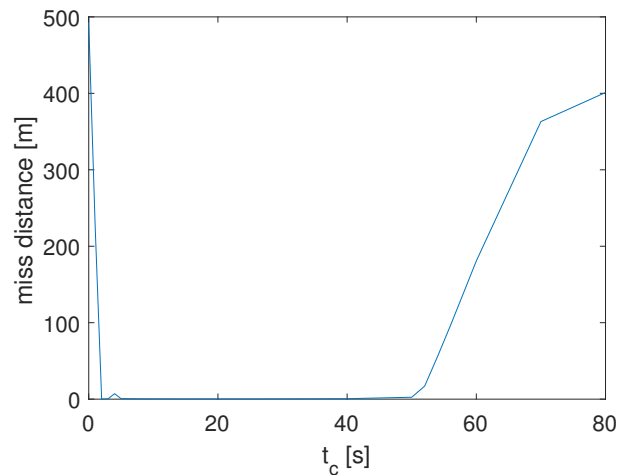


**Figure 4-6:**  $t_c$  sensitivity analysis

A sensitivity analysis of  $t_c$  on the final miss distance is performed, as can be seen in figure 4-6. An initial offset of  $+1^\circ$  in pitch and yaw angle is used for this simulation. As can be seen any starting time between  $2s$  and  $50s$  will result in a zero miss distance. As this uncontrolled trajectory hits the ground after  $75.5s$  any  $t_c > 75.5s$  will result in the uncontrolled trajectory. Applying control from the start results in larger miss distance than the uncontrolled trajectory. The controller starting time of  $t_c = 10$  is chosen, this allows some margin for other trajectories that might need longer to stabilize, but allows control for the most part of the trajectory resulting in larger possible course corrections.

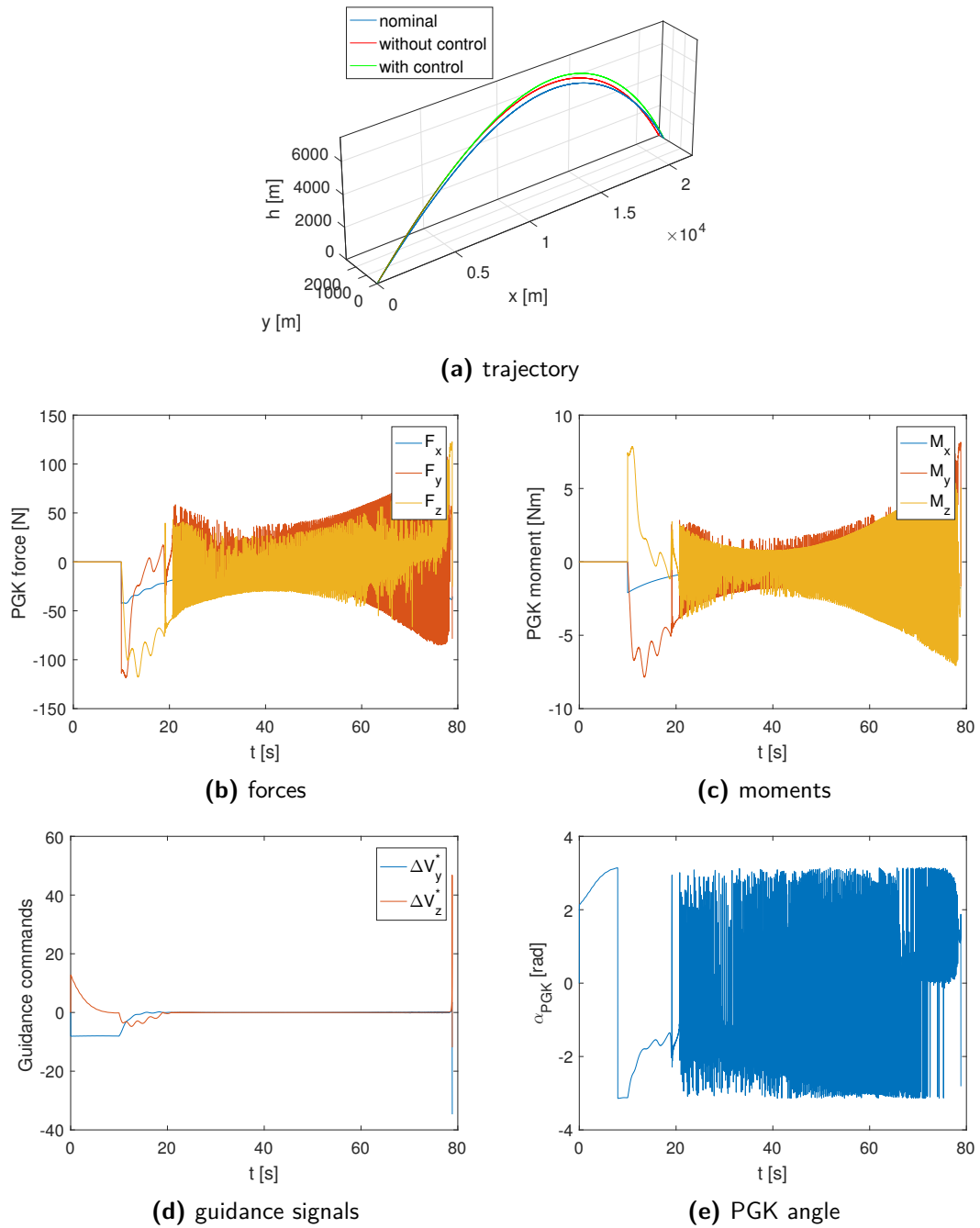


Figure 4-7:  $t_c = 10s$

As can be seen in figure 4-7 adding the first of the switching criteria results in an improvement in miss distance, from  $401m$  without a controller, to  $0.4m$  with this controller. The

figure also shows that for the first 10s the actuator is switched off, the actuator forces and moments are zero. When the PGK is activated it takes roughly from 10s to 20s to set the projectile on a new ideal trajectory. The guidance commands are close to zero after 20s, so no further course correction is required. However the only thing this controller can change is the direction of the actuator forces and moments by changing  $\alpha_{PGK}$ , it does not have the capability yet to switch off the actuator. As shown in figure 4-7, the PGK angle is extremely noisy from 20s until impact, this results in a noisy actuator force and moment. That's why the second switching law is added, the guidance threshold  $G_c$ , which switches the actuator off when the trajectory is within a certain margin of a new ideal trajectory.

### Guidance threshold $G_c$

$$\begin{bmatrix} F_a \\ M_a \end{bmatrix} = \begin{cases} 0 & \text{if } t < t_c, \text{ or } \begin{vmatrix} \Delta V_y^* \\ \Delta V_z^* \end{vmatrix} < G_c, \\ f_{PGK}(x(t), \alpha_{PGK}) & \text{for all other situations.} \end{cases} \quad (4-4)$$

A same sort of analysis is done on the guidance threshold  $G_c$ . When the guidance signals are too small, i.e. the current trajectory is within the boundaries of  $G_c$ , the controller will shut off the actuator. This is described in equation (5-1) by switching condition

$$\begin{vmatrix} \Delta V_y^* \\ \Delta V_z^* \end{vmatrix} < G_c.$$

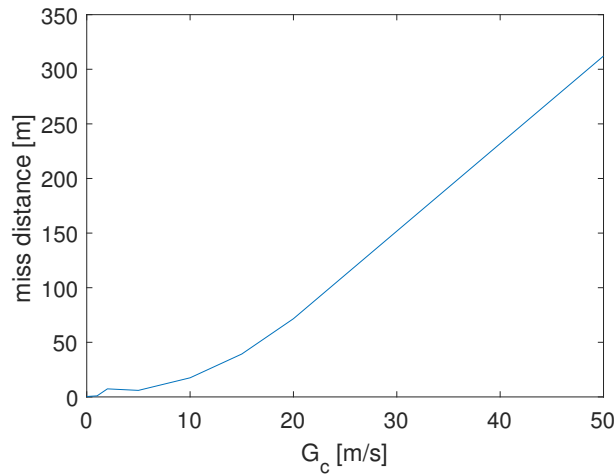
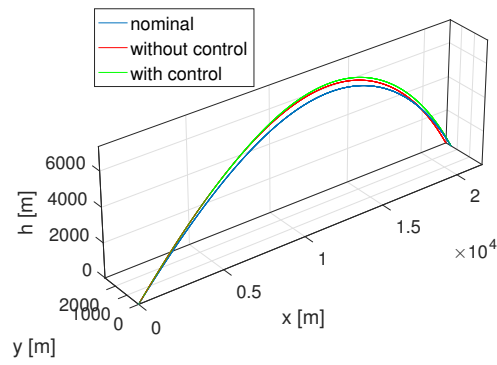


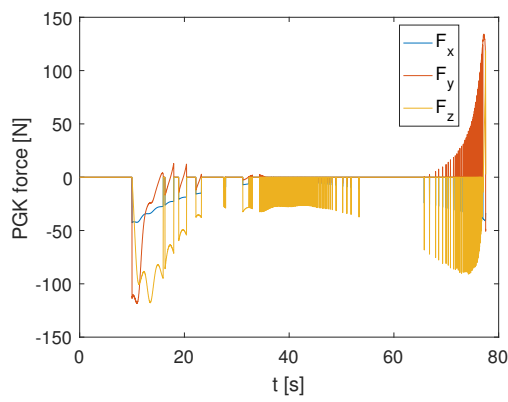
**Figure 4-8:**  $G_c$  sensitivity analysis

As to be expected the addition of the guidance threshold switching criterium does not increase performance when looking at the final miss distance. However it should eliminate the excessive changes in  $\alpha_{PGK}$ . A threshold value  $G_c = 2m/s$  is chosen as a

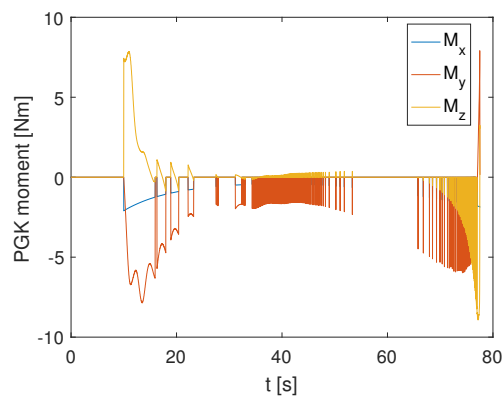
compromise, this eliminates the undesired changes in the PGK angle, without increasing the miss distance too much. Figure 4-9 shows that the PGK ring is not excessively rotated. However figures 4-9b, and 4-9c show that the actuator is switched on and off multiple times per second, which is undesirable and unrealistic. There are no dynamics in the actuator model, but as the PGK ring is freely spinning when switched 'off' the 'on' switching is not instant. Therefore the downtime switching constraint is added as the third and last of the switching criteria.



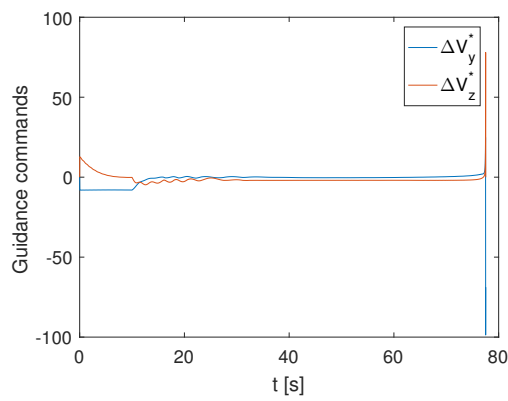
(a) trajectory



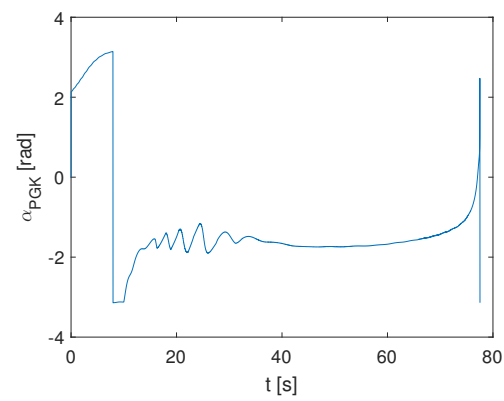
(b) forces



(c) moments



(d) guidance signals



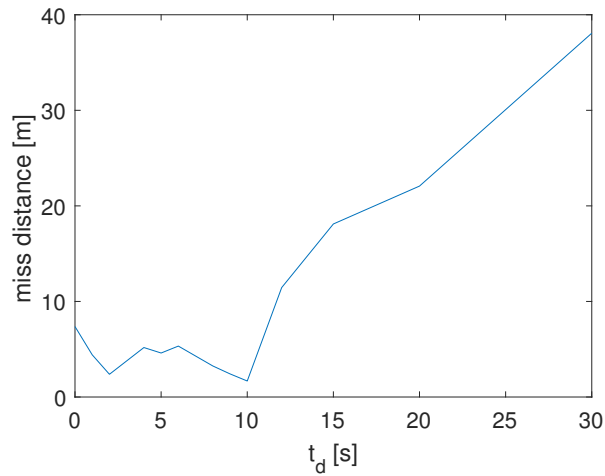
(e) PGK angle

Figure 4-9:  $G_c = 2 \text{ m/s}$

### Actuator downtime $t_d$

To avoid excessive on and off switching of the actuator a downtime  $t_d$  is introduced. When the actuator is switched off, at  $t = t_{off}$ , the actuator cannot be switched on before  $t = t_{off} + t_d$ . Just as the guidance threshold this constraint will not decrease the miss distance, but this will more accurately describe reality. As the delivery error should not increase too much, an analysis is done showing the effect of  $t_d$  on miss distance.

$$\begin{bmatrix} F_a \\ M_a \end{bmatrix} = \begin{cases} 0 & \text{if } t < t_c, \text{ or } \begin{vmatrix} \Delta V_y^* \\ \Delta V_z^* \end{vmatrix} < G_c, \text{ or } t < t_{off} + t_d, \\ f_{PGK}(x(t), \alpha_{PGK}) & \text{for all other situations.} \end{cases} \quad (4-5)$$



**Figure 4-10:**  $t_d$  sensitivity analysis

As can be seen from figure 4-10 any downtime smaller than 10s doesn't significantly change the miss distance. A downtime of  $t_d = 5s$  is chosen to have a safety margin on both sides. This results in the trajectory, forces, moments, guidance signals and PGK angle as displayed in figure 4-11

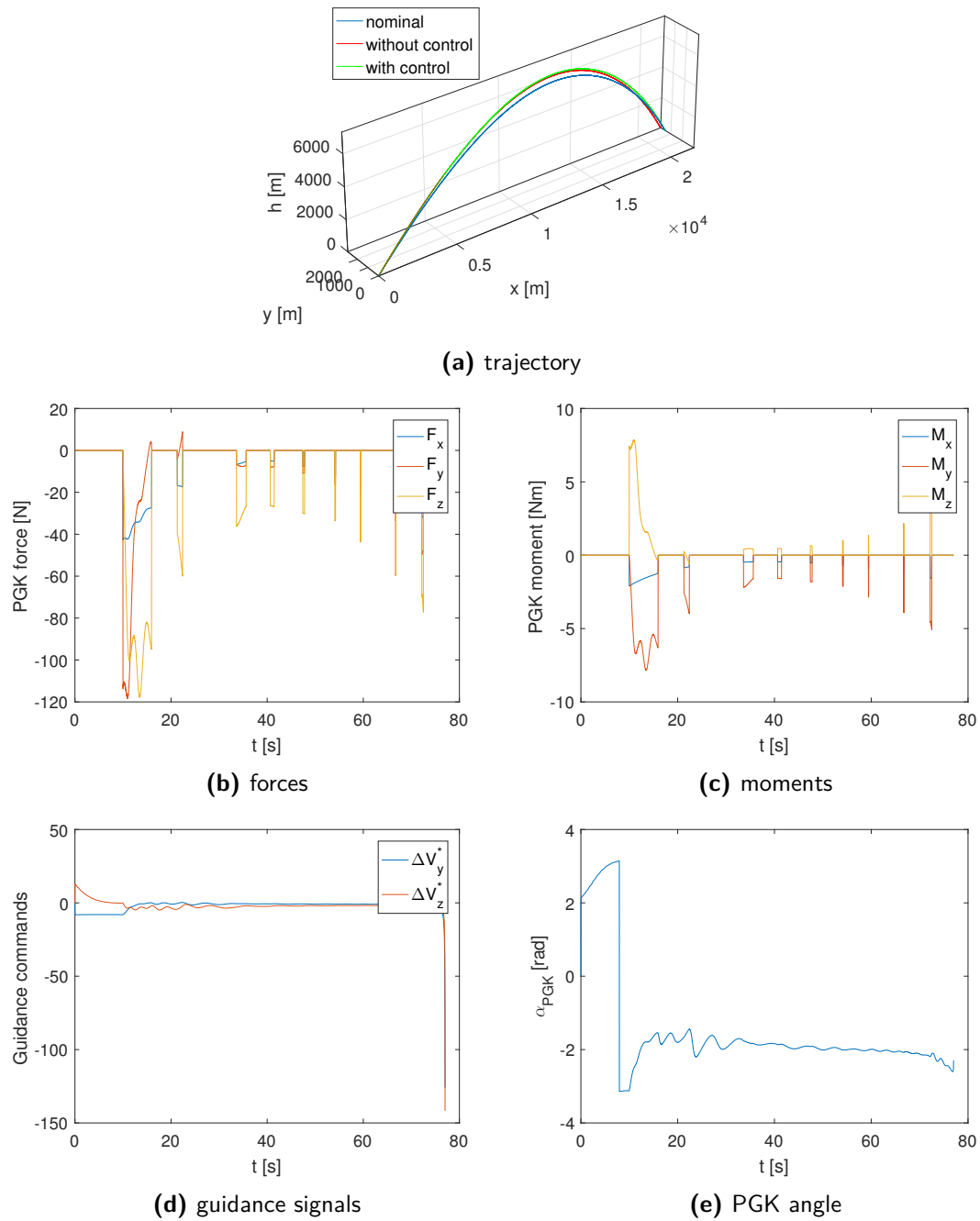


Figure 4-11:  $t_d = 5s$

### Tuning for a depressed trajectory

The switching controller is tuned for a specific trajectory, and these settings will be used in chapter 5, however they might not be optimal for other trajectories. To give insight into the optimality of the settings, a shorter, more depressed trajectory is used. This nominal trajectory has an initial condition

$$\begin{aligned} x_0 &= [u_0 \ v_0 \ w_0 \ p_0 \ q_0 \ r_0 \ x_{E_0} \ y_{E_0} \ z_{E_0} \ \phi_0 \ \theta_0 \ \psi_0]^T \\ &= [330\text{m/s} \ 0 \ 0 \ 800/s \ 0 \ 0 \ 0 \ 0 \ 0 \ 0 \ 25^\circ \ 0]^T, \end{aligned}$$

and a final position of  $[x_E \ y_E \ z_E] = [7352 \ 78 \ 0]$  m. An offset of  $+1^\circ$  in initial pitch and yaw angle is used to perform the controller tuning following the same steps as before.

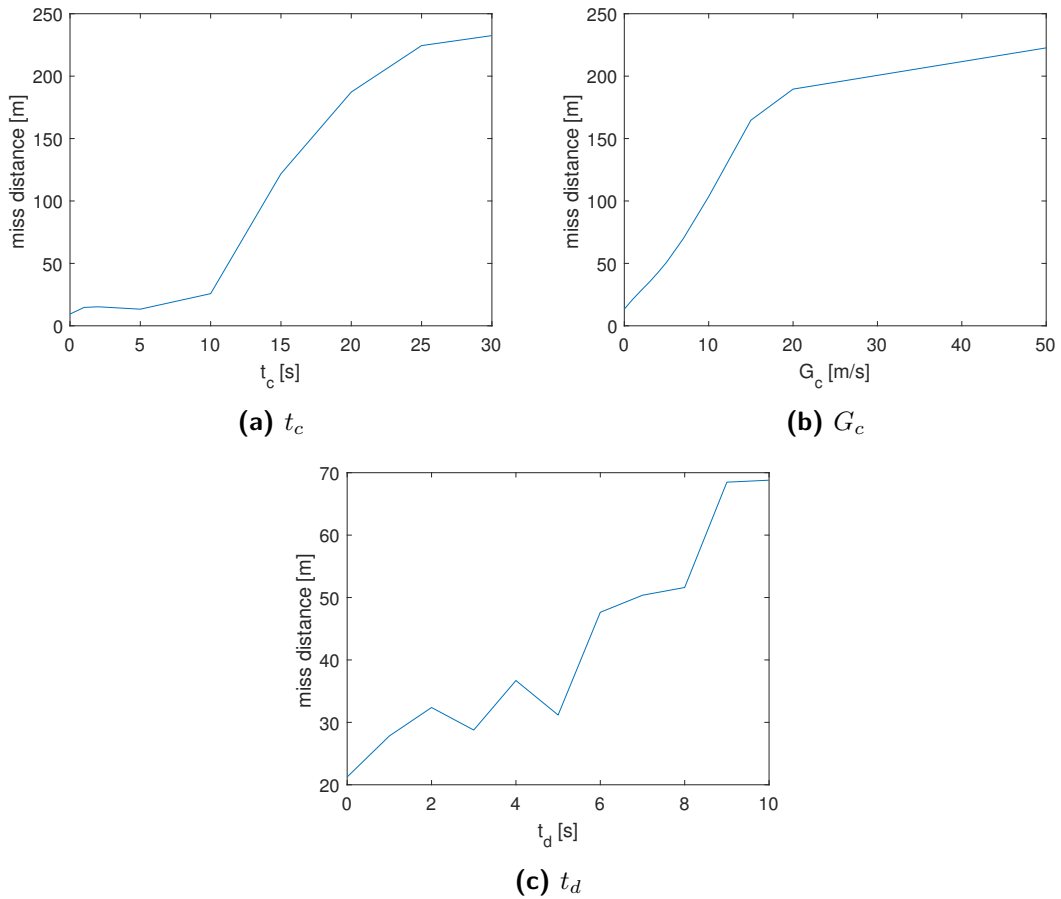


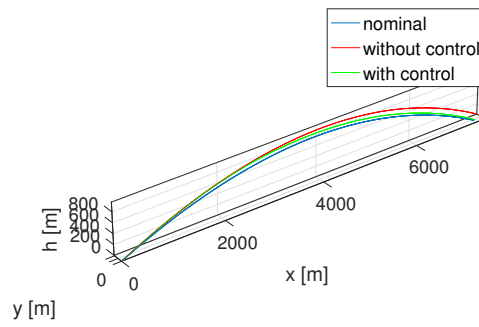
**Figure 4-12:** switching parameters analyses for depressed trajectory

The analyses are based on the plots shown in figure 4-12. The controller starting time,  $t_c$ , should be below 10s and is set to 5s to have some safety margins. The miss distance

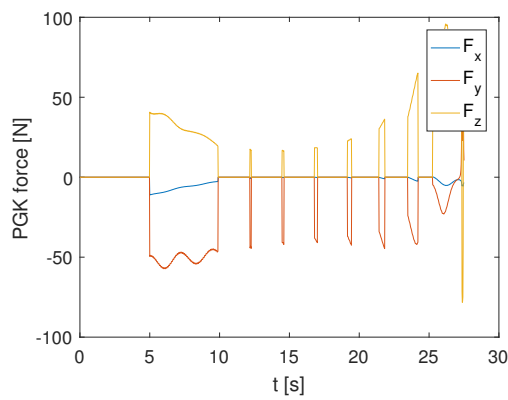
increases twice as fast with the guidance threshold,  $G_c$ , which is therefore set at  $1m/s$ . Increasing the downtime,  $t_d$  also causes the miss distance to increase, so it's set to  $1s$ . These settings result in the following trajectory, forces, moments, guidance signals and PGK angle as displayed in figure 4-13.

If for this trajectory the previous tuning is used, where the controller starting time is  $t_c = 10s$ , the guidance threshold  $G_c = 2m/s$ , and the downtime  $t_d = 5s$ . The trajectory, forces, moments, guidance signals and PGK angle are different as displayed in figure 4-14. From the PGK force and moment plots it can be seen that these settings are less suitable for these kind of trajectories. Which can be explained by the shorter flight time. When the controller starts at  $10s$  more than a third of the depressed trajectory has passed, leaving less time for course correction. Not changing the downtime has the same effect.

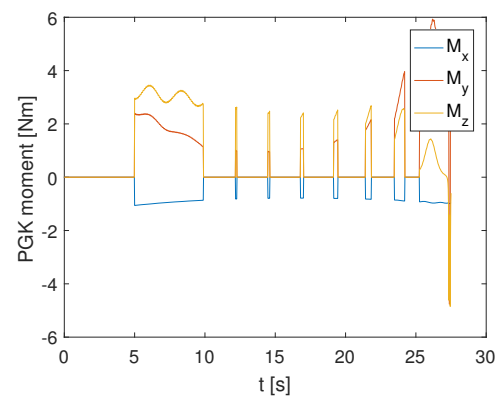
Even though the tuning in the second case is far from optimal, the miss distance is still decreased from  $232m$  to  $65m$ , however the specific tuning results in a miss distance of  $28m$ . Therefore a tuning for every nominal trajectory, or a class of nominal trajectories is advised. To derive such a tuning schedule requires a too large effort to include in this report. The tuning for the first nominal trajectory,  $t_c = 10s$ ,  $G_c = 2m/s$ , and  $t_d = 5s$  is used for simulations in the following chapter.



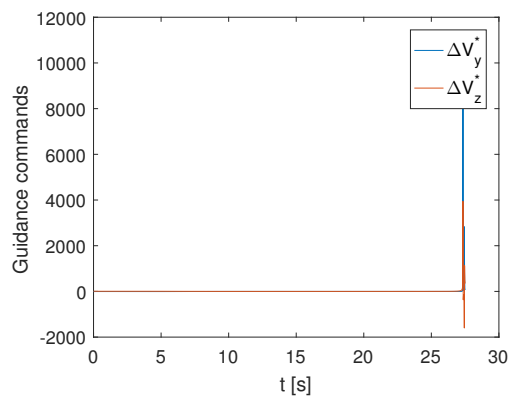
(a) trajectory



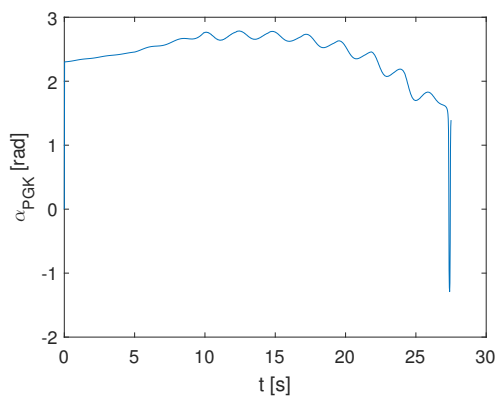
(b) forces



(c) moments

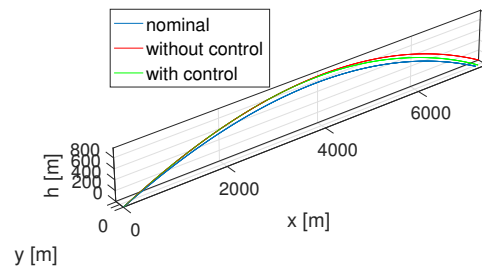


(d) guidance signals

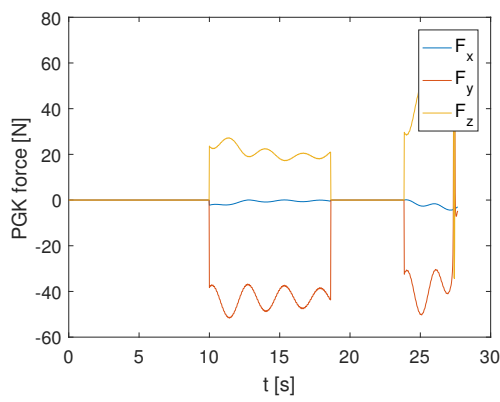


(e) PGK angle

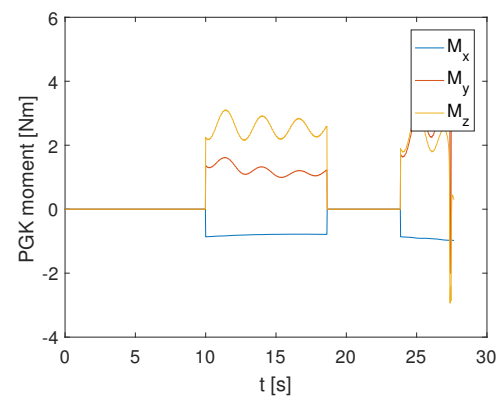
Figure 4-13:  $t_d = 5s$



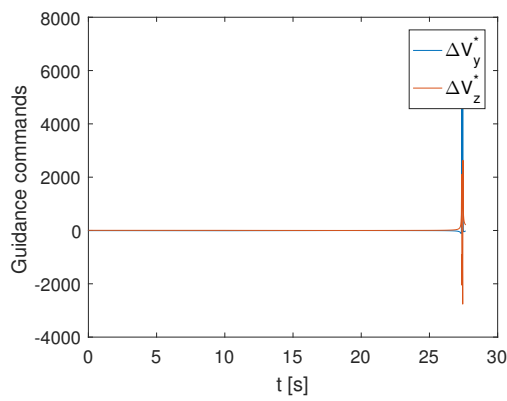
(a) trajectory



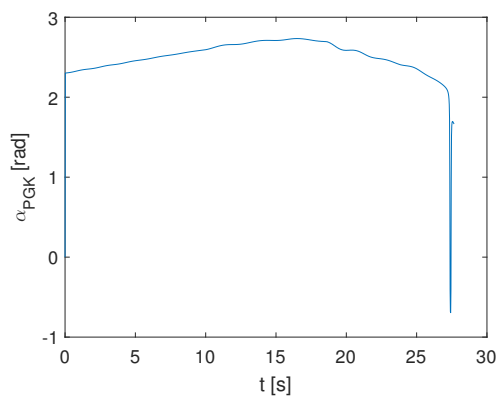
(b) forces



(c) moments



(d) guidance signals



(e) PGK angle

Figure 4-14:  $t_d = 5s$

## 4-2 Model predictive control

Model Predictive Control (MPC) is, as the name says, a control method that uses a model of the system to predict the system states into the future, depending on the control inputs. These control inputs are optimized to obtain desired predicted states. MPC is carried out in the time domain, and uses a discrete state-space model, also called plant, to describe the system, which will generally look like

$$\begin{aligned} x(k+1) &= Ax(k) + Bu(k) \\ y(k) &= Cx(k) + Du(k) \end{aligned}$$

Where  $k$  denotes the discrete time,  $x(k)$  the state vector,  $u(k)$  the control input vector,  $y(k)$  the measured output vector, and  $A$ ,  $B$ ,  $C$ , and  $D$  matrices specifying the static and dynamic behavior of the plant model.

An MPC controller is implemented by solving an optimization program, such as 4-6 [35]. As can be seen one of the benefits of MPC is that constraints can be added. In the case of guided projectiles the constraints will for example guarantee stability, and the cost function will optimize the control actions given these constraints.

$$\left\{ \begin{array}{l} \min_u J(k, N_p, N_m, x(k), \hat{x}_k, u_k) \\ \text{subject to} \\ \hat{x}(k+1) = A\hat{x}(k) + Bu(k) \\ G_1 u_k \leq g_1 \\ G_2 u_k \leq g_2 \\ \text{"stability constraints"} \end{array} \right. \quad (4-6)$$

Where  $J(k, N_p, N_m, x(k), \hat{x}_k, u_k)$  is the cost function,  $\hat{x}_k$  the predicted plant states, and  $u_k$  the control outputs. The subscript  $k$  is the instant at which these sequences are computed. The plant states are predicted a number of steps into the future, until the prediction horizon, and the control inputs are calculated until the control horizon and look like this:

$$\hat{x}_k = (\hat{x}(k+1|k), \hat{x}(k+2|k), \dots, \hat{x}(k+N_p|k)) \quad (4-7)$$

$$u_k = (u(k|k), u(k+1|k), \dots, u(k+N_m-1|k)) \quad (4-8)$$

where  $N_p$  is the prediction horizon and  $N_m$  the control horizon. As shown in figure 4-15, the control horizon or input horizon is the number of future optimal control actions taken into account when calculating the current optimal control, and the prediction horizon or output horizon is the number of predicted outputs taken into account. When  $N_m < N_p$  the input at the control horizon is taken constant for all predicted outputs until the

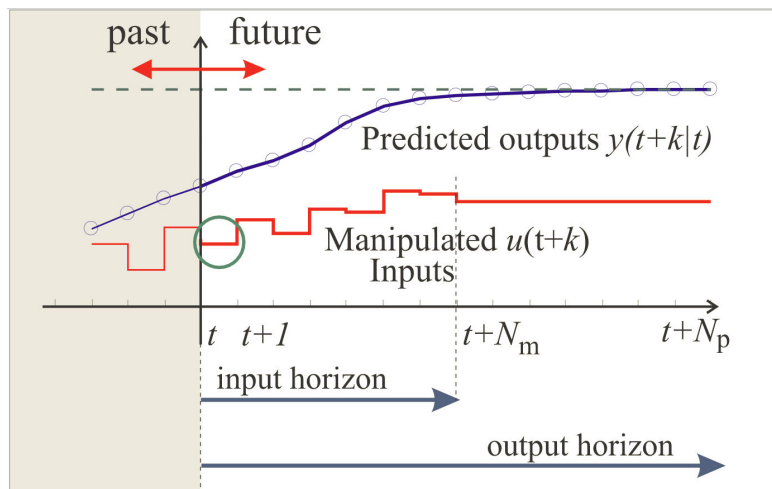


**Figure 4-15:** Model Predictive Control Scheme

Source: [36]

prediction horizon.

Depending on the optimization algorithm used (linear programming, quadratic programming, etc.) the form of the cost function  $J$  may differ.

The following basic MPC algorithm [36] shows how the optimization program 4-6 is used:

- 1) Get the new state  $x(k)$
  - 2) Solve the optimization program 4-6
  - 3) Apply  $u(k)$
  - 4)  $k \leftarrow k + 1$ . Go to 1)
- (4-9)

Even though the control actions until the control horizon are calculated, only the current action  $u(k)$  is applied to the plant. The remaining optimal control inputs are not used as inputs and a new optimal control problem is solved at all future time steps.

To show the MPC structure designed in this section a simple test-case is used. Finally a first step is made to apply this method to provide course correction for the projectile using the PGK.

### 4-2-1 Pendulum

A frictionless pendulum is used as test-case, where  $m$  is the mass of the bob,  $l$  the length of the weightless rod,  $g$  the gravitational constant,  $\theta$  the angle of the pendulum, and  $\tau$ , the torque at the rotating point as control action. The pendulum is controlled

in the downward position, cause this is a stable equilibrium. This resembles the true objective, the projectile control. The projectile is also stable along the trajectory because of the high spin rate. This example is noiseless, and unconstrained which results in an optimization problem that can be solved analytically.

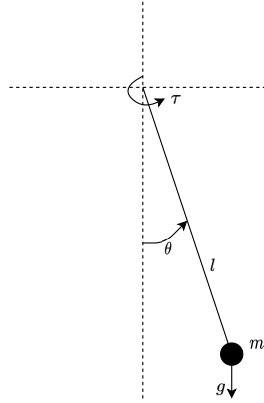


**Figure 4-16:** pendulum schematic

The dynamics of the pendulum model as in figure 4-16 are as follows

$$I\ddot{\theta} + mgl \sin \theta = \tau \quad (4-10)$$

where

$$I = ml^2, \quad x_1 = \theta, \quad x_2 = \dot{\theta}, \quad u = \tau \quad (4-11)$$

this results in nonlinear system description  $f(x, u)$ , which will be used for simulation.

$$\dot{x} = f(x, u) = \begin{bmatrix} \dot{x}_1 \\ \dot{x}_2 \end{bmatrix} = \begin{bmatrix} x_2 \\ \frac{1}{ml^2} (u - mgl \sin x_1) \end{bmatrix} \quad (4-12)$$

A linear model is needed since linear MPC is used for controlling the system. The linear model is obtained by small angle approximation,  $\sin \theta \approx \theta$ , substituting this in equation (4-12) results in

$$\dot{x} = \begin{bmatrix} x_2 \\ \frac{1}{ml^2} (u - mglx_1) \end{bmatrix}. \quad (4-13)$$

In state-space representation, assuming the pendulum angle  $\theta$  can be measured directly, this will be

$$\dot{x} = Ax + Bu \quad (4-14)$$

$$y = Cx + Du, \quad (4-15)$$

with

$$A = \begin{bmatrix} 0 & 1 \\ -\frac{g}{l} & 0 \end{bmatrix}, \quad B = \begin{bmatrix} 0 \\ \frac{1}{ml^2} \end{bmatrix}, \quad C = [1 \quad 0], \quad D = 0.$$

### MPC structure

The MPC structure is based on the TU Delft DCSC lecture notes on MPC [37]. As a control model, and as base for the prediction model, the state space representation of the pendulum dynamics as described in equation (4-14) are used.

The cost function  $J$ , which the MPC will minimize by optimizing the future inputs, is based on the performance signal  $z$ .

$$J(u, k) = \sum_{j=0}^{N-1} z^T(k+j|k)z(k+j|k) \quad (4-16)$$

The predictions of a signal over horizon  $N$  are denoted with a tilde. So with the predictions of the performance signal  $\tilde{z}(k)$ , and the prediction of the control inputs  $\tilde{v}(k)$

$$\tilde{z}(k) = \begin{bmatrix} z(k|k) \\ z(k+1|k) \\ \vdots \\ z(k+N-1|k) \end{bmatrix}, \quad \tilde{v}(k) = \begin{bmatrix} u(k|k) \\ u(k+1|k) \\ \vdots \\ u(k+N-1|k) \end{bmatrix} \quad (4-17)$$

the cost function can be written as

$$J(\tilde{v}, k) = \tilde{z}^T(k)\tilde{z}(k) \quad (4-18)$$

The performance signal  $z(k)$  is constructed to track a reference signal, but also includes a control penalty to avoid excessive control action.

$$z(k) = \begin{bmatrix} Q^{1/2}(r(k) - y(k)) \\ R^{1/2}u(k) \end{bmatrix} = \begin{bmatrix} -Q^{1/2}C \\ 0 \end{bmatrix} x(k) + \begin{bmatrix} Q^{1/2} \\ 0 \end{bmatrix} r(k) + \begin{bmatrix} 0 \\ R^{1/2} \end{bmatrix} u(k) \quad (4-19)$$

where  $Q$  and  $R$  are weights.

$$z(k) = C_2x(k) + D_{22}r(k) + D_{23}u(k) \quad (4-20)$$

where

$$C_2 = \begin{bmatrix} -Q^{1/2}C \\ 0 \end{bmatrix}, \quad D_{22} = \begin{bmatrix} Q^{1/2} \\ 0 \end{bmatrix}, \quad D_{23} = \begin{bmatrix} 0 \\ R^{1/2} \end{bmatrix} \quad (4-21)$$

The signal  $z(k)$  can be split in two parts, one part influenced by the control inputs, and a part that is unaffected by the control input. The second part is called the free-response signal,  $z_0(k)$ [37]. And  $z(k) = z_0(k)$  when the control input is set to zero (for instance after the control horizon):

$$z(k) = z_0(k) + D_{23}u(k) \quad (4-22)$$

$$z_0(k) = C_2x(k) + D_{22}r(k) \quad (4-23)$$

So the predictions  $\tilde{z}(k)$  are

$$\tilde{z}(k) = \tilde{z}_0(k) + \tilde{D}_{23}\tilde{v}(k) \quad (4-24)$$

$$\tilde{z}_0(k) = \tilde{C}_2x(k) + \tilde{D}_{22}\tilde{r}(k) \quad (4-25)$$

with

$$\tilde{C}_2 = \begin{bmatrix} C_2 \\ C_2A \\ C_2A^2 \\ \vdots \\ C_2A^{N-1} \end{bmatrix}, \quad \tilde{D}_{22} = \begin{bmatrix} D_{22} & 0 & \dots & 0 & 0 \\ 0 & D_{22} & \dots & 0 & 0 \\ 0 & 0 & \ddots & \vdots & \vdots \\ \vdots & & \ddots & D_{22} & 0 \\ 0 & & \dots & 0 & D_{22} \end{bmatrix},$$

$$\tilde{D}_{23} = \begin{bmatrix} D_{23} & 0 & \dots & 0 & 0 \\ C_2B & D_{23} & \dots & 0 & 0 \\ C_2AB_3 & C_2B_3 & \ddots & \vdots & \vdots \\ \vdots & & \ddots & D_{23} & 0 \\ C_2A^{N-2}B_3 & \dots & C_2B_3 & D_{23} \end{bmatrix}$$

This makes the cost function to minimize  $J(\tilde{v}, k)$

$$J(\tilde{v}, k) = \tilde{z}^T(k) \tilde{z}(k) \quad (4-26)$$

$$= \left( \tilde{z}_0^T(k) + \tilde{v}^T(k) \tilde{D}_{23}^T \right) \left( \tilde{z}_0(k) + \tilde{D}_{23} \tilde{v}(k) \right) \quad (4-27)$$

$$= \tilde{v}^T(k) \tilde{D}_{23}^T \tilde{D}_{23} \tilde{v}(k) + 2\tilde{v}^T(k) \tilde{D}_{23}^T \tilde{z}_0(k) + \tilde{z}_0^T(k) \tilde{z}_0(k) \quad (4-28)$$

choose

$$H = 2\tilde{D}_{23}^T \tilde{D}_{23}, \quad f(k) = 2\tilde{D}_{23}^T \tilde{z}_0(k), \quad c(k) = \tilde{z}_0^T(k) \tilde{z}_0(k) \quad (4-29)$$

then

$$J(\tilde{v}, k) = \tilde{v}^T(k) H \tilde{v}(k) + 2\tilde{v}^T(k) f(k) + c(k) \quad (4-30)$$

minimizing  $J(\tilde{v}, k)$  can be done by setting the gradient of  $J$  to zero:

$$\frac{\partial J(\tilde{v}, k)}{\partial \tilde{v}} = H \tilde{v}(k) + f(k) = 0 \quad (4-31)$$

for invertible  $H$  the solution is

$$\tilde{v}(k) = -H^{-1} f(k) \quad (4-32)$$

$$= -(\tilde{D}_{23}^T \tilde{D}_{23})^{-1} \tilde{D}_{23}^T \tilde{z}_0(k) \quad (4-33)$$

$$= -(\tilde{D}_{23}^T \tilde{D}_{23})^{-1} \tilde{D}_{23}^T (\tilde{C}_2 x(k) + \tilde{D}_{22} \tilde{r}(k)) \quad (4-34)$$

This vector  $\tilde{v}(k)$  contains all future control inputs the MPC has determined on timestep  $k$ , the first control action  $v(k|k)$  of vector  $\tilde{v}(k)$  is selected and applied to the system. According to the receding horizon principle a new vector  $\tilde{v}$  is calculated at the next timestep  $k+1$  with the horizon also moved one timestep.

$$v(k|k) = \begin{bmatrix} I & 0 & \dots & 0 \end{bmatrix} \tilde{v}(k) = E_v \tilde{v}(k) \quad (4-35)$$

so finally the control signal at time  $k$  is

$$v(k|k) = E_v \tilde{v}(k) \quad (4-36)$$

$$= -E_v (\tilde{D}_{23}^T \tilde{D}_{23})^{-1} \tilde{D}_{23}^T (\tilde{C}_2 x(k) + \tilde{D}_{22} \tilde{r}(k)) \quad (4-37)$$

$$= -F x(k) + D_r \tilde{r}(k) \quad (4-38)$$

where

$$F = E_v (\tilde{D}_{23}^T \tilde{D}_{23})^{-1} \tilde{D}_{23}^T \tilde{C}_2 \quad (4-39)$$

$$D_r = -(\tilde{D}_{23}^T \tilde{D}_{23})^{-1} \tilde{D}_{23}^T \tilde{D}_{22} \quad (4-40)$$

$$E_v = \begin{bmatrix} I & 0 & \dots & 0 \end{bmatrix} \quad (4-41)$$

## Simulations

The nonlinear simulations are started with pendulum the pendulum at an angle of  $\theta = 10^\circ$ , and the angular velocity  $\dot{\theta} = 0^\circ/s$ . The reference is set to the stable position of  $r = 0^\circ$ .

simulation settings		
sampling time	$dt$	0.01 s
initial state	$x_0$	$[10 \ 0]^T$ °, °/s
reference	$r$	$0^\circ$
gravitational acceleration	$g$	9.81 m/s <sup>2</sup>
length	$l$	0.3 m
mass	$m$	0.2 kg

MPC settings		
sampling time	$dt$	0.01 s
prediction horizon	$N$	100
reference tracking weights	$Q$	1
control penalty weight	$R$	0.1

In figure 4-17 the controlled state, control inputs and delta reference are plotted. As can be seen the controller is able to set the pendulum in the desired, stable, position  $\theta = r = 0^\circ$ .

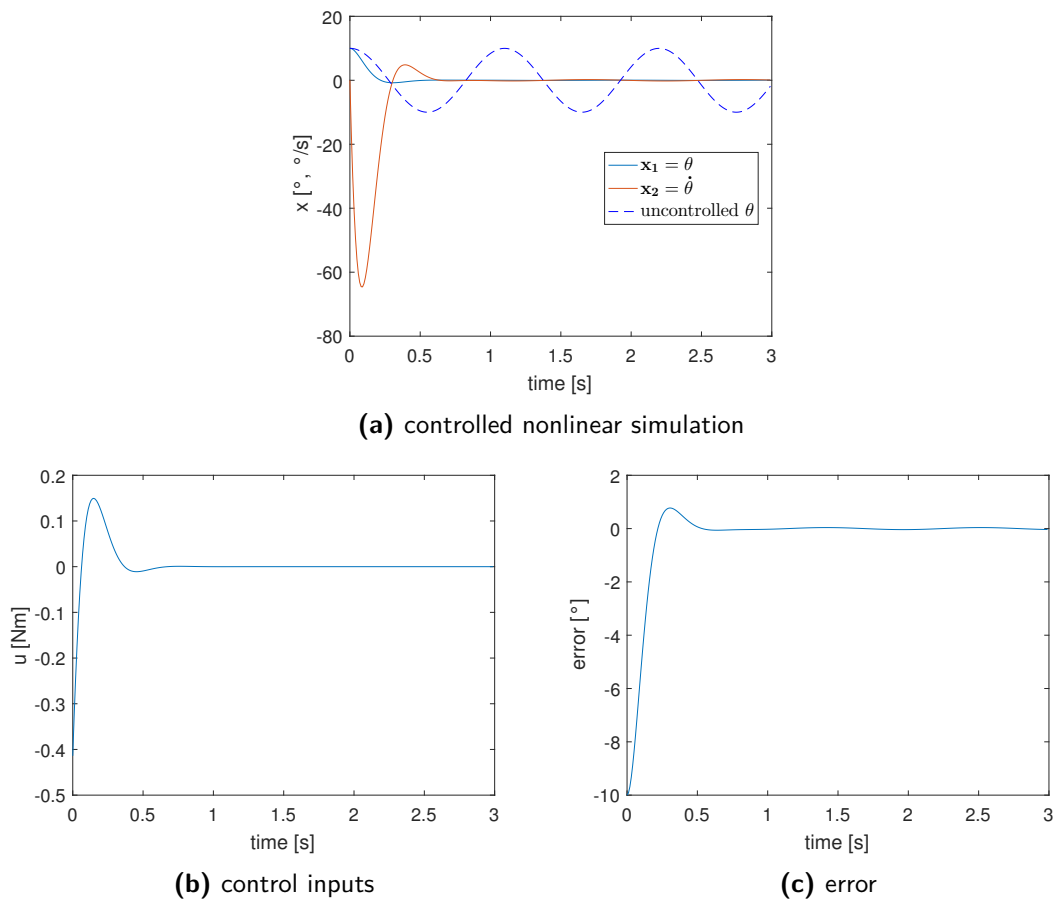


**Figure 4-17:** MPC stabilizing pendulum at  $\theta = 0$  degrees

To show how the receding horizon principle works a look at the predicted control inputs and state over the prediction horizon. Figure 4-18 shows how the predictions from discrete time  $k$  to  $k + N$  change for increasing  $k$ . Only the current control action is applied, before a new optimization is done according to the receding horizon principle. So when all first elements of these predictions are plotted over time this will by definition result in figure 4-17.

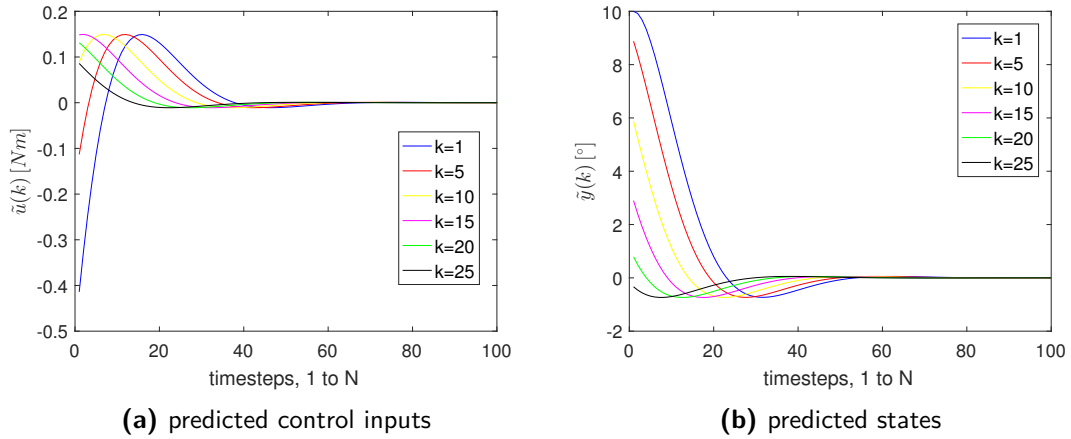
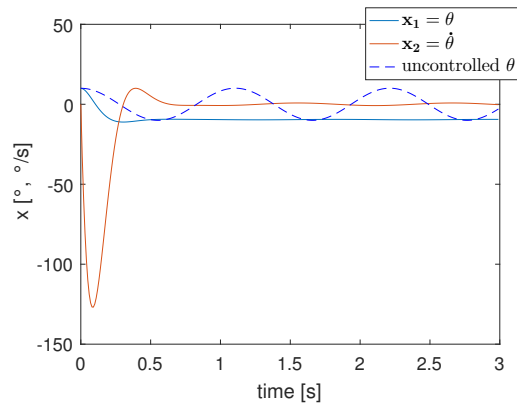
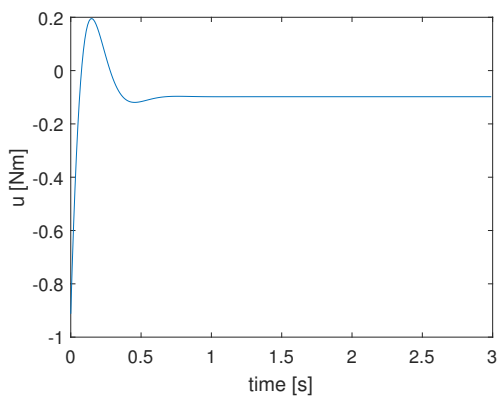


**Figure 4-18:** MPC predictions from discrete times  $k$  to  $k + N$

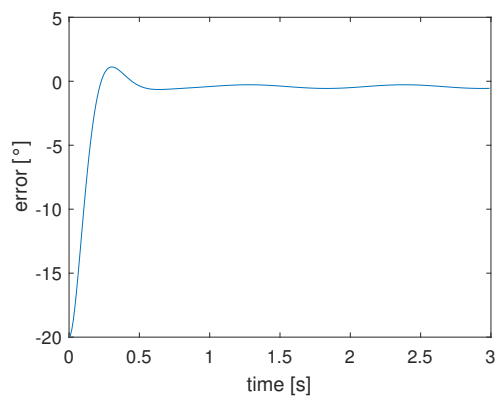
The controller is also able to stabilize the pendulum at another angle, where the system is not stable, for example at  $r = -10^\circ$  as can be seen in figure 4-19. Contrary to the previous example, when the pendulum was stabilized at an equilibrium point, these plots show a steady state error, and a non-zero steady state control input. This steady state error is not caused by a mismatch between the nonlinear simulation model and the linear control model. This can be seen from the predictions  $\tilde{y}$  and  $\tilde{v}$  in figures 4-19e and 4-19d. These figures show the predictions, based on the linear control model, and they also show a steady state error. The steady state error is caused by the mismatch in control objectives, minimizing the control action, and minimizing the error, these cannot both be fulfilled. An optimum is found between the size of the steady state error and the control input based on tuning weights  $Q$  and  $R$ . Increasing  $R$ , the control penalty, the steady state control input will decrease, but this will increase the steady state error.



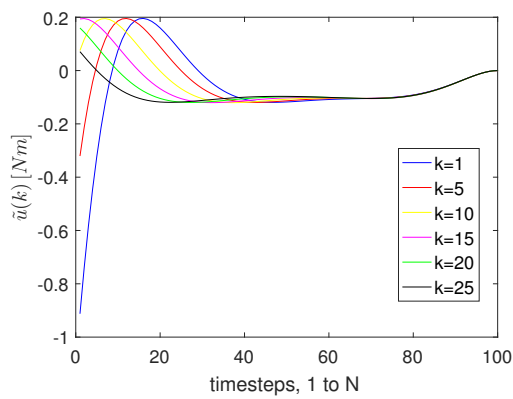
(a) controlled nonlinear simulation



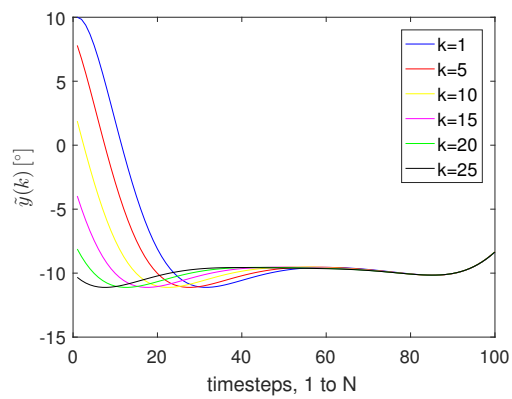
(b) control inputs



(c) delta reference



(d) predicted control inputs



(e) predicted states

Figure 4-19: MPC stabilizing pendulum at  $\theta = -10$  degrees

### 4-2-2 PGK

The same MPC structure can be used to provide course correction by controlling the PGK actuator. However there are some fundamental differences caused by the linearization of both the projectile and the actuator model. As previously stated in chapter 2 the linearization of these models results in them describing the deviation dynamics rather than directly deriving the current state.

So control model will be

$$\dot{x} = A dx + B du \quad (4-42)$$

$$dy = C dx + D du, \quad (4-43)$$

with  $A$  the linearized projectile model from equation (2-30),  $B$  the linearized actuator model from equation (2-40),  $C = \begin{bmatrix} 1 & 0 & 0 & 0 \\ 0 & 1 & 0 & 0 \end{bmatrix}$  as they can be derived from the Global Positioning System (GPS) measurements, and  $D = 0$ .

The Guidance as described in chapter 3 is used as the reference signal for this controller to track. As the guidance signals are already delta velocities, they can directly be used in this linearized MPC structure. The result of this controller will be an incremental control action  $du$  with respect to the  $u_0$  around which is linearized. The control action used for simulation is therefore  $u = u_0 + du$ .

This MPC framework can be seen as a foundation for course correction by the PGK actuator, but needs further elaboration as is suggested in the recommendations in chapter 6.

## 4-3 Conclusion

In this chapter the empirical switching mode controller is described. A sensitivity analysis on the switching parameters  $t_c$ , the controller starting time,  $G_c$ , the guidance threshold, and  $t_d$  the controller downtime in between switches, is performed, resulting in the following controller.

$$\begin{bmatrix} F_a \\ M_a \end{bmatrix} = \begin{cases} 0 & \text{if } t < t_c, \text{ or } \begin{vmatrix} \Delta V_y^* \\ \Delta V_z^* \end{vmatrix} < G_c, \text{ or } t < t_{off} + t_d, \\ f_{PGK}(x(t), \alpha_{PGK}) & \text{for all other situations.} \end{cases}$$

$$t_c = 10s, G_c = 2m/s, \text{ and } t_d = 5s.$$

with  $F_a$ , and  $M_a$  the actuator forces and moments,  $\Delta V_{y,z}^*$  the guidance commands,  $t_{off}$  the last time at which the controller is switched off,  $f_{PGK}$  the nonlinear actuator model as described in section 2-2-2,  $x(t)$  the state at time  $t$ , and  $\alpha_{PGK}$  the angle of the

---

PGK ring. This tuning is specific to one nominal trajectory and it is shown that it still provides course correction without causing instability for a depressed trajectory, however the performance could be improved by changing the tuning for different trajectories.



---

# Chapter 5

---

## Simulations

The Precision Guidance Kit (PGK) and switching controller are simulated on four different nominal trajectories using the models as described in chapter 2. The switching controller designed in chapter 4 is tested on four different nominal trajectories. For each trajectory 100 simulations are performed with random offsets, as in a Monte-Carlo simulation, for which the controller will provide course correction to end up as close as possible to the target. These offsets are applied to the initial pitch angle  $\theta_0$ , yaw angle  $\psi_0$ , and initial velocity  $V_0$  and are uniformly distributed. The offset is uniformly distributed between  $-1^\circ$  and  $1^\circ$  for the pitch and yaw angle, and between  $-5m/s$  and  $5m/s$  for the initial velocity.

The two main parameters that determine a nominal trajectory are the initial velocity and pitch angle, so these are varied, resulting in four different nominal trajectories.

- trajectory 1: high velocity, high pitch angle
- trajectory 2: high velocity, low pitch angle
- trajectory 3: low velocity, high pitch angle
- trajectory 4: low velocity, low pitch angle

The initial state is shown for each scenario, and the resulting nominal trajectory. The impact point of the nominal trajectory is used as the target for the trajectories with the offsets on the initial state. As the impact point is per definition at  $z_E = 0$ , the  $z_E$  coordinates of impact points are omitted from the analysis. Therefore the miss distance, or delivery error,  $\varepsilon_{x,y}$  is

$$\begin{bmatrix} \varepsilon_x \\ \varepsilon_y \end{bmatrix} = \begin{bmatrix} x_E(t_{impact}) \\ y_E(t_{impact}) \end{bmatrix} - \begin{bmatrix} T_x \\ T_y \end{bmatrix}, \quad (5-1)$$

where  $(x, y)_E(t_{impact})$  are the  $x$  and  $y$  coordinates in the Earth reference frame at the time of impact, and  $T_{x,y}$  the target coordinates in the same reference frame.

For each trajectory the miss distances of the impact points for the uncontrolled and controlled trajectories are analyzed. The Circular Error Probable (CEP) is a common measure for accuracy of weapon systems, it is defined as the radius of the circle in which 50% of the projectiles are expected to land. This circle is centered on the mean of all the impact points, which does not have to be the target point. The deviation of the mean impact point and the target, the so called bias, is therefore added to the analysis.

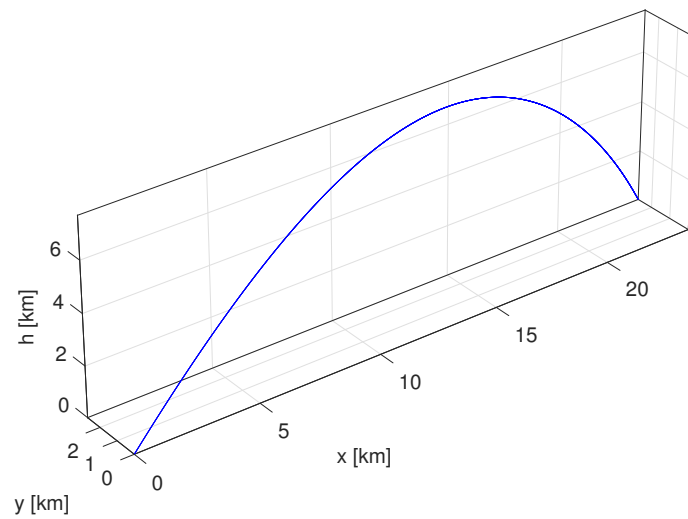
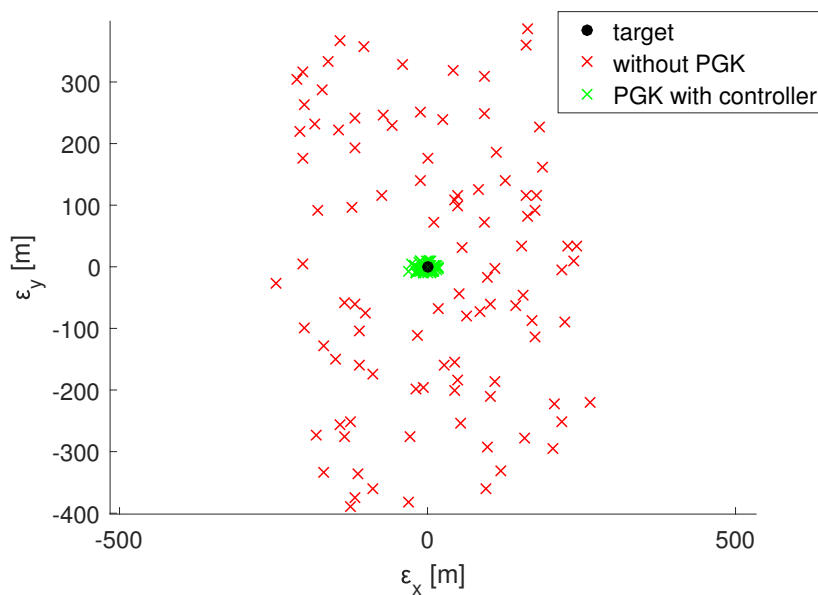
## 5-1 trajectory 1: high velocity, high pitch angle

The initial state of the first nominal trajectory is

$$\begin{aligned} x_0 &= \begin{bmatrix} u_0 & v_0 & w_0 & p_0 & q_0 & r_0 & x_{E_0} & y_{E_0} & z_{E_0} & \phi_0 & \theta_0 & \psi_0 \end{bmatrix}^T \\ &= \begin{bmatrix} 700m/s & 0 & 0 & 1200/s & 0 & 0 & 0 & 0 & 0 & 0 & 45^\circ & 5^\circ \end{bmatrix}^T \end{aligned}$$

resulting in the nominal trajectory as shown in figure 5-1, with final coordinates  $x_E(t_{impact})$ , and  $y_E(t_{impact})$ .

$$\begin{bmatrix} x_E(t_{impact}) \\ y_E(t_{impact}) \end{bmatrix} = \begin{bmatrix} T_x \\ T_y \end{bmatrix} = \begin{bmatrix} 23785m \\ 2738m \end{bmatrix}$$

**Figure 5-1:** nominal trajectory 1**Figure 5-2:** miss distance trajectory 1

The miss distances of the 100 simulations are plotted in figure 5-2. As can be seen from the figure the PGK combined with the switching mode controller greatly reduces the spread of impact points. Even though the offset in initial conditions is uniformly

distributed, it can be seen that the uncontrolled impact points are not. These have a larger spread in  $\varepsilon_y$ , approximately between  $-400m$  and  $400m$ , than in  $\varepsilon_x$ , which is approximately between  $-250m$  and  $250m$ . This can be explained by the initial pitch angle of the nominal trajectory, which is  $\theta_0 = 45^\circ$ . This is the optimal pitch angle for long trajectories, any increase or decrease in pitch angle will shorten the trajectory only slightly. So the main cause of  $\varepsilon_x$  is the offset of the initial velocity, which is shown to have less of an effect on the impact point in the range direction than an offset in yaw angle has in the cross-range direction.

A more zoomed in plot of the controlled miss distances is shown in figure 5-3. As can be seen the spread of the impact points of the controlled trajectories are slightly oval, with a larger spread in the range direction. This has to be caused by the PGK since the spread of the uncontrolled impact points is larger in the cross-range direction. This will be discussed further for the next trajectories, where spread of the controlled miss distances is more clearly oval shaped.

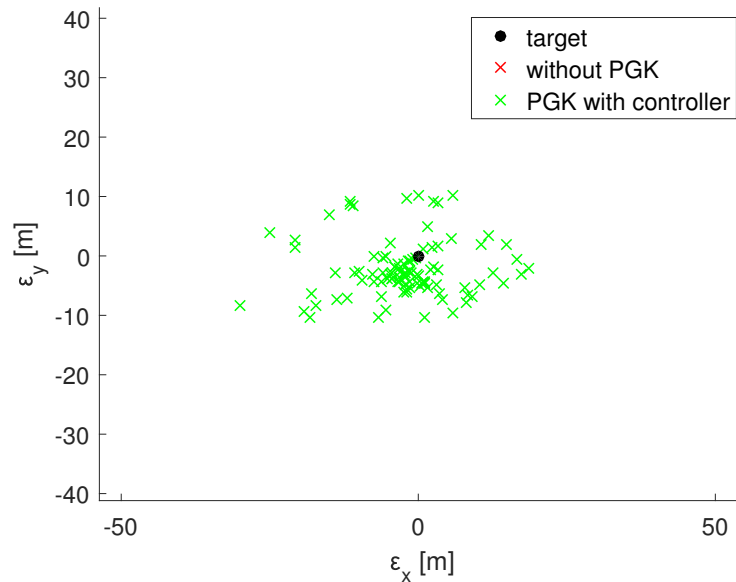


**Figure 5-3:** miss distance trajectory 1 close up

The average distance is listed in table 5-1, as well as the CEP and the bias. The average miss distance is reduced by 96%, and the CEP is reduced by 98%.

**Table 5-1:** simulations results trajectory 1

	uncontrolled	controlled
average miss distance [m]	257	10
CEP [m]	264	6
bias [m]	$[3.8 \ -8.1]^T$	$[-1.0 \ -5.2]^T$

## 5-2 trajectory 2: high velocity, low pitch angle

The initial state of the second nominal trajectory is

$$\begin{aligned} x_0 &= [u_0 \ v_0 \ w_0 \ p_0 \ q_0 \ r_0 \ x_{E_0} \ y_{E_0} \ z_{E_0} \ \phi_0 \ \theta_0 \ \psi_0]^T \\ &= [700\text{m/s} \ 0 \ 0 \ 1200/\text{s} \ 0 \ 0 \ 0 \ 0 \ 0 \ 0 \ 25^\circ \ 5^\circ]^T \end{aligned}$$

resulting in the nominal trajectory as shown in figure 5-4, with final coordinates and target

$$\begin{bmatrix} x_E(t_{\text{impact}}) \\ y_E(t_{\text{impact}}) \end{bmatrix} = \begin{bmatrix} T_x \\ T_y \end{bmatrix} = \begin{bmatrix} 19481\text{m} \\ 1945\text{m} \end{bmatrix}.$$

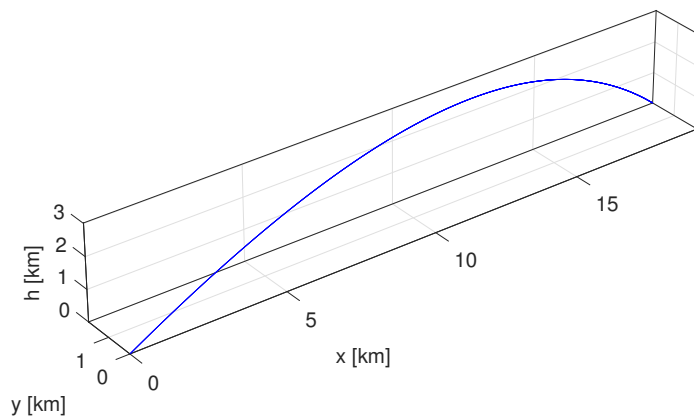


**Figure 5-4:** nominal trajectory 2

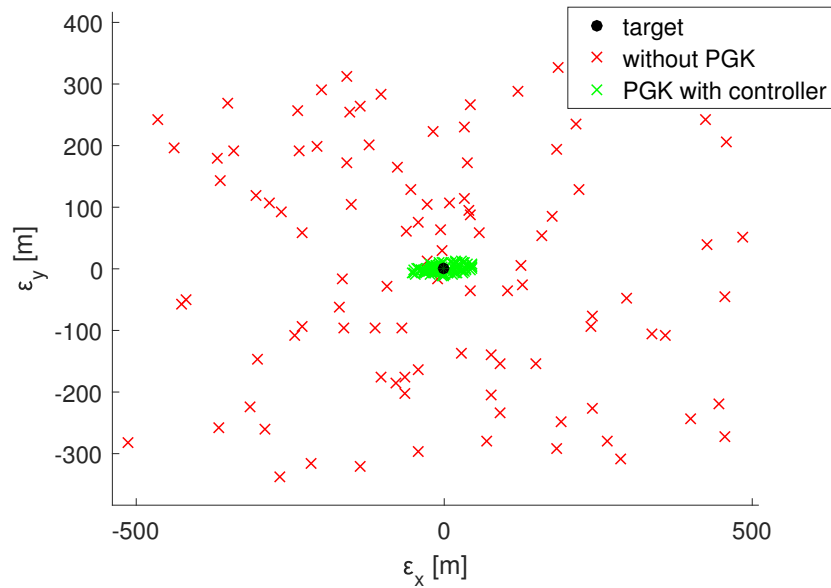


**Figure 5-5:** miss distance trajectory 2

The miss distances of the 100 simulations are plotted in figure 5-5. As can be seen from the figure the PGK combined with the switching mode controller also reduces the spread of impact points for this trajectory with lower initial pitch angle. The figure shows also that the spread in impact points from the controlled trajectories are not shaped like a circle.  $\varepsilon_x$  is harder to control to zero than  $\varepsilon_y$ . This is not caused by a low Jacobian elements in the guidance as can be seen in figure 5-6. This plot shows that the impact point in range direction could be corrected by manipulating  $\Delta V_z$  up to the end of the trajectory. So the miss distance and its distribution is caused by the controller.

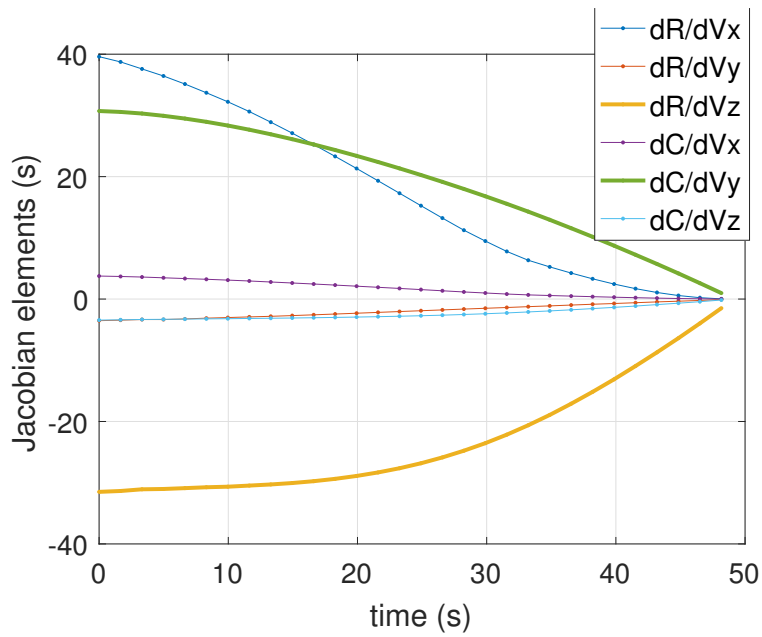


**Figure 5-6:** Jacobian elements nominal trajectory

The average miss distance is listed in table 5-2, as well as the CEP and the bias. The average miss distance is reduced by 92%, and the CEP is reduced by 93%.

**Table 5-2:** simulations results trajectory 2

	uncontrolled	controlled
average miss distance [m]	274	22
CEP [m]	270	18
bias [m]	$[-15 \ 3.2]^T$	$[-3.9 \ -0.1]^T$

### 5-3 trajectory 3: low velocity, high pitch angle

The initial state of the third nominal trajectory is

$$\begin{aligned} x_0 &= [u_0 \quad v_0 \quad w_0 \quad p_0 \quad q_0 \quad r_0 \quad x_{E_0} \quad y_{E_0} \quad z_{E_0} \quad \phi_0 \quad \theta_0 \quad \psi_0]^T \\ &= [330m/s \quad 0 \quad 0 \quad 800/s \quad 0 \quad 0 \quad 0 \quad 0 \quad 0 \quad 0 \quad 45^\circ \quad 0]^T \end{aligned}$$

resulting in the nominal trajectory as shown in figure 5-7, with final coordinates and target

$$\begin{bmatrix} x_E(t_{impact}) \\ y_E(t_{impact}) \end{bmatrix} = \begin{bmatrix} T_x \\ T_y \end{bmatrix} = \begin{bmatrix} 9275m \\ 229m \end{bmatrix}.$$

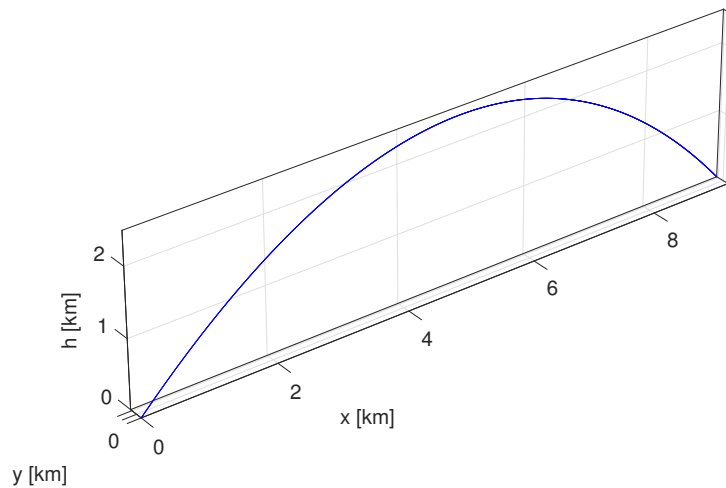


**Figure 5-7:** nominal trajectory 3

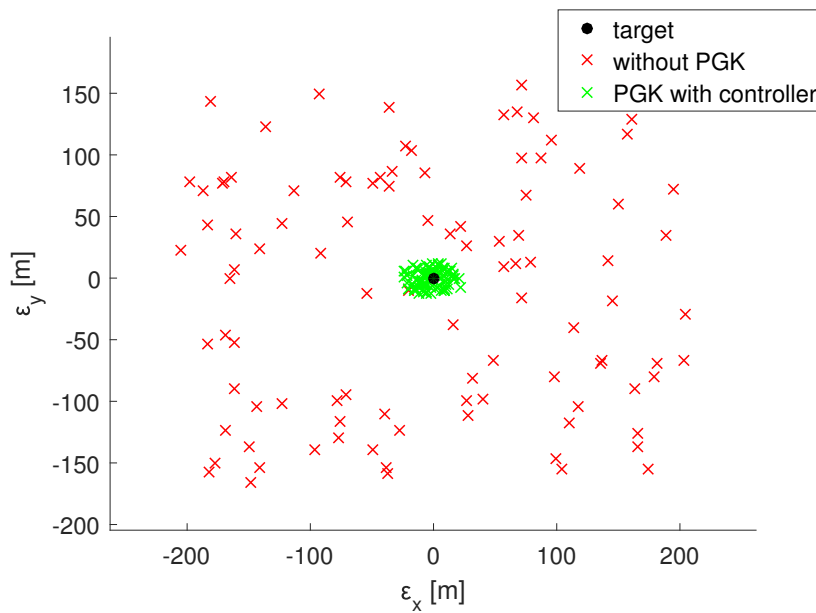


**Figure 5-8:** miss distance trajectory 3

The miss distances of the 100 simulations are plotted in figure 5-8. As can be seen from the figure the PGK combined with the switching mode controller also reduces the spread of impact points for a trajectory with lower initial velocity. The mean miss distance is listed in table 5-3, as well as the CEP and the bias. The average miss distance is reduced by 92%, and the CEP is reduced by 92%.

**Table 5-3:** simulations results trajectory 3

	uncontrolled	controlled
mean miss distance [m]	144	12
CEP [m]	154	12
bias [m]	$[-8.2 \ 9.6]^T$	$[-2.4 \ -0.7]^T$

## 5-4 trajectory 4: low velocity, low pitch angle

The initial state of the fourth nominal trajectory is

$$\begin{aligned} x_0 &= [u_0 \quad v_0 \quad w_0 \quad p_0 \quad q_0 \quad r_0 \quad x_{E_0} \quad y_{E_0} \quad z_{E_0} \quad \phi_0 \quad \theta_0 \quad \psi_0]^T \\ &= [330m/s \quad 0 \quad 0 \quad 800/s \quad 0 \quad 0 \quad 0 \quad 0 \quad 0 \quad 0 \quad 25^\circ \quad 0]^T \end{aligned}$$

resulting in the nominal trajectory as shown in figure 5-9, with final coordinates and target

$$\begin{bmatrix} x_E(t_{impact}) \\ y_E(t_{impact}) \end{bmatrix} = \begin{bmatrix} T_x \\ T_y \end{bmatrix} = \begin{bmatrix} 7352m \\ 78m \end{bmatrix}.$$

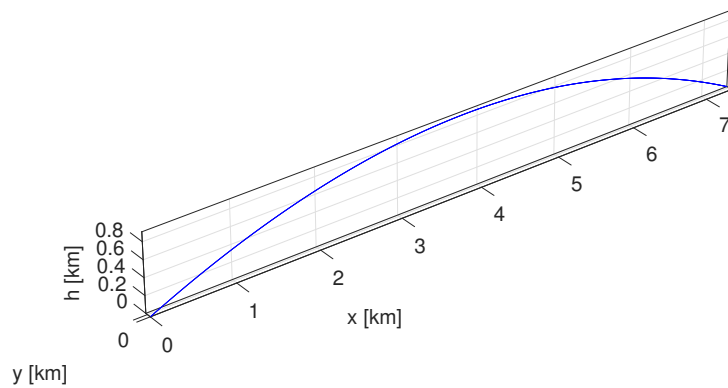


**Figure 5-9:** nominal trajectory 4

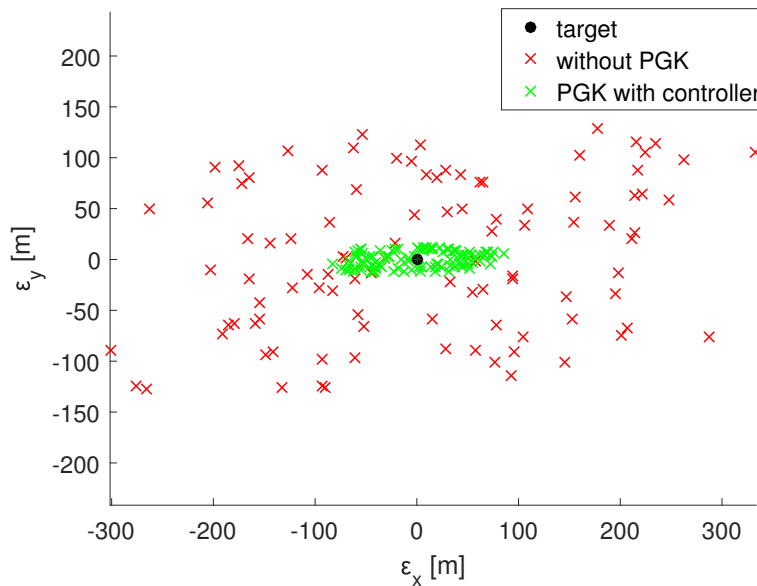


**Figure 5-10:** miss distance trajectory 4

The miss distances of the 100 simulations are plotted in figure 5-10. As can be seen from the figure the PGK combined with the switching mode controller also reduces the spread of impact points for trajectories with a lower initial velocity and pitch angle. The mean miss distance is listed in table 5-4, as well as the CEP and the bias. The average miss distance is reduced by 72%, and the CEP is reduced by 70%. As can be seen in the figure and the table this shorter and flatter trajectory is harder to control. The CEP is still lower than the goal of 50m, but the relative improvements in miss distance and CEP for this trajectory are the lowest of these four scenarios. The nominal trajectory of this scenario varies the most from the trajectory on which the controller tuning is based. As previously stated in section the performance could be improved by tuning for each nominal trajectory. This simulation is repeated using the controller tuning specific for this trajectory as found in section 4-1-3. This miss distance for the simulations with the new tuning is shown in figure 5-11. The mean miss distance, CEP and bias are listed in table 5-4 along with a new uncontrolled set, which is not equal to the first one, since other random seeds are used. As can be seen the controlled miss distances are decreased using this specific tuning, the average miss distance is reduced by 91% and the CEP by 92% with respect to the uncontrolled case. By using specific tuning an extra decrease of 20 percentage points in average miss distance and CEP is achieved. However the specific tuning does not change the spread of the miss distance, which remains oval shaped.

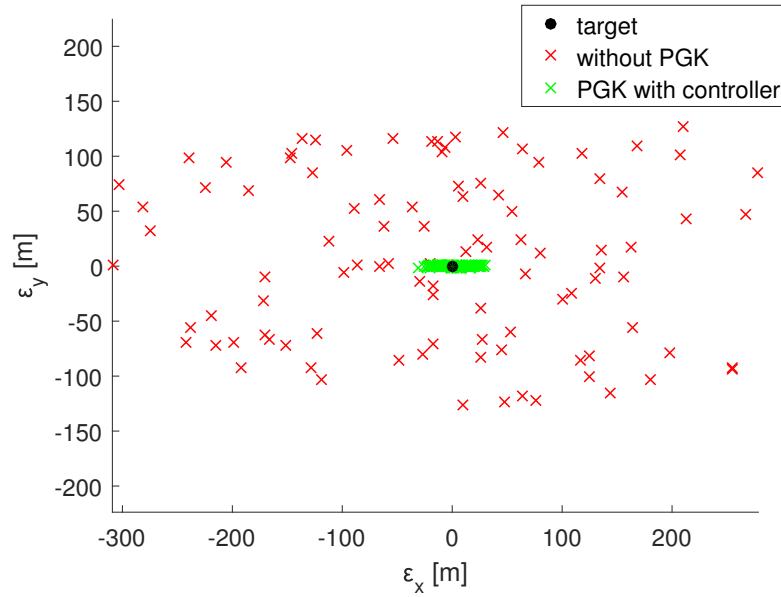


**Figure 5-11:** miss distance trajectory 4 with specific tuning

**Table 5-4:** simulations results trajectory 4

	uncontrolled	controlled	uncontrolled 2	controlled with specific tuning
mean miss distance [m]	149	41	143	13
CEP [m]	144	43	143	12
bias [m]	$[5.6 \ 3.5]^T$	$[0.0 \ -0.3]^T$	$[-10.8 \ 6.8]^T$	$[1.6 \ 0.2]^T$

## 5-5 conclusion

In this chapter Monte-Carlo simulations of the PGK and the switching controller are performed. This is done for four different nominal trajectories, varying in velocity and pitch angle since these are the parameters with the largest influence on the trajectory. For each simulation the initial velocity, pitch angle and yaw angle have a random offset, for which the controller and actuator combination successfully compensates. It is shown that the CEP is reduced to less than  $50m$ , therefore the controller meets the design criteria stated in section 1-2. The reduction in average miss distance and CEP are relatively smaller for shorter and flatter trajectories. For trajectories with an even lower velocity and/or pitch angle the PGK and switching controller designed in this thesis might not be able to result in a CEP less than  $50m$ . It is shown that specific tuning for a set of launch conditions increases performance using a shorter and depressed trajectory as an example. The controller provides more adequate control in cross-range direction

than in range direction, however both remain within the desired boundaries as specified by the design criteria.



---

## Chapter 6

---

# Conclusions

The projectile dynamics are formulated as a nonlinear 6Degrees of Freedom (DoF) non-rolling body frame model, and a nonlinear model is constructed for the Precision Guidance Kit (PGK) actuator. Both these models are linearized for computational efficiency and to be used in linear control applications. The principles of the Jacobian guidance are explained. The mathematical derivation of the guidance signals are included. These signals are desired changes in normal body velocities  $\Delta V_{y,z}^*$ , and function as a reference to be tracked by a controller. To demonstrate the capabilities of the guidance, two simple proportional actuators are used, one providing only forces, and one only moments. These actuators are combined with a proportional controller. This combination results in a decrease of delivery errors by at least 95% for initial offsets in pitch and yaw angles of  $1^\circ$ .

While the actuator and controller are to be changed for more realistic ones in the next chapter, the guidance is as described in this chapter. So any increase in delivery error can be attributed to the actuator and controller. The switching mode controller is described. A sensitivity analysis on the switching parameters  $t_c$ , the controller starting time,  $G_c$ , the guidance threshold, and  $t_d$  the controller downtime in between switches, is performed, resulting in an empirically tuned switching controller. This tuning is specific to one nominal trajectory and it is shown that it still provides course correction without causing instability for a depressed trajectory, however the performance could be improved by changing the tuning for different trajectories. Monte-Carlo simulations of the PGK and the switching controller are performed. This is done for four different nominal trajectories, varying in velocity and pitch angle since these are the parameters with the largest influence on the trajectory. For each simulation the initial velocity, pitch angle and yaw angle have a uniformly distributed random offset, for which the controller and actuator combination successfully compensates. It is shown that the Circular Error Probable (CEP) is reduced to less than  $50m$ , therefore the controller meets the design

criteria. The reduction in average miss distance and CEP are relatively smaller for shorter and flatter trajectories, since the controller is not tuned specifically for such a trajectory. It is shown that specific tuning for a specific launch conditions increases performance, using a shorter and depressed trajectory as an example. The controller results in higher miss distances in range direction than in cross-range direction, however both remain within the desired boundaries as specified by the design criteria. The switching controller has easy to tune settings. It calculates the PGK angle,  $\alpha_{PGK}$  continuously, and uses state-dependent switching to turn the actuator on or off. Even though the design might be simple, the combination between this controller, the actuator model, and the guidance algorithm decreases the average miss distance and CEP by 90%.

As the guidance algorithm in combination with an ideal, proportional actuator decreases the average miss distance by 95%, there is only a 5 percentage point drop in performance caused by the switching controller in combination with the PGK. As the PGK actuator is not ideal, it accounts for a part of this reduction in performance which cannot be solved by using different control methods. Still the selection of other, more sophisticated, controllers might further increase the performance, however small, if this is desired.

## 6-1 Recommendations

The first recommendation is to complete the Model Predictive Control (MPC) controller. Although the linear projectile model and the linear model for the PGK will decrease the computational requirements, it looks like the actuator's behavior is too nonlinear. With a small enough time step a linear model should closely resemble the nonlinear model so it should be able to work, but the computational benefits will disappear too. Therefore it is recommended to consider a nonlinear MPC for the control of the PGK.

Other nonlinear control approaches could also be used to control the PGK actuator more efficiently. For example nonlinear dynamic inversion, this control strategy is used mostly in aircraft control and has proven to be an easy and robust option for controlling nonlinear systems.

Stability of the switching mode controller is shown in simulation, but this should be proven theoretically as well. This is left out of the scope of this report, but is recommended for further research.

The PGK model is simplified and assumed to be static, for a given projectile state and angle of the PGK ring the actuator forces and moments are calculated. In reality the angle cannot be set directly, a torque caused by the brake in the actuator will slow the spin rate of the ring and allows it to be set in at a certain angle. This step is recommended to resemble reality more closely. It will however complicate the actuator model, and provides an extra (highly nonlinear) challenge for the controller. One of the problems that will rise are the actuator forces and moments that will disturb the

trajectory when the actuator ring is despun, or when the brake is released and the ring will start to spin because of the anti-roll canards.

In this thesis the guidance is benchmarked with an ideal proportional actuator resulting in miss distances within  $1m$ , so it is safe to say that the error caused by the guidance is small. But the remaining delivery error will be partly caused by the controller and partly by the actuator. If the largest part is caused by limitations of the actuator even an ideal controller only provides a slight performance increase. This is advised to analyze for further research.

The switching mode controller is tuned for a specific case, resulting in a controller that provides course correction successfully for the four different scenario's tested in this thesis. However it is shown that the performance can be improved by tuning the controller for each launch. Another recommendation is to do this by scheduling controller settings for sets of launch conditions. For example actuation can start earlier on the trajectory if the initial velocity is lower, since the vibration caused by the launch will be dampened earlier as well. The downtime of the controller might also be adjusted according to the distance to the target. In practice this would provide no additional action, since the target coordinates are loaded into the PGK pre-launch, so the controller tuning could be adjusted automatically based on the target information.

The inaccuracy of the GPS and angle measurements used by the guidance is not taken into account. The navigation, or state estimation is assumed to be perfect. This is left out of the scope of this report, however this should be included to complete this control engineering problem.



---

# Appendix A

---

## Jacobian linearization

The Linear Parameter Varying (LPV) based linear projectile model derived in chapter 2 is linearized around the nominal trajectory. So this model describes the deviations around the nominal trajectory and not the projectile dynamics directly. In equations (2-30 - 2-36) the Jacobian matrix that describes the deviation dynamics is shown. In this Appendix the derivation will be shown in more detail, based on [38].

### A-1 Deviation dynamics

Linearization around a trajectory is done in the following way. The general idea is to make a Taylor expansion around a known solution so let  $(x_0, u_0)$  denote a solution to  $\dot{x} = f(x, u)$  and consider another known solution. And consider another solution  $(x(t), u(t)) = (x_0 + \delta_x, u_0 + \delta_u)$ :

$$\dot{x}(t) = f(x_0 + \delta_x, u_0 + \delta_u) \quad (\text{A-1})$$

$$= f(x_0, u_0) + \frac{\partial f}{\partial x}(x_0, u_0)\delta_x + \frac{\partial f}{\partial u}(x_0, u_0)\delta_u + \mathcal{O}(\|\delta_x, \delta_u\|^2), \quad (\text{A-2})$$

so the deviation dynamics are

$$\dot{\delta}_x = \frac{\partial f}{\partial x}(x_0, u_0)\delta_x + \frac{\partial f}{\partial u}(x_0, u_0)\delta_u + \mathcal{O}(\|\delta_x, \delta_u\|). \quad (\text{A-3})$$

For small deviations  $(\delta_x, \delta_u)$  this results in

$$\dot{\delta}_x(t) = A(t)\delta_x(t) + B(t)\delta_u(t) \quad (\text{A-4})$$

$$A(t) = \left. \frac{\partial f}{\partial x} \right|_{\substack{x(t) = \bar{x}(t) \\ u(t) = \bar{u}(t)}} \quad (\text{A-5})$$

$$B(t) = \left. \frac{\partial f}{\partial u} \right|_{\substack{x(t) = \bar{x}(t) \\ u(t) = \bar{u}(t)}} \quad (\text{A-6})$$

Note that in contrast to linearization around an equilibrium, matrices  $A$ , and  $B$  are time dependent when linearizing along the trajectory.

## A-2 Jacobian Linearization of projectile model

$$A = \begin{bmatrix} \frac{\partial \dot{v}}{\partial v} & \frac{\partial \dot{v}}{\partial w} & \frac{\partial \dot{v}}{\partial q} & \frac{\partial \dot{v}}{\partial r} \\ \frac{\partial \dot{w}}{\partial v} & \frac{\partial \dot{w}}{\partial w} & \frac{\partial \dot{w}}{\partial q} & \frac{\partial \dot{w}}{\partial r} \\ \frac{\partial \dot{q}}{\partial v} & \frac{\partial \dot{q}}{\partial w} & \frac{\partial \dot{q}}{\partial q} & \frac{\partial \dot{q}}{\partial r} \\ \frac{\partial \dot{r}}{\partial v} & \frac{\partial \dot{r}}{\partial w} & \frac{\partial \dot{r}}{\partial q} & \frac{\partial \dot{r}}{\partial r} \end{bmatrix} \quad (\text{A-7})$$

$$\dot{v} = -V_0 r + \frac{1}{m} Y \quad (\text{A-8})$$

$$Y = -\bar{q} S \left( C_{N\alpha} \frac{v}{V_0} + \frac{p_0 d}{V_0} C_{yp\alpha} \frac{w}{V} \right) \quad (\text{A-9})$$

$$\frac{\partial \dot{v}}{\partial v} = - \left( \frac{1}{m V_0} \right) \bar{q} S C_{N\alpha} \quad (\text{A-10})$$

$$\frac{\partial \dot{v}}{\partial w} = - \left( \frac{1}{m V_0} \right) \bar{q} S \left( \frac{p_0 d}{V_0} \right) C_{yp\alpha} \quad (\text{A-11})$$

$$\frac{\partial \dot{v}}{\partial q} = 0 \quad (\text{A-12})$$

$$\frac{\partial \dot{v}}{\partial r} = -V_0 \quad (\text{A-13})$$

$$\dot{w} = V_0 q + \frac{1}{m} Z \quad (\text{A-14})$$

$$Z = -\bar{q} S \left( C_{N\alpha} \frac{w}{V_0} - \frac{p_0 d}{V_0} C_{yp\alpha} \frac{v}{V_0} \right) + mg \cos \theta \quad (\text{A-15})$$

$$\frac{\partial \dot{w}}{\partial v} = \left( \frac{1}{mV_0} \right) \bar{q} S \left( \frac{p_0 d}{V_0} \right) C_{ypa} \quad (\text{A-16})$$

$$\frac{\partial \dot{w}}{\partial w} = - \left( \frac{1}{mV_0} \right) \bar{q} S C_{Na} \quad (\text{A-17})$$

$$\frac{\partial \dot{w}}{\partial q} = V_0 \quad (\text{A-18})$$

$$\frac{\partial \dot{w}}{\partial r} = 0 \quad (\text{A-19})$$

$$\dot{q} = -I_{yy}^{-1} I_{xx} p_0 r + I_{yy}^{-1} M \quad (\text{A-20})$$

$$M = \bar{q} S d \left( C_{m\alpha} \frac{w}{V_0} - \frac{p_0 d}{V_0} C_{np\alpha} \frac{v}{V_0} + \frac{d}{V_0} C_{mq} q \right) \quad (\text{A-21})$$

$$\frac{\partial \dot{q}}{\partial v} = -I_{yy}^{-1} \frac{\bar{q} S d}{V_0} \left( \frac{p_0 d}{V_0} \right) C_{npa} \quad (\text{A-22})$$

$$\frac{\partial \dot{q}}{\partial w} = I_{yy}^{-1} \frac{\bar{q} S d}{V_0} C_{ma} \quad (\text{A-23})$$

$$\frac{\partial \dot{q}}{\partial q} = I_{yy}^{-1} \frac{\bar{q} S d}{V_0} d C_{mq} \quad (\text{A-24})$$

$$\frac{\partial \dot{q}}{\partial r} = -I_{yy}^{-1} I_{xx} p_0 \quad (\text{A-25})$$

$$\dot{r} = I_{yy}^{-1} I_{xx} p_0 q + I_{yy}^{-1} N \quad (\text{A-26})$$

$$N = \bar{q} S d \left( -C_{m\alpha} \frac{v}{V_0} - \frac{p_0 d}{V_0} C_{np\alpha} \frac{w}{V_0} + \frac{d}{V_0} C_{nr} r \right) \quad (\text{A-27})$$

$$\frac{\partial \dot{r}}{\partial v} = -I_{yy}^{-1} \frac{\bar{q} S d}{V_0} C_{ma} \quad (\text{A-28})$$

$$\frac{\partial \dot{r}}{\partial w} = -I_{yy}^{-1} \frac{\bar{q} S d}{V_0} \left( \frac{p_0 d}{V_0} \right) C_{npa} \quad (\text{A-29})$$

$$\frac{\partial \dot{r}}{\partial q} = I_{yy}^{-1} I_{xx} p_0 \quad (\text{A-30})$$

$$\frac{\partial \dot{r}}{\partial r} = I_{yy}^{-1} \frac{\bar{q} S d}{V_0} d C_{nr} \quad (\text{A-31})$$

Resulting in:

$$A = \begin{bmatrix} \frac{\partial \dot{v}}{\partial v} & \frac{\partial \dot{v}}{\partial w} & \frac{\partial \dot{v}}{\partial q} & \frac{\partial \dot{v}}{\partial r} \\ \frac{\partial \dot{w}}{\partial v} & \frac{\partial \dot{w}}{\partial w} & \frac{\partial \dot{w}}{\partial q} & \frac{\partial \dot{w}}{\partial r} \\ \frac{\partial \dot{q}}{\partial v} & \frac{\partial \dot{q}}{\partial w} & \frac{\partial \dot{q}}{\partial q} & \frac{\partial \dot{q}}{\partial r} \\ \frac{\partial \dot{r}}{\partial v} & \frac{\partial \dot{r}}{\partial w} & \frac{\partial \dot{r}}{\partial q} & \frac{\partial \dot{r}}{\partial r} \end{bmatrix} = \begin{bmatrix} -A_j & -B_j & 0 & -V_0 \\ B_j & -A_j & V_0 & 0 \\ -C_j & E_j & F_j & -G_j \\ -E_j & -C_j & G_j & F_j \end{bmatrix} \quad (\text{A-32})$$

where

$$A_j = \frac{1}{mV_0} \bar{q} S C_{Na} \quad (\text{A-33})$$

$$B_j = \frac{1}{mV_0} \bar{q} S \frac{p_0 d}{V_0} C_{ypa} \quad (\text{A-34})$$

$$C_j = I_{yy}^{-1} \frac{\bar{q} S d}{V_0} \frac{p_0 d}{V_0} C_{npa} \quad (\text{A-35})$$

$$E_j = I_{yy}^{-1} \frac{\bar{q} S d}{V_0} C_{ma} \quad (\text{A-36})$$

$$F_j = I_{yy}^{-1} \frac{\bar{q} S d}{V_0} d C_{nr} \quad (\text{A-37})$$

$$G_j = I_{yy}^{-1} I_{xx} p_0 \quad (\text{A-38})$$

---

# Bibliography

- [1] T. Hillstrom and P. Osborne, "United Defense Course Correcting Fuze for the Projectile Guidance Kit Program The Need for Accuracy Direct Fire," *NDIA 49th Annual Fuze Conference*, pp. 1–11, 2005.
- [2] T. Bybee, "Precision guidance kit," *45th Annual NDIA Gun and Missile Systems Conference*, vol. 4, no. May, 2010.
- [3] B. Etkin, *Dynamics of Atmospheric Flight*. Wiley, 1972.
- [4] C. Murphy, *Free flight motion of symmetric missiles*. Ballistic Research Laboratories, 1963.
- [5] R. L. McCoy, *Modern Exterior Ballistics: The Launch and Flight Dynamics of Symmetric Projectiles*. Schiffer, 1999.
- [6] P. Wernert, S. Theodoulis, and Y. Morel, "Flight dynamics properties of 155 mm spin-stabilized projectiles analyzed in different body frames," *AIAA Atmospheric Flight Mechanics Conference*, vol. August, 2010.
- [7] D. Ollerenshaw and M. Costello, "Model Predictive Control of a Direct Fire Projectile Equipped With Canards," *Journal of Dynamic Systems, Measurement, and Control*, vol. 130, November 2008.
- [8] F. Fresconi and M. Ilg, "Model Predictive Control of Agile Projectiles," *AIAA Atmospheric Flight Mechanics Conference*, pp. 2012–4860, August 2012.
- [9] A. Elsaadany and Y. Wen-Jun, "Accuracy improvement capability of advanced projectile based on course correction fuze concept," *The Scientific World Journal*, July 2014.

- [10] A. J. Calise, M. Sharma, and J. E. Corban, "Adaptive Autopilot Design for Guided Munitions," *Journal of Guidance, Control, and Dynamics*, vol. 23, no. 5, September-October, pp. 837–843, 2000.
- [11] E. Gagnon and M. Lauzon, "Maneuverability Analysis of the Conventional 155 mm Gunnery Projectile," *AIAA Guidance, Navigation and Control Conference and Exhibit*, pp. 20–23, August 2007.
- [12] E. Gagnon, "Low cost guidance and control solution for in-service unguided 155 mm artillery shell," tech. rep., DRDC Valcartier, July 2009.
- [13] M. Costello and A. Peterson, "Linear Theory of a Dual-Spin Projectile in Atmospheric Flight," *Journal of Guidance, Control, and Dynamics*, vol. 23, no. 5, September-October, 2000.
- [14] L. C. Hainz and M. Costello, "Modified projectile linear theory for rapid trajectory prediction," *Journal of Guidance, Control, and Dynamics*, vol. 28, pp. 1006–1014, September-October 2005.
- [15] S. Theodoulis, F. Sève, and P. Wernert, "Robust gain-scheduled autopilot design for spin-stabilized projectiles with a course-correction fuze," *Aerospace Science and Technology*, vol. 42, pp. 477–489, 2015.
- [16] S.-H. Cho and M. Zaheer-uddin, "An experimental study of multiple parameter switching control for radiant floor heating systems," *Energy*, vol. 24, no. 5, pp. 433 – 444, 1999.
- [17] D. Liberzon, *Switching in Systems and Control*. Birkhäuser Boston, 2003.
- [18] S. Lim and J. P. How, "Modeling and h-infinity control for switched linear parameter-varying missile autopilot," *IEEE Transactions on Control Systems Technology*, vol. 11, no. 6, pp. 830–838, 2003.
- [19] C. Yuan, Y. Liu, F. Wu, and C. Duan, "Hybrid switched gain-scheduling control for missile autopilot design," *Journal of Guidance, Control, and Dynamics*, vol. 39, 08 2016.
- [20] D. E. Miller, M. Chang, and E. J. Davison, "An approach to switching control: Theory and application," in *Control Using Logic-Based Switching*, pp. 234–247, Springer-Verlag.
- [21] F. Fresconi, I. Celmins, S. Sifton, and M. Costello, "High maneuverability projectile flight using low cost components," *Aerospace Science and Technology*, 2015.
- [22] J. W. C. Robinson and P. Strömbäck, "Velocity To Be Gained Guidance for a Generic 2D Course Correcting Fuze," *AIAA Guidance, Navigation and Control Conference*, January 2015.

- 
- [23] S. Theodoulis, V. Gassmann, T. Brunner, and P. Wernert, "Robust Bank-to-Turn Autopilot Design for a Class of 155mm Spin-Stabilized Canard-Guided Projectiles," *AIAA Atmospheric Flight Mechanics (AFM) Conference*, August 2013.
- [24] S. Theodoulis, V. Gassmann, P. Wernert, L. Dritsas, I. Kitsios, and A. Tzes, "Guidance and Control Design for a Class of Spin-Stabilized Fin-Controlled Projectiles," *Journal of Guidance, Control, and Dynamics*, vol. 36, no. 2, March-April, 2013.
- [25] F. Sève, S. Theodoulis, P. Wernert, M. Zasadzinski, and M. Boutayeb, "Pitch/Yaw Channels Control Design for a 155mm Projectile with Rotating Canards, using a  $\mathcal{H}_\infty$  Loop-Shaping Design Procedure," *AIAA Guidance, Navigation and Control Conference*, January 2014.
- [26] F. Sève, S. Theodoulis, P. Wernert, M. Zasadzinski, and M. Boutayeb, "Gain-Scheduled  $\mathcal{H}_\infty$  Loop-Shaping Autopilot design for spin-stabilized canard-guided projectiles," *AerospaceLab*, pp. 1–24, September 2017.
- [27] M. Costello, "Extended range of a gun launched smart projectile using controllable canards," *9th Annual Gun Dynamic Symposium*, November 1998.
- [28] A. J. Calise and H. A. El-Shirbiny, "An Analysis of Aerodynamic Control for Direct Fire Spinning Projectiles," *AIAA Guidance, Navigation and Control Conference and Exhibit*, August 2001.
- [29] J. Rogers and M. Costello, "Design of a Roll-Stabilized Mortar Projectile with Reciprocating Canards," *Journal of Guidance, Control, and Dynamics*, vol. July-August, 2010.
- [30] D. Zhu, S. Tang, J. Guo, and R. Chen, "Flight stability of a dual-spin projectile with canards," *Proceedings of the Institution of Mechanical Engineers, Part G: Journal of Aerospace Engineering*, vol. 229, no. 4, pp. 703–716, 2015.
- [31] P. Burke and T. Pergolizzi, "XM1156 Precision Guidance Kit (PGK)," *52nd Annual Fuze Conference*, 2008.
- [32] F. J. Regan and J. Smith, "Aeroballistics of a Terminally Corrected Spinning Projectile (TCSP)," *Journal of Spacecraft and Rockets*, vol. 12, p. 733, Dec. 1975.
- [33] Orbital ATK, "M1156 pgk factsheet." Advertising data from Orbital ATK, "<https://www.orbitalatk.com/defense-systems/armament-systems/pgk/>", accessed 1 2018.
- [34] A. S. Morse, ed., *Control Using Logic-Based Switching*. Springer Berlin Heidelberg, 1997.
- [35] S. Misik, A. Cela, and Z. Bradac, "Optimal Predictive Control - A brief review of theory and practice," *IFAC-PapersOnLine*, 2016.

- 
- [36] A. Bemporad and M. Morari, “Robust Model Predictive Control: A Survey,” in *Garulli, A. and Tesi, A. (eds) Robustness in identification and control. Lecture Notes in Control and Information Sciences*, vol. 245, pp. 207–226, Springer, London, 1999.
- [37] T. van de Boom and T. Backx, “Model predictive control, lecture notes for the course sc4060,” September 2005.
- [38] Packard, Poola, and Horowitz, “Dynamic systems and feedback,” 2002.

---

# Glossary

## List of Acronyms

<b>3mE</b>	Mechanical, Maritime and Materials Engineering
<b>DCSC</b>	Delft Center for Systems and Control
<b>TU Delft</b>	Delft University of Technology
<b>DUT</b>	Delft University of Technology
<b>TNO</b>	the Netherlands organization for applied scientific research
<b>MPC</b>	Model Predictive Control
<b>PGK</b>	Precision Guidance Kit
<b>CCF</b>	Course Correction Fuze
<b>GNC</b>	Guidance Navigation and Control
<b>DoF</b>	Degrees of Freedom
<b>CEP</b>	Circular Error Probable
<b>GPS</b>	Global Positioning System
<b>LPV</b>	Linear Parameter Varying
<b>PID</b>	Proportional-Integral-Derivative
<b>ISL</b>	Institute of Saint Louis
<b>EoM</b>	Equations of Motion
<b>RMSE</b>	Root-Mean-Square Error

<b>CFD</b>	Computational Fluid Dynamics
<b>WS</b>	Weapon Systems
<b>DSS</b>	Defence Safety and Security

## List of Symbols

$\alpha$	Angle of attack [ <i>rad</i> ]
$\alpha'$	The angle of incidence [ <i>rad</i> ]
$\alpha_{PGK}$	Angle of the PGK ring [ <i>rad</i> ]
$\beta$	Angle of sideslip [ <i>rad</i> ]
$\delta_x(t)$	Small deviation of state at time t [–]
$\delta_{\alpha_{PGK}}$	Increment of the angle of the PGK ring [ <i>rad</i> ]
$\delta_{\alpha_{PGK}}$	Small deviation of the angle of the PGK ring [ <i>rad</i> ]
$\Delta CR$	Deviation of the impact point in cross-range direction [ <i>m</i> ]
$\Delta R$	Deviation of the impact point in range direction [ <i>m</i> ]
$\Delta V_{x,y,z}$	Deviation in velocity in x,y,z direction [ <i>m/s</i> ]
$\Delta V_{y,z}^*$	Desired deviation in velocity in y,z direction, also guidance signals [ <i>m/s</i> ]
$\phi, \theta, \psi$	Euler angles for roll, pitch and yaw [ <i>rad</i> ]
$\varepsilon$	Miss distance, or delivery error [ <i>m</i> ]
$\bar{q}$	Dynamic pressure [ <i>Pa</i> ]
$\bar{x}(t)$	Nominal state at time t [–]
$\mathcal{M}$	Mach number [–]
$\tilde{C}_2, \tilde{D}_{22}, \tilde{D}_{23}$	Prediction matrices
$\tilde{v}$	Prediction of control input
$\tilde{y}$	Prediction of measurement signal
$\tilde{z}$	Prediction of performance signal
$A_{y,z}$	Specific force [ <i>m/s<sup>2</sup></i> ]
$C_*$	Aerodynamic coefficients [–]
$C_{A0,A2}$	Aerodynamic drag force coefficient
$C_{lp,mq,nr}$	Damping moment coefficients
$C_{m\alpha}$	Aerodynamic overturning moment coefficient
$C_{N\alpha}$	Aerodynamic normal force coefficient
$C_{np\alpha}$	Magnus moment coefficient
$C_{yp\alpha}$	Magnus force coefficient
$d$	Diameter of the projectile [ <i>m<sup>2</sup></i> ]

---

$dt$	Sampling time
$F_a$	Actuator force [ $N$ ]
$F_b$	Aerodynamic force acting on the projectile body [ $N$ ]
$F_F$	Actuator force in fin frame [ $Nm$ ]
$F_g$	Gravity [ $N$ ]
$F_m$	Magnus force [ $N$ ]
$F_X, F_Y, F_Z$	Force components [ $N$ ]
$g$	Gravitational acceleration
$G_C$	Guidance threshold [ $m/s$ ]
$I$	Inertia matrix
$J$	Cost function
$K$	Control gains $[-]$
$k$	Discrete time
$l_r$	Reference length of the fins [ $m$ ]
$m$	Mass [ $kg$ ]
$M_a$	Actuator moment [ $Nm$ ]
$M_b$	Moment caused by aerodynamics on the projectile body [ $Nm$ ]
$M_d$	Damping moment [ $Nm$ ]
$M_F$	Actuator moment in fin frame [ $Nm$ ]
$M_m$	Magnus moment [ $Nm$ ]
$M_X, M_Y, M_Z$	Moment components [ $Nm$ ]
$N$	Prediction horizon
$p, q, r$	Angular velocity vector components [ $rad/s$ ]
$Q$	Reference tracking weight
$R$	Control penalty weight
$r(k)$	Reference at time $k$
$S$	Aerodynamic reference surface of the projectile [ $m^2$ ]
$S_r$	Reference surface of the fins [ $m^2$ ]
$t$	Time [ $s$ ]
$T_s$	Sampling time [ $s$ ]
$t_c$	Controller starting time [ $s$ ]
$t_c$	Downtime of the controller [ $s$ ]
$t_{impact}$	Time at impact [ $s$ ]
$t_{off}$	Time at which the controller is switched off [ $s$ ]
$T_{x,y}$	Target position $x$ and $y$ [ $m/s$ ]
$u, v, w$	Velocity vector components [ $m/s$ ]
$V$	Total velocity [ $m/s$ ]
$v(k)$	Control input at time $k$

---

$x(t)$	State at time $t$ [-]
$x_E, y_E, z_E$	Position components in earth frame [ $m$ ]
$z$	Performance signal
$A, B, C, D$	State space matrices
$f_{PGK}$	Nonlinear actuator model